AD-A063 253 HUGHES RESEARCH LABS MALIBU CALIF F/G 20/3
ROCKET MODEL SATELLITE POSITIVE ION BEAM SYSTEM.(U)
OCT 78 T MASEK F19628-76-C-0272
UNCLASSIFIED AFGL-TR-78-0179 NL

OF 2
AD
A063253

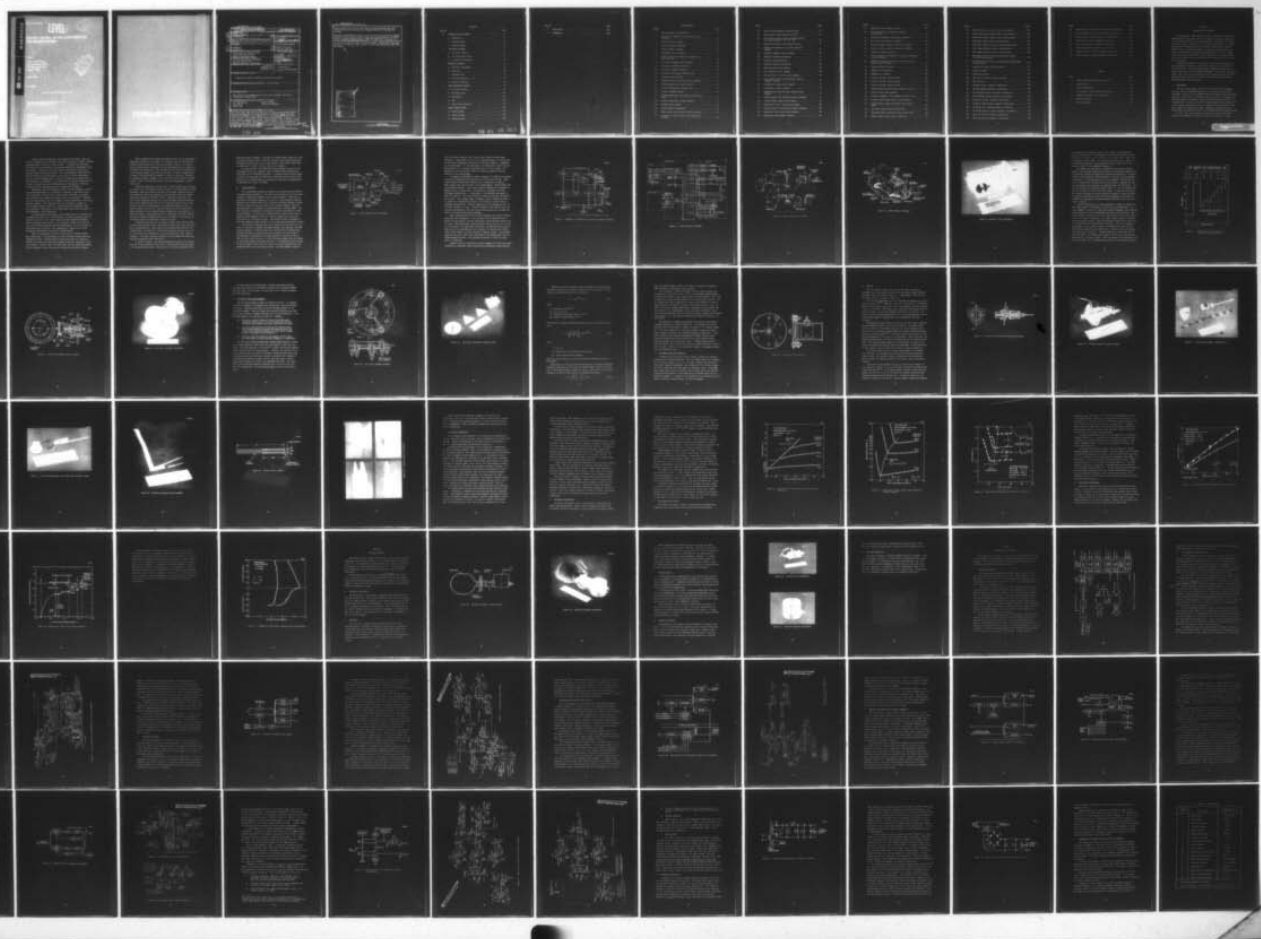

DDC FILE COPY

AD A063253

AFGL-TR-78-0178

LEVEL II

12

ROCKET MODEL SATELLITE POSITIVE ION BEAM SYSTEM

T. Hunt

Hughes Aircraft Company
Research Laboratories Division
3011 Malibu Canyon Road
Malibu, CA 90265

DDC
DEC 27 1978
D

UNCLASSIFIED

SECURITY CLASSIFICATION OF THIS PAGE (When Data Entered)

REPORT DOCUMENTATION PAGE

READ INSTRUCTIONS BEFORE COMPLETING FORM

1. REPORT NUMBER: AFGL-TR-78-0179	2. GOVT ACCESSION NO.
3. RECIPIENT'S CATALOG NUMBER	
4. TITLE (and Subtitle): ROCKET MODEL SATELLITE POSITIVE ION BEAM SYSTEM	5. TYPE OF REPORT & PERIOD COVERED: Final Report 1 Jul 1976 - 1 Oct 1977
6. PERFORMING ORG. REPORT NUMBER	
7. AUTHOR(s): T. Masek	8. CONTRACT OR GRANT NUMBER(s): F19628-76-C-0272
9. PERFORMING ORGANIZATION NAME AND ADDRESS: Hughes Research Laboratories, 3011 Malibu Canyon Road, Malibu, California 90265	10. PROGRAM ELEMENT, PROJECT, TASK AREA & WORK UNIT NUMBERS: 61101F; ILIR6J01; 6J
11. CONTROLLING OFFICE NAME AND ADDRESS: Air Force Geophysics Laboratory, Hanscom AFB, MA 01731, Monitor: Herbert A. Cohen/LKB	12. REPORT DATE: October 1978 13. NUMBER OF PAGES: 170
14. MONITORING AGENCY NAME & ADDRESS (if different from Controlling Office) 172p.	15. SECURITY CLASS. (of this report): UNCLASSIFIED 15a. DECLASSIFICATION DOWNGRADING SCHEDULE

16. DISTRIBUTION STATEMENT (of this Report)

Approved for public release; distribution unlimited.

17. DISTRIBUTION STATEMENT (of the abstract entered in Block 20, if different from Report)

18. SUPPLEMENTARY NOTES

This research was supported by the Air Force In-House Laboratory Independent Research Fund.

19. KEY WORDS (Continue on reverse side if necessary and identify by block number)

Ion beam systems
Ion sources
Xenon ions
Hollow cathodes
Spacecraft charging

20. ABSTRACT (Continue on reverse side if necessary and identify by block number)

The Rocket Model (RM) Satellite Positive Ion Beam System (SPIBS) instrument was built under Air Force Geophysics Laboratory (AFGL) Contract F19628-76-C-0272, to be one experiment in an Astrobee F Rocket scientific payload. The purpose of the rocket experiment was to obtain electrostatic charging data in the altitude range of 100 to 300 km. SPIBS provides a controllable means of ejecting a positive xenon ion beam or a neutralized ion beam at ion energies of 1 or 2 keV. Rocket flight test

→ next page

DD FORM 1 JAN 73 1473 EDITION OF 1 NOV 65 IS OBSOLETE

UNCLASSIFIED

SECURITY CLASSIFICATION OF THIS PAGE (When Data Entered)

172 600

results showed that surface potentials of several hundred volts were achieved by ion ejection and that charging varied as a function of altitude.

Although the RM-SPIBS was built for its own distinct purpose, an equally important function of the rocket flight was the evaluation of the SPIBS design. The main SPIBS program (F19628-76-C-0066) was conducted concurrently with the RM-SPIBS program. The SPIBS primary development effort was in fact carried out under the main program. The RM-SPIBS instrument was built to a quality level similar to the SPIBS engineering model (EM) instrument.

ACCESSION for
NTIS [illegible] Section
DDC B ff Section
UNANNOUNCED
JUSTIFICATION
BY
DISTRIBUTION/AVAILABILITY CODES
Dist. SPECIAL
A

CONTENTS

79 01 15 015

ILLUSTRATIONS

TABLES

SECTION 1

INTRODUCTION AND SUMMARY

The Rocket Model (RM) Satellite Positive Ion Beam System (SPIBS) instrument was built, under Air Force Geophysics Laboratory (AFGL) Contract F19628-76-C-0272, to be one experiment in an Astrobee "F" Rocket scientific payload. The purpose of the rocket experiment was to obtain electrostatic charging data in the altitude range of 100 to 300 km. SPIBS provides a controllable means of ejecting a positive xenon ion beam or a neutralized ion beam at ion energies of 1 or 2 keV. Rocket flight test results showed that surface potentials of several hundred volts were achieved by ion ejection and that charging varied as a function of altitude.

Although the RM-SPIBS was built for its own distinct purpose, an equally important function of the rocket flight was the evaluation of the SPIBS design. The main SPIBS program (F19628-76-C-0066) was conducted concurrently with the RM-SPIBS program.[1] The SPIBS primary development effort was in fact carried out under the main program. The RM-SPIBS instrument was built to a quality level similar to the SPIBS engineering model (EM) instrument.

A. BACKGROUND

The main SPIBS program, initiated in 1975 by the AFGL Aeronomy Division, had the long-range objective of operating an ion ejection instrument on the Air Force SCATHA (Spacecraft Charging at High Altitude) satellite. Within the overall AFGL program, the task of developing the SPIBS instrument was awarded to Hughes Research Laboratories (HRL). The responsibility for other tasks such as requirements definition, qualification testing, integration with the satellite, flight operations, and data reduction was retained by AFGL. Breadboard, engineering, and flight model instruments were built and developed under the SPIBS contract.

For the rocket test, which was conducted in January 1970, AFGL designed and assembled the payload section and provided the launch

PRECEDING PAGE NOT FILMED BLANK

support team. RM-SPIBS integration into the payload, prelaunch checkout, and in-flight operations were performed by AFGL with Hughes support.

The motivation for the SCATHA program, the rocket test program, and SPIBS is the general interest in developing a better understanding of space vehicle charging processes. Several papers related to this subject are available in the literature.[2-7] The SPIBS requirements were derived by AFGL from consideration of spacecraft charging in general and the objectives of SCATHA in particular. The requirements defined for SPIBS are presented in Table 1 and are discussed in some length in Ref. 8. Requirements for RM-SPIBS were identical to the SPIBS requirements except for a mounting interface needed for the rocket payload.

The ion beam current levels, chosen to be greater than the maximum photoelectron emission expected from SCATHA spacecraft grounds, were set at 0.3 mA, 1 mA, and greater than or equal to 2 mA. The upper value was chosen to provide a dynamic range for possible ion-beam currents consistent with power and weight limitations. To minimize interference with other SCATHA experiments, the SPIBS structure exposed to the ambient plasma must be kept close to spacecraft ground potential. This translates into the requirement for a grounded-surface (decel grid) following the ion accelerator grid.

The SPIBS instrument design evolved through several cycles, primarily as a result of ion source design evolution. Initially, the system input power goal was about 25 W with a lifetime requirement of 100 hr. Ion sources then available in the 1 to 2 mA beam current range used filament cathodes and met neither of the basic requirements. The key factor in meeting the power and life requirements was lower cathode temperature. The lower temperature is only available by using "oxide-coated" emitters. In addition, the initially available ion sources were operated on argon simply as a carryover from previous work and as a matter of convenience.

Table 1. SPIBS Requirements and Characteristics

Parameter	Requirement	Characteristic
Ion beam		
Current, mA	0.3 to 2.0	0.3 to 2.0
Energy, keV	1 to 2	1 and 2
Input power, W		
Maximum startup	60	55
1 mA beam, 1 keV	25	30
2 mA beam, 2 keV	--	45
Full beam and biased neutralizer	--	55
Expellant	Noble gas	Xenon
Weight	7.8 maximum	7.4
Operating life, hr	300 minimum	>300
On/Off cycles	200 minimum	>200
Neutralizer		
Control	Ion beam on or off	On/off control
Emission range	2 μA to 2 mA	2.5 μA to 2.5 mA
Biasing	-1 kV to +1 kV	-1 kV to +1 kV in 10 steps
Ion source enclosure and cover	Preflight test capability	Blowoff cover
External magnetic field	<1 G at 10 cm	1 G at 12 cm
EMI	MIL STD 461 A	AFGL to test
Vibration	20 g rms random	AFGL to test
Decel grid	Shielding from space plasma	Decel grid operated at PPA ground potential

6327

Several cathode designs were investigated in prototype argon ion sources including coated filaments and various miniature "flower" cathodes using wire mesh to store the oxide mixture. Lifetimes were generally less than 50 hr, and methods for producing significant improvements were not obvious. Generally, the power required to maintain a given discharge current increased with time. This trend probably indicated that the work function was increasing as the result of several mechanisms. The free surface elements (e.g., barium or strontium) are maintained in equilibrium by the transport of new atoms from the oxide storage site to replace the atoms lost by ion bombardment and evaporation. Both the transport process and evaporation are temperature dependent.

Apparently, when ion bombardment losses are not dominant, a stable equilibrium temperature is achieved and reasonably long cathode lives can be obtained. For instance, flower cathode lifetimes of several thousand hours were demonstrated with mercury ion thrusters.[9] However, when ion sputtering of the free elements becomes significant, the process becomes unstable. The temperature must be increased to supply the active oxide elements being lost by sputtering; the evaporation rate then increases. Eventually, the cathode heater fails from hot spots or from weakness at high temperature.

To avoid cathode sputtering, the ion energy must be relatively low (probably less than 30 V). Unfortunately, the argon discharge tends to operate in the 40 to 50 V region with the plasma conditions needed to obtain reasonable beam currents. The discharge voltage can be driven down with increased discharge neutral atom density, but this results in unacceptable gas flowrates. The combination of argon with an oxide cathode was subsequently rejected as a SPIBS option.

With the recognition that both the gas and the cathode design were significant, a limited number of tests of oxide cathodes were performed with xenon. Although long duration tests were not conducted, operation on xenon with discharge voltages around 30 V appeared to have more promise. However, when it became clear that ion sputtering energy was the dominant factor, interest was focused on the hollow cathode.

Hollow cathodes were rejected initially because of the anticipated high power required for starting. For instance, the 8-cm ion thruster cathode required about 30 to 35 W for starting. However, the typical hollow cathode has the advantage that the emitting surface is exposed to relatively low energy ions. This probably results from the high-density, low-resistance plasma in and near the cathode. In most configurations, a "keeper" electrode near the cathode is used for starting. Generally, the cathode-to-keeper voltage is 10 to 20 V less than the main discharge voltage. Thus, the emitting surface experiences bombardment by lower energy ions.

Since the probability was high that a hollow cathode would provide the needed life, the primary concern was power. By isolating the cathode thermally, using a re-entrant thin wall tube design, conduction losses were minimized. With this approach, starting power (into the cathode heater) was reduced to about 20 to 25 W. Xenon was retained as the first choice expellant because of its more desirable plasma properties. The hollow cathode design selected was eventually found to have a life of more than 1,000 hr operating at acceptable gas flowrates with a keeper voltage of 20 to 25 V. Because time was of the essence, only minor variations in the original cathode design were investigated. In addition, argon or other gases were not tested with the hollow cathode because the primary program objective was to develop a satisfactory system design within the available resources and time.

A significant benefit of the hollow cathode that probably would not have been available from a conventional oxide cathode was low steady state operating power. After keeper and main discharge ignition, the cathode heater is turned off. The keeper discharge requires about 5 W, but this power also contributes to ion production and is not totally parasitic. The oxide cathodes originally tested undoubtedly would have required substantial power continously.

As noted in Table 1, the system maximum input power was increased from the initial optimistic 25-W level. The 60-W peak level was found to be conservative for both startup and for full-power operation (2 mA

beam with biased filament). Although the cathode heater draws less than 25 W during startup, power processing efficiency and housekeeping power contribute significantly to the power demand. Under normal conditions, an input power of about 55 W was found to be adequate.

The time phasing of the RM-SPIBS program allowed essentially all development work to be completed under the main SPIBS program before fabrication of the RM-SPIBS instrument. Although several design changes possibly would have made the SPIBS more compatible with the rocket test objectives, the SPIBS design was unchanged to maximize the applicability of RM-SPIBS test results to SCATHA.

B. SYSTEM CONCEPTS

The requirements and goals outlined in the previous section led to the system shown in Figure 1. The basic system consists of an ion source assembly, an expellant assembly, and a power processor. Xenon gas is delivered to the porous plug in the source at 7 psia through a pressure regulator and latching valve from a reservoir initially charged to about 800 psig. Power for the ion source valve, analog telemetry, and command functions are provided by the power processor assembly (PPA). The PPA circuitry is packaged on conventional circuit cards within a structural enclosure. An ion source vacuum enclosure, with a cover that is opened by electroexplosive devices, provides protection for the ion source prior to operation in space. This blowoff cover is designed to allow for complete ground checkout of ion source and system before launch.

Ion thruster technology was used to develop the ion source in the areas of ion optics, cathode, discharge chamber, and expellant line high voltage isolation. Positive xenon ions extracted from a Penning-type discharge plasma are accelerated electrostatically to high velocity. The discharge is operated at the beam potential to allow the ions to exit at near-ground potential. In the discharge plasma, ions are formed by collisions between atoms and electrons. A conventional hollow cathode is used to generate the electrons, which are then accelerated into the plasma by means of the discharge voltage. An axial magnetic field is

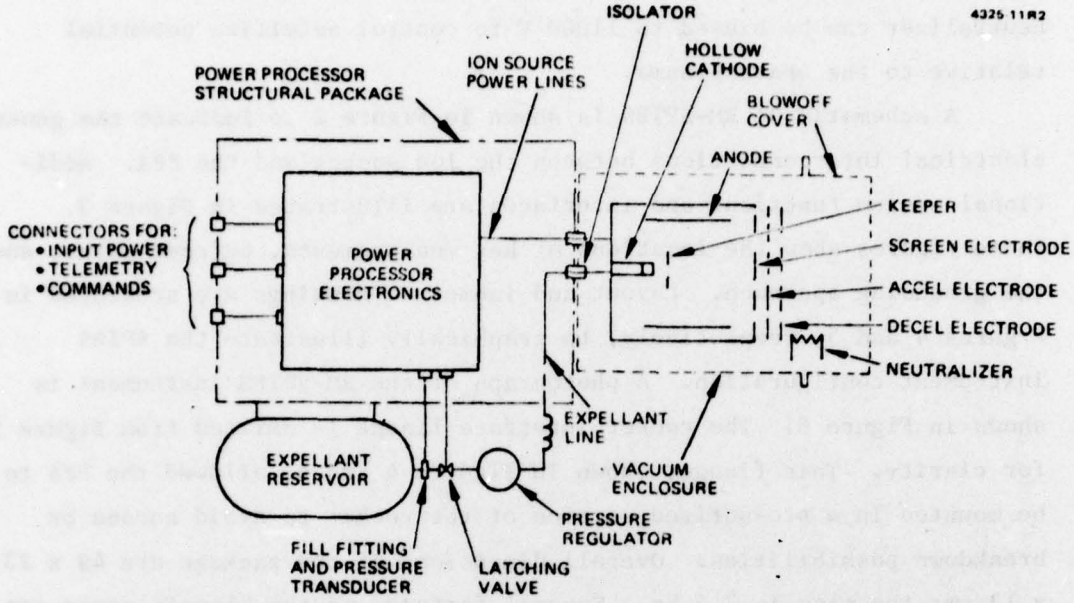

Figure 1. Block diagram of the RM-SPIBS.

used to restrict electron flow radially and increase electron-atom collisions. Downstream from the ion accelerating grids is a neutralizer in the form of redundant thermionically emitting filaments. Depending on the requirements of the experiment, the neutralizer could be used to neutralize all or a fraction (including zero) of the ion beam. The neutralizer can be biased to ±1000 V to control satellite potential relative to the space plasma.

A schematic of RM-SPIBS is shown in Figure 2 to indicate the general electrical interconnections between the ion source and the PPA. Additional system functions and interfaces are illustrated in Figure 3. These figures show the locations of key measurements, current paths, and the grounding approach. Layout and isometric drawings are presented in Figures 4 and 5, respectively, to graphically illustrate the SPIBS instrument configuration. A photograph of the RM-SPIBS instrument is shown in Figure 6. The rocket interface flange is omitted from Figure 5 for clarity. This flange, shown in Figures 4 and 6, allowed the PPA to be mounted in a pressurized section of the rocket to avoid corona or breakdown possibilities. Overall dimensions of the package are 49 x 23 x 13 cm; the mass is 7.4 kg. Several features of the blowoff cover can be noted, including the open and closed positions and the ion beam collector to be used during ground checkout.

Major characteristics of the SPIBS instrument are listed in Table 1 along with the requirements. The ion source can be operated with or without the neutralizer, and the neutralizer can be operated without the ion beam. Five neutralizer electron emission levels from 2 μA to 2.2 mA can be obtained. For additional flexibility in studying vehicle potential control, the neutralizer can be biased at 10 levels from -1000 to +1000 V with respect to vehicle ground (telemetry return). The minimum operating life and on/off cycle requirements were demonstrated with the SPIBS breadboard system. The expellant reservoir is sized for about 200 hr of operation.

Command capability includes 29 ground commands for relatively great flexibility in EM-SPIBS flight operation and convenient ground testing.

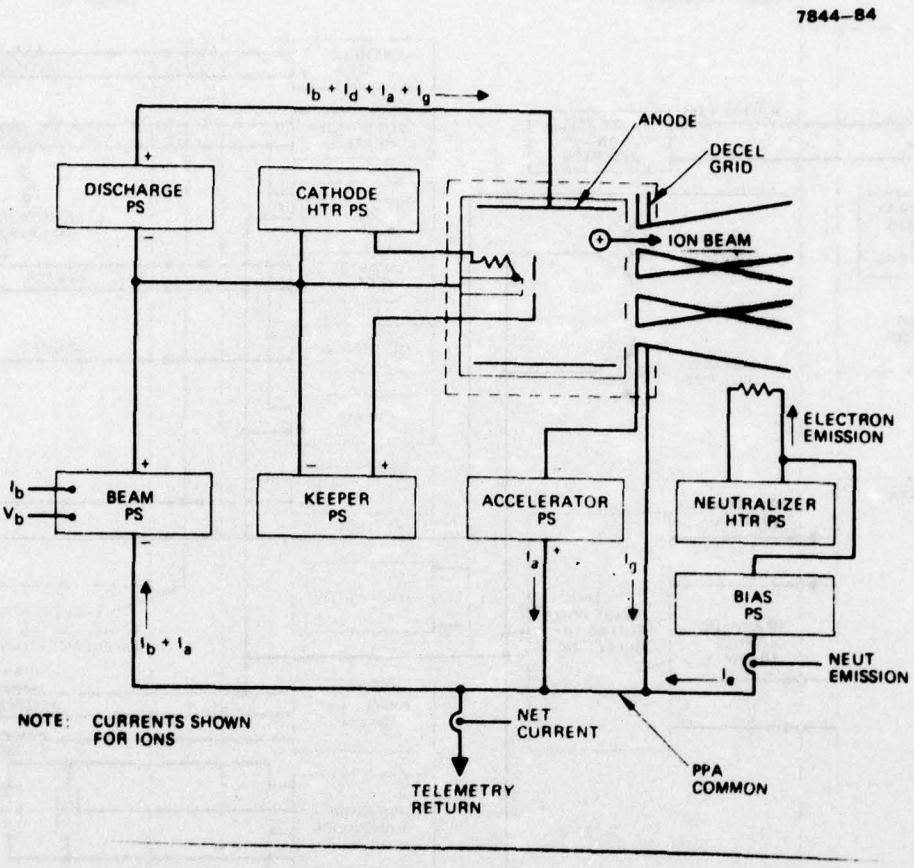

Figure 2. Schematic of SPIBS for ion source and power processor.

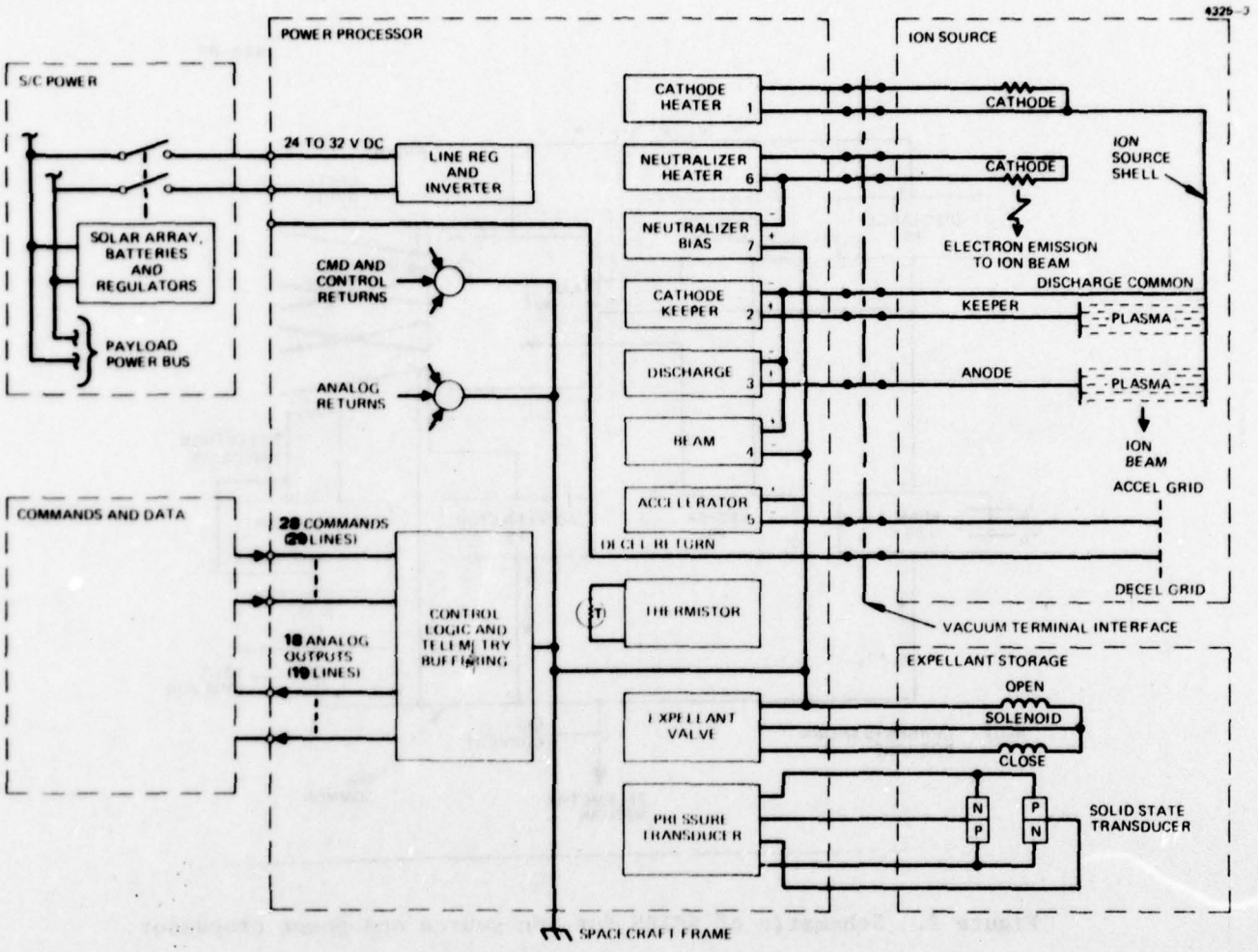

Figure 3. System interface diagram.

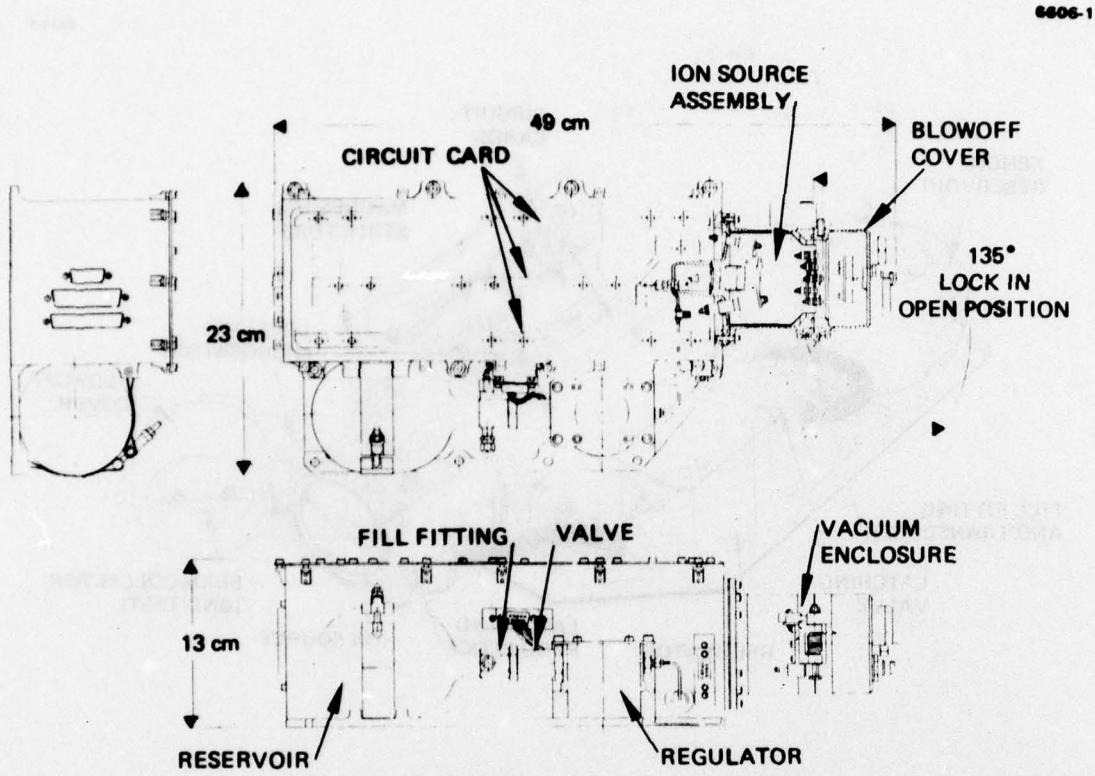

Figure 4. Layout drawing of RM-SPIBS.

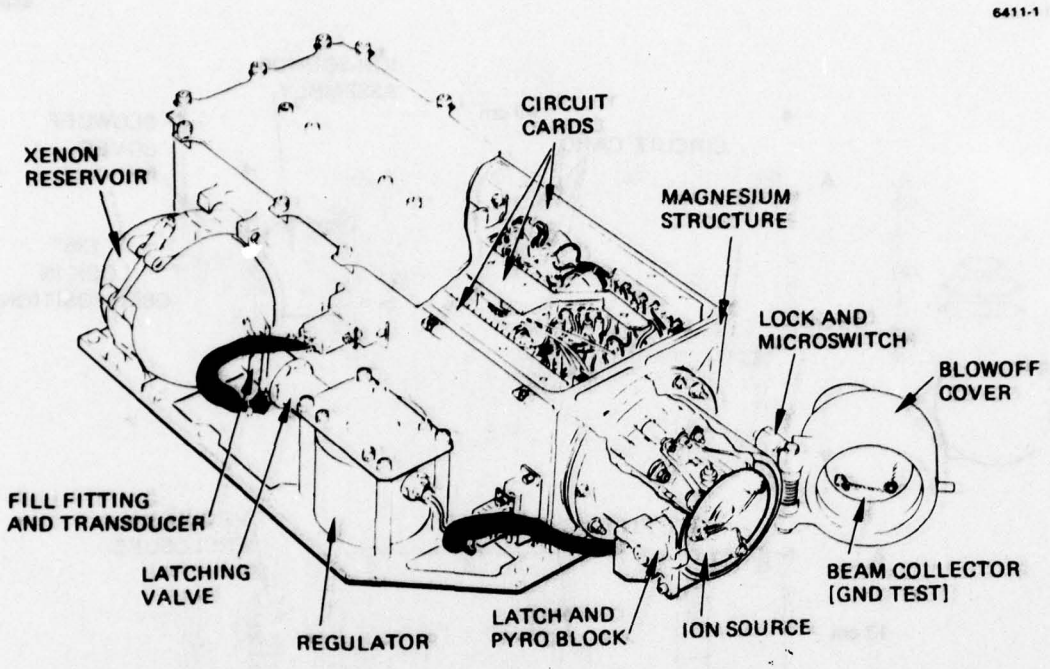

Figure 5. SPIBS isometric drawing.

MC12153

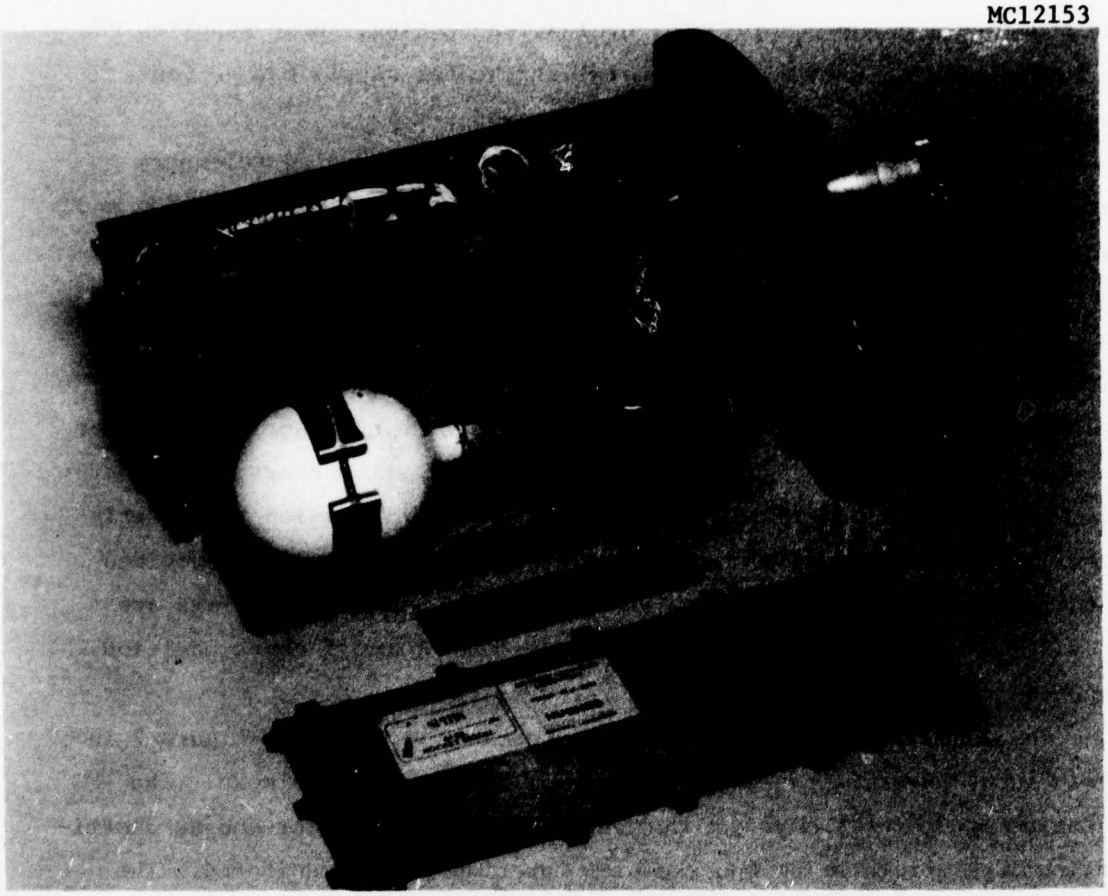

Figure 6. RM-SPIBS flight instrument.

The cathode can be heated at either of two levels, corresponding to initial conditioning of a new cathode or to lower power normal startup. Commands are provided to turn on and off the cathode keeper supply and the beam/accel power supply. For evaluation testing, these supplies can be turned off separately. The neutralizer heater supply can be connected to either of the redundant filaments.

Performance and operation are monitored by 18 analog telemetry outputs. Two extremely important currents, the neutralizer emission and the SPIBS net current, are measured by bipolar electrometers. The electrometers are designed to operate between -2.5 mA and +2.5 mA (positive corresponds to a net electron flow off the filament). The bipolar feature is required only for detecting the net current to ground, but the two electrometers are identical to simplify design and fabrication. For currents (positive or negative) greater than 2 μA, the electrometer outputs are accurate to ±10% of the true current. In addition to the primary outputs defining ion source operation, telemetry is also provided for expellant reservoir pressure and PPA housekeeping. Two flags are provided for defining bias voltage polarity and blowoff cover position (open or closed).

A good illustration of system performance is shown in Figure 7 in which input power is presented as a function of operating mode. The first command, *instrument on*, activates the line regulator and ac distribution inverter to allow housekeeping functions to be monitored. The *cathode preheat* command turns on the cathode heater and discharge supply. After a few minutes (typically, 1 to 5 min), keeper voltage is applied and the discharge ignites. When the discharge voltage falls below 40 V, the cathode heater is automatically turned off. Once the discharge is established, a wide range of options is available for beam current, beam voltage, neutralization, and biasing. A few of the typical modes are illustrated in Figure 7. Although biasing is illustrated only for full beam power, the complete bias range of ±1 kV can be used with any beam current or voltage setting. Since the system can be operated as an ion source alone, as a neutralized ion source, or as an electron source

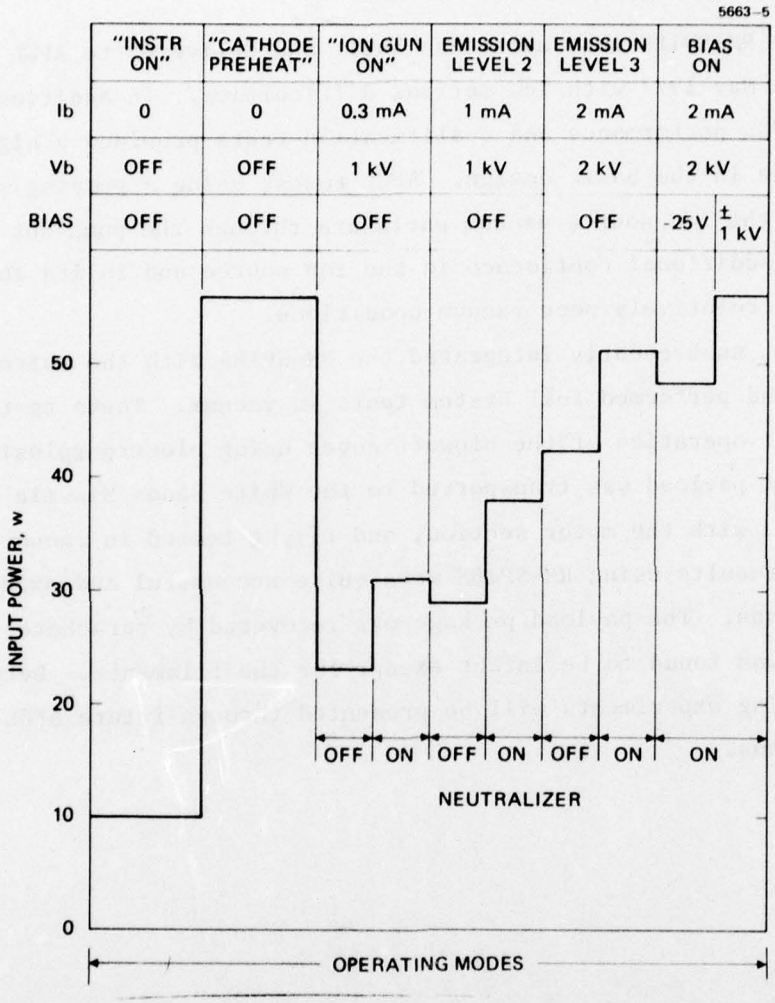

Figure 7. SPIBS typical input power as a function of operating mode.

alone, each with and without biasing, a total of 290 operating modes are available with RM-SPIBS.

C. PROGRAM SUMMARY AND CONCLUSIONS

The RM-SPIBS instrument was built and delivered to AFGL in a timely manner in May 1977 with few serious difficulties. In addition to Hughes tests, AFGL performance and qualification tests provided a high level of confidence in the basic design. AFGL tests, using a pumping station to evacuate the ion source vacuum enclosure through the pump-out port, provided additional confidence in the ion source and in its ability to withstand relatively poor vacuum conditions.

AFGL subsequently integrated the RM-SPIBS with the Astrobee "F" payload and performed full system tests in vacuum. These tests included successful operation of the blowoff cover using electroexplosive devices. The rocket payload was transported to the White Sands Missile Range, integrated with the motor section, and flight tested in January 1978. Charging results using RM-SPIBS were quite successful and exceeded many expectations. The payload package was recovered by parachute, and RM-SPIBS was found to be intact except for the filaments. Details of the charging experiments will be presented through future AFGL publications.

SECTION 2

ION SOURCE ASSEMBLY

The key element of the SPIBS instrument is the ion source assembly (ISA) shown in Figure 8. The ISA produces the ion beam, provides a mount for the neutralizer filaments, and incorporates a vacuum enclosure flange for interfacing with the vacuum-tight cover. ISA design, fabrication processes, and performance are discussed below. This information applies to the SPIBS and RM-SPIBS instruments, although RM-SPIBS data are used where ever possible. Additional information regarding design evolution, various test results, and specific problems is presented in the SPIBS final report.[1]

A. ION SOURCE DESIGN

A photograph of the ion source is presented in Figure 9 to aid in visualizing some of the design details shown in Figure 8. The major elements of the source are (1) ion optics, including neutralizer filaments; (2) source body, which supports the magnets and anode; and (3) cathode-isolator-porous plug (CIP). The CIP subassembly supports the keeper and interfaces with the expellant assembly.

The ion source consists of a 2.4-cm-diameter cylindrical discharge chamber with a concentric cylindrical anode. A hollow cathode-keeper assembly is located at the end of the discharge chamber cylinder; the ion optics assembly is attached to the exit end of this cylinder. The ion source is cantilevered from three insulated and shielded feedthroughs (cable and terminals) attached to the vacuum enclosure endplate. The feedthroughs are tilted toward the center line of the source at a 10° angle to form a rigid conical support base. This configuration allows using a small vacuum enclosure endplate while maintaining sufficient clearance for the isolator assembly, which lies within the conical space formed by the three insulators. Nine wiring insulator feedthroughs are arranged in a circular pattern around the enclosure endplate. These are also tilted toward the axis to allow sputter shields to be placed on the source end of the electrical feedthroughs.

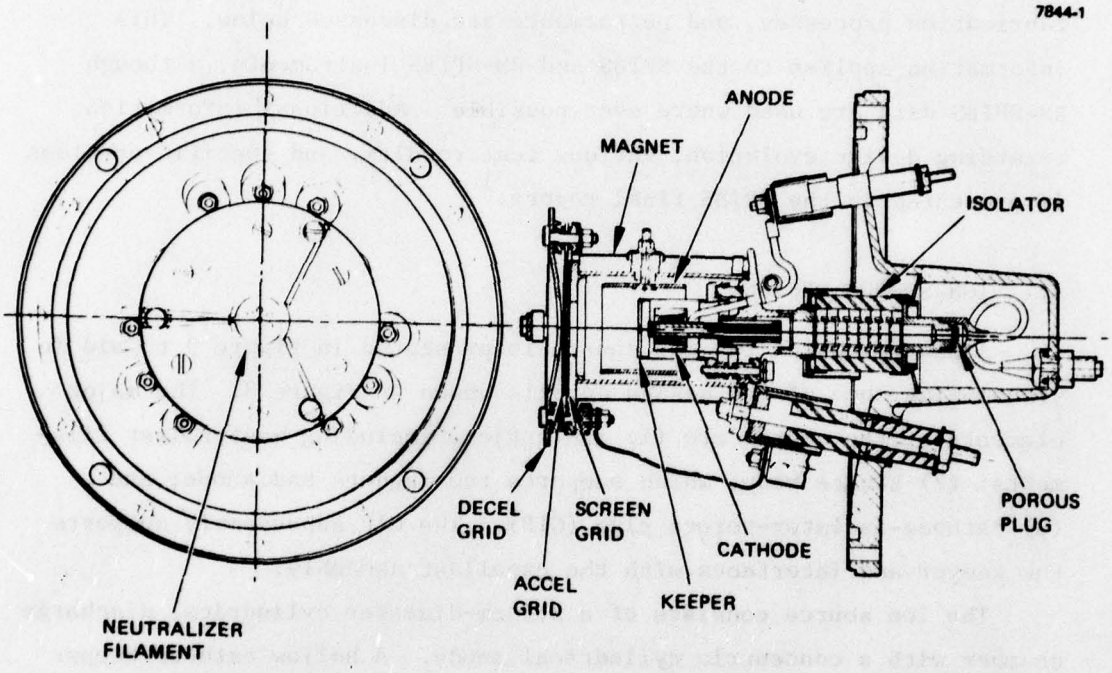

Figure 8. Ion source assembly layout drawing.

M11950

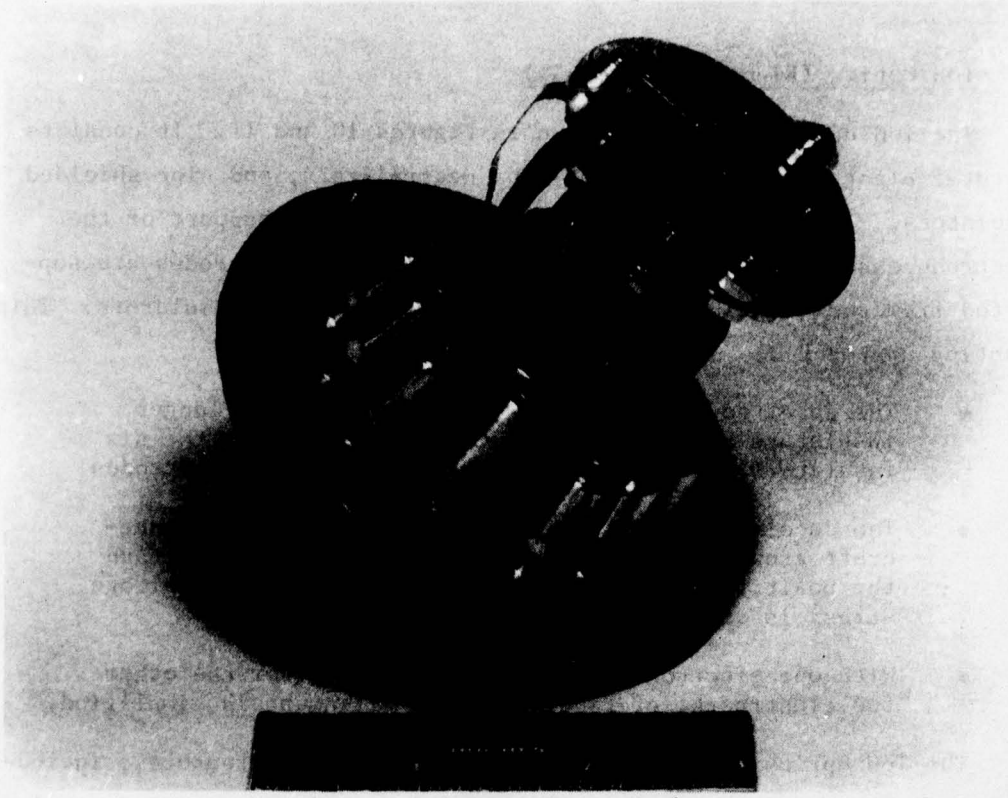

Figure 9. Ion source assembly photograph.

The open end of the feedthroughs, outside the vacuum enclosure, was potted with Uralane polyurathane to prevent high voltage breakdown. This was found to be necessary for operation in air, using the pumpout port for evacuation.

1. Ion Optics (Electrode Assembly)

The ion optics design is shown in Figures 10 and 11. It consists of three electrodes, two filament-type neutralizers, and nine shielded insulators. The decel electrode is used as the main support of the electrode assembly. Both the screen and the accel electrodes are supported from the decel through individual sets of three insulators. This mounting approach was selected for three main reasons:

- The decel could be centrally dished, allowing longer insulators and the use of sputter shields over the six insulators that support the screen and accel electrodes.
- The decel electrode will be operated at nominal spacecraft ground potential (between the negative accel and the positive screen potential) and thus a lower voltage stress is applied to the insulators.
- With one electrode acting as the support for the other two electrodes, critical aperture alignment is simplified.

The ion optics design incorporates several novel features, including a single-aperature steel decel grid and graphite screen and accel grids. Steel was selected for the decel to reduce the external magnetic field created by the ion source magnets. Graphite was selected for the screen aperture and accel grids to minimize charge-exchange sputtering. A single-aperture decel grid was selected to minimize the trapping of sputtered accel material, which in early tests was found to cause a significant buildup on the decel and subsequent shorting. The decel, accel, and screen grid aperture diameters are 1.27 cm, 0.12 cm, and 0.15 cm, respectively. Grid-to-grid spacings of 0.04 to 0.05 cm are used.

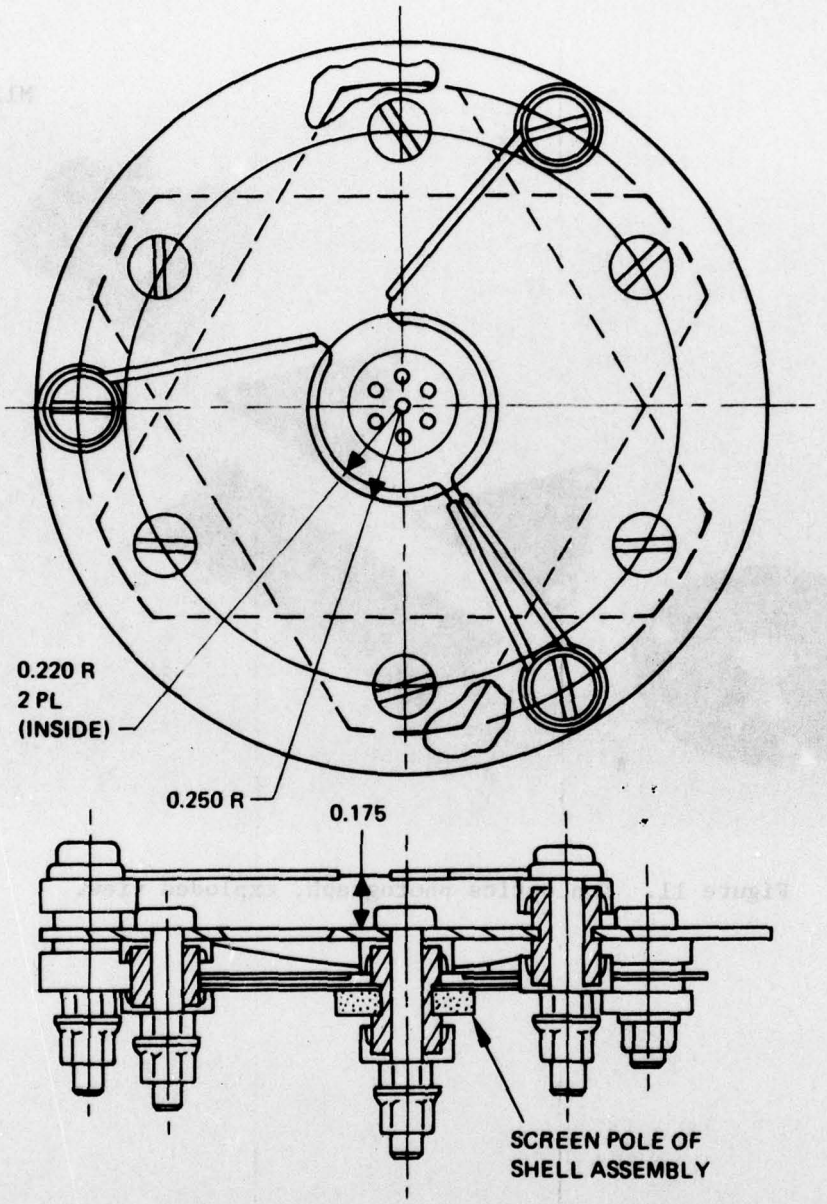

Figure 10. Ion optics assembly drawing.

M12001

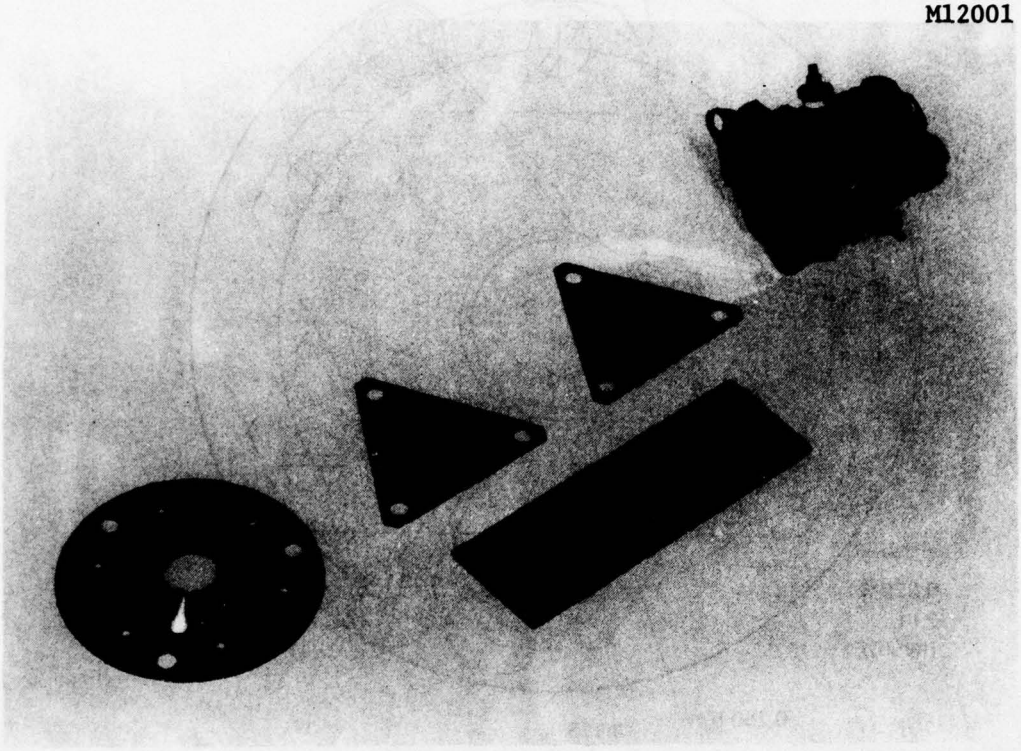

Figure 11. Ion optics photograph, exploded view.

Selection of aperture number, aperture diameter, and grid spacing was based on empirical relations developed for ion thrusters.[10] Beam current I_b and beam voltage V_t are related by

$$I_b = PV_t^{3/2} \text{ (in A)} , \tag{2-1}$$

where

P = perveance (in $A/V^{3/2}$)

$V_t = V_b + V_a$ (in V)

V_a = negative accelerator voltage (in V)

V_b = positive beam voltage (in V)

Perveance for a single aperture and xenon ions can be expressed in the form

$$P_a = \frac{6.8 \times 10^{-9}}{\left(0.336 + \frac{\ell}{d_s}\right)} \text{ (in } A/V^{3/2}) , \tag{2-2}$$

where

$\ell = \ell_g + d_s$

ℓ_g = screen grid to accelerator grid spacing

d_s = screen grid aperture diameter.

Using ℓ_g = 0.05 cm and d_s = 0.15 cm, the Xe ion perveance is $\approx 4.1 \times 10^{-9}$ $A/V^{3/2}$.

Empirically, it has also been established that a minimum accelerator voltage is required to avoid "electron backstreaming," from the neutralizer or downstream plasma, through the optics. The ratio of V_b to total voltage V_t is used to characterize the backstreaming limit:

$$R = \frac{V_b}{V_b + V_a} = \frac{V_b}{V_t} \leq 0.8 . \tag{2-3}$$

Thus, for beam voltages of 1000 V and 2000 V, accelerator voltages of 300 V and 600 V, respectively, were selected.

Total voltages of 1300 V and 2600 V result in beam currents (per aperture) of 0.19 mA and 5.4 mA. Since the ion chamber plasma density is nonuniform radially, these values must be reduced somewhat (about 25%) to obtain an average current capability for a given optics design. With an average beam current capability of about 0.14 A/aperture at 1300 V, seven apertures are needed to obtain a total beam current of 1 mA. At 2600 V, the optics design would support substantially more current than the required 2 mA. Experimental results presented in Section 5 show that these calculations, used in selecting an optics design, were slightly conservative (i.e., the measured perveance was found to be about 4.3×10^{-9} $A/V^{3/2}$).

The neutralizer filaments are mounted from the decel grid using shielded insulators as shown in Figure 10. The filament material is tantalum with yttrium added to reduce brittleness.[11] A filament length of 1.27 cm and a diameter of 0.18 mm was found to combine low heater power, adequate emission, and reasonable operating temperature. Filament location was determined experimentally through coupling tests (which determined beam neutralization versus the filament-to-beam coupling voltage) and through life tests. A downstream position of 0.44 cm from the face of the decel grid and a radial position of 0.64 cm were selected. Details of the experiments related to filament positioning are presented in Ref. 1.

2. Ion Source Body (Ion Chamber)

A drawing of the ion source body is shown in Figure 12; exterior features can be seen in Figure 11. The ion chamber shell has a diameter of 2.4 cm and a length of 3.6 cm. The anode, mounted from the shell with three insulator assemblies, has a diameter of 1.9 cm and a length of 1.8 cm. Both the shell and anode are stainless steel. A ferromagnetic (1018 steel) pole is attached to the optical end of the shell to provide internal magnetic field shaping and a mounting point for the electrode assembly. A flange is also attached to the cathode end of the shell to provide a mounting point for the CIP assembly.

7844-2

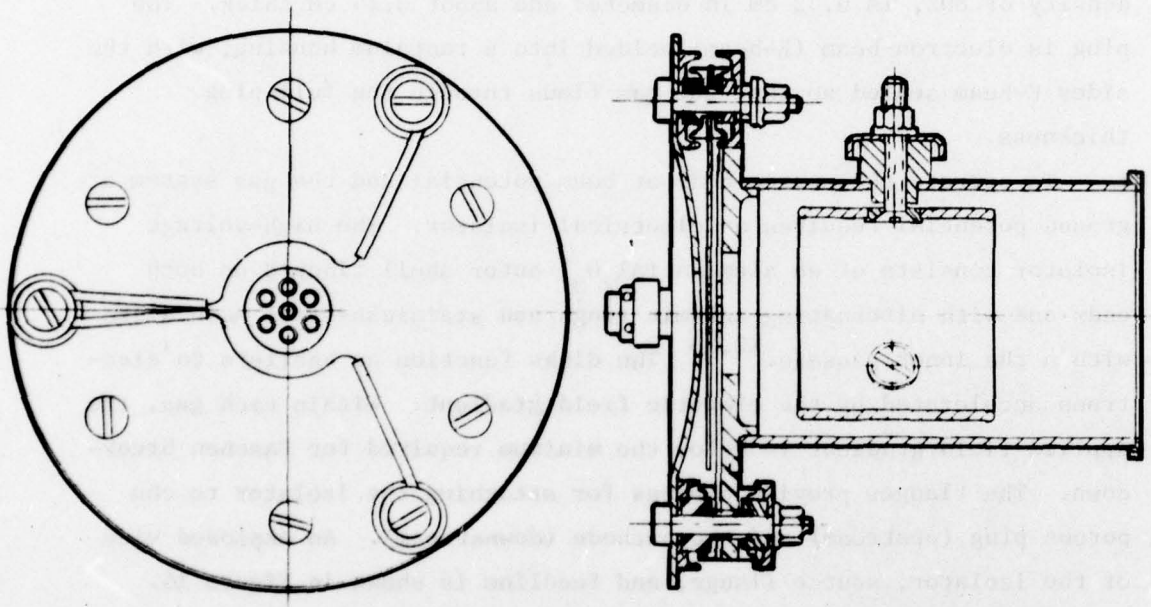

Figure 12. Ion source body drawing.

3. The CIP

The CIP includes several key parts of the SPIBS ion source, including the hollow cathode, keeper electrode, high voltage isolator, and porous plug, as shown in Figure 13. A photograph of the CIP with the keeper removed is shown in Figure 14.

The CIP plug subassembly uses the technology developed for the 8-cm mercury thruster.[12,13] Xenon gas flow rate to the source is determined mainly by the porous plug, which reduces the pressure from the regulated 7 psia to a few Torr. The porous plug, fabricated from tungsten with a density of 80%, is 0.32 cm in diameter and about 0.14 cm thick. The plug is electron-beam (E-beam) welded into a tantalum housing, with the sides E-beam sealed so that the gas flows through the full plug thickness.

To operate the source body at beam potential and the gas system at ground potential requires an electrical isolator. The high-voltage isolator consists of an alumina (Al_2O_3) outer shell flanged on both ends and with alternating ceramic rings and stainless-steel mesh disks within the inner passage.[12,13] The disks function as barriers to electrons accelerated by the electric field gradient. Within each gap, the applied field gradient is below the minimum required for Paschen breakdown. The flanges provide a means for attaching the isolator to the porous plug (upstream) and the cathode (downstream). An exploded view of the isolator, source flange, and feedline is shown in Figure 15.

The structural part of the isolator subassembly is the alumina outer housing. Since alumina can withstand only limited bending or tension loads, the isolator housing is supported by the belleville washer between the upstream flange of the isolator and the enclosure endplate.

The hollow cathode assembly design is illustrated in Figure 16. This cathode is similar to the 5-cm and 8-cm ion-thruster cathodes with a modified mount.[12,13] The cathode assembly includes a reentrant-type mount; this has the effect of increasing the thermal conduction path length and decreasing the thermal loss. As shown in Figure 13, the cathode is mounted to one end of a central passage through the endplate

7835-2

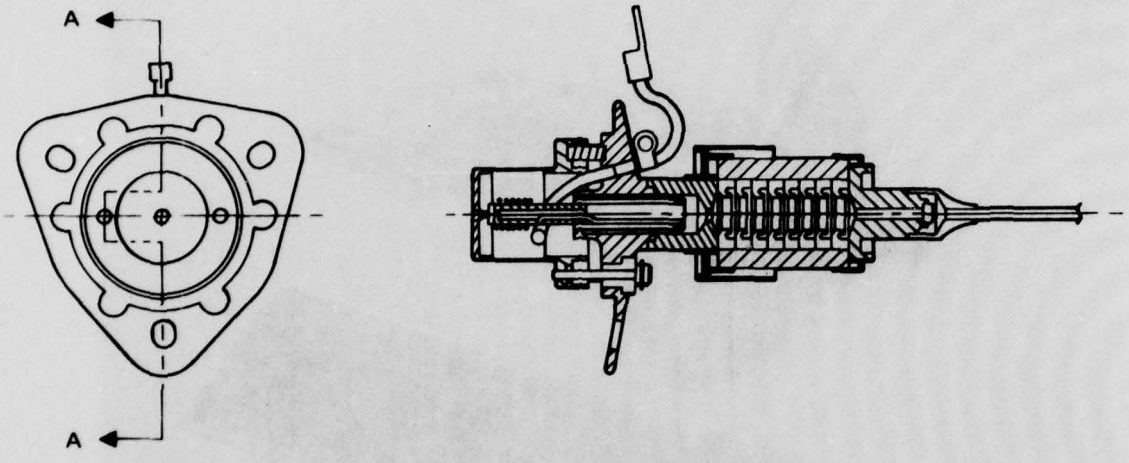

Figure 13. Cathode-isolator-porous plug (CIP) assembly.

M11999

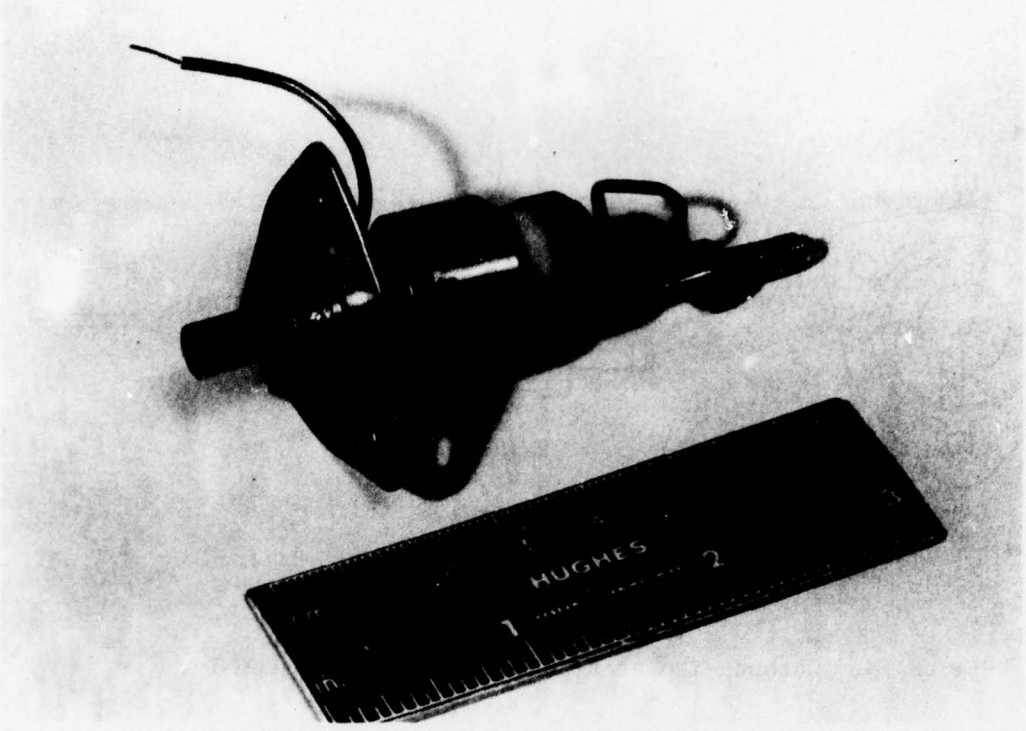

Figure 14. CIP photograph with keeper removed.

M12003

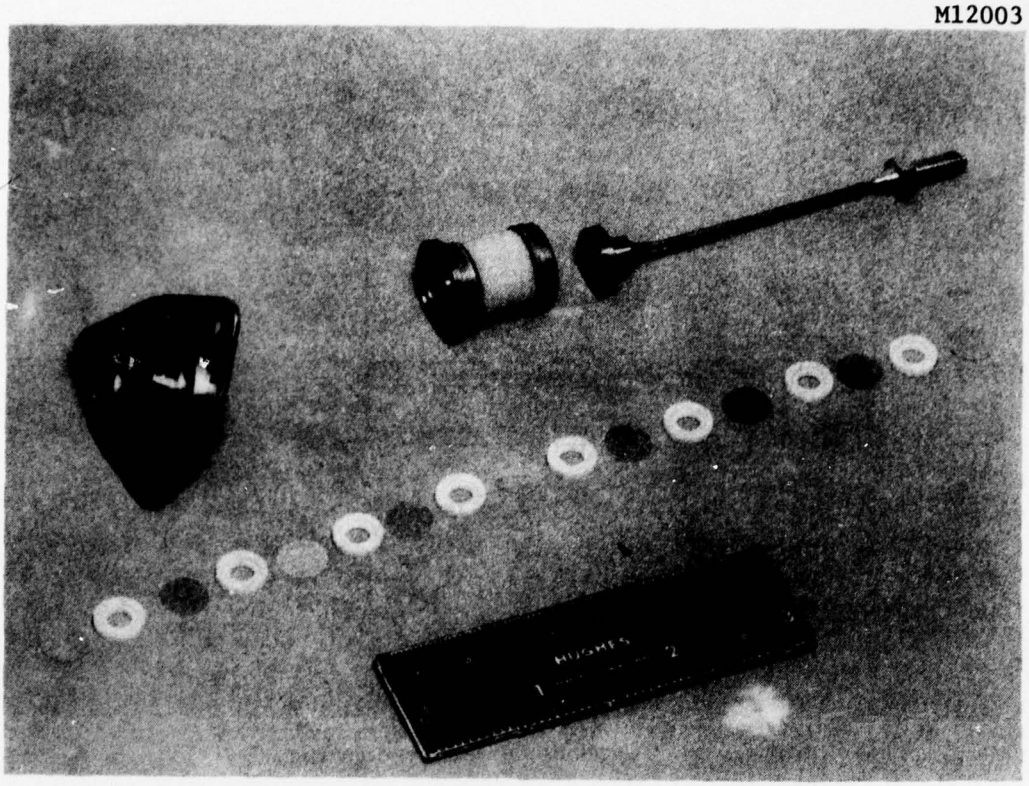

Figure 15. Isolator photograph, exploded view.

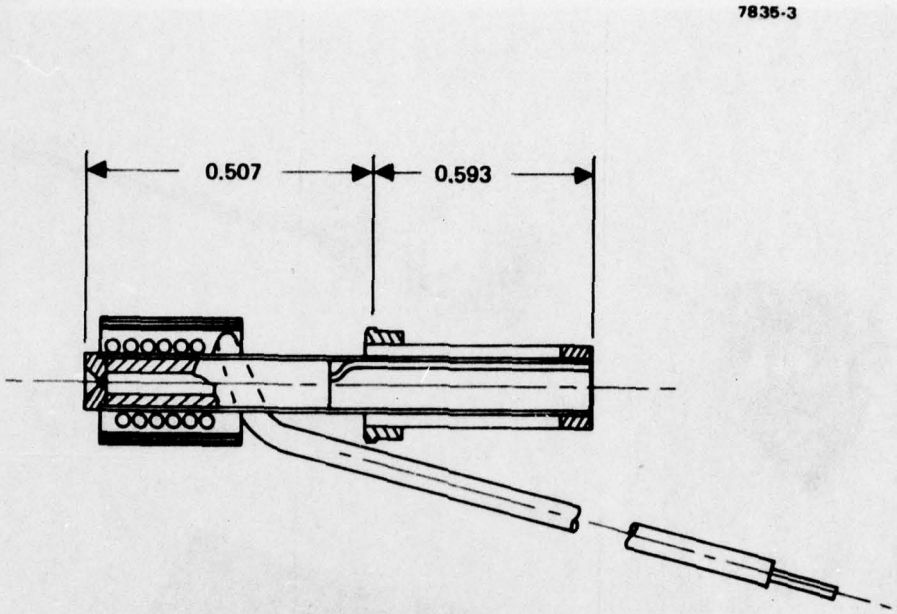

Figure 16. Cathode assembly drawing.

of the source body. The other end of the central passage is attached to the isolator. Photographs of the cathode are shown in Figures 17 and 18. In Figure 17, the keeper and its insulator rings are shown with the cathode. Details of the cathode construction are shown in Figure 18, including the heater, tantalum heat shielding, and the cathode insert.

The cathode tip is fabricated from thoriated tungsten. The orifice throat and chamber is machined using electrical discharge erosion (EDM). The tip is E-beam welded to a tantalum tube having a 3.18-mm diameter, 2.79-cm length, and an 0.25-mm wall thickness. The tantalum mounting tube is 4.00 mm in diameter, 0.13 mm in wall thickness, and about 1.0 cm in length. Spacer rings are used between the feed tube and the mounting tube and between the mounting tube and the endplate. The parts must be carefully held in alignment by fixtures during assembly to provide accurate cathode tip alignment.

To achieve stable and repeatable low-power operation with hollow cathodes, a low work function insert is usually placed inside the cathode tube. The SPIBS cathode insert, which is made of oxide-impregnated porous tungsten, is shown in Figures 19 and 20. It is attached to the cathode tube by four rhenium wires that are brazed to the insert and spot welded to the tube. The wires are attached to the insert before the oxide mixture is put into the tungsten. This approach was selected after an evaluation of rolled tantalum foil inserts and other impregnated configurations.

B. ION SOURCE FABRICATION

To ensure reliable and repeatable ion source performance, an assembly procedure was developed. This procedure identifies all process steps required to fabricate the parts for the source and to assemble it. In conjunction with the detailed drawings, the assembly procedure provides a written record for each source. A copy of the RM-SPIBS assembly record was supplied to AFGL.

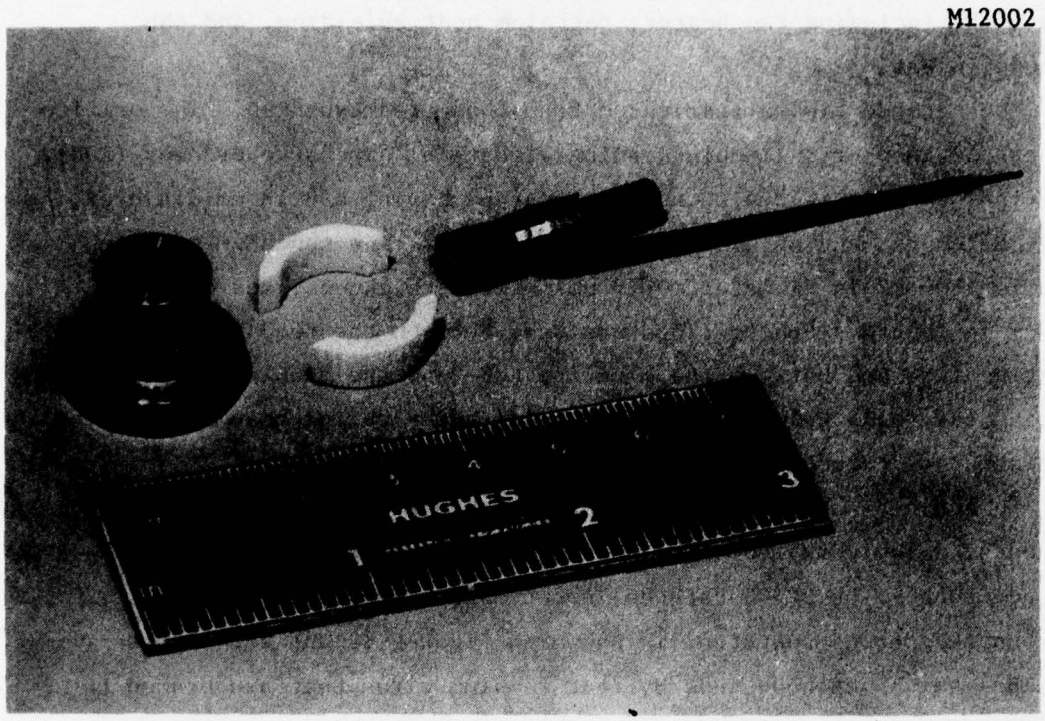

Figure 17. Cathode photography, with keeper and insulator rings.

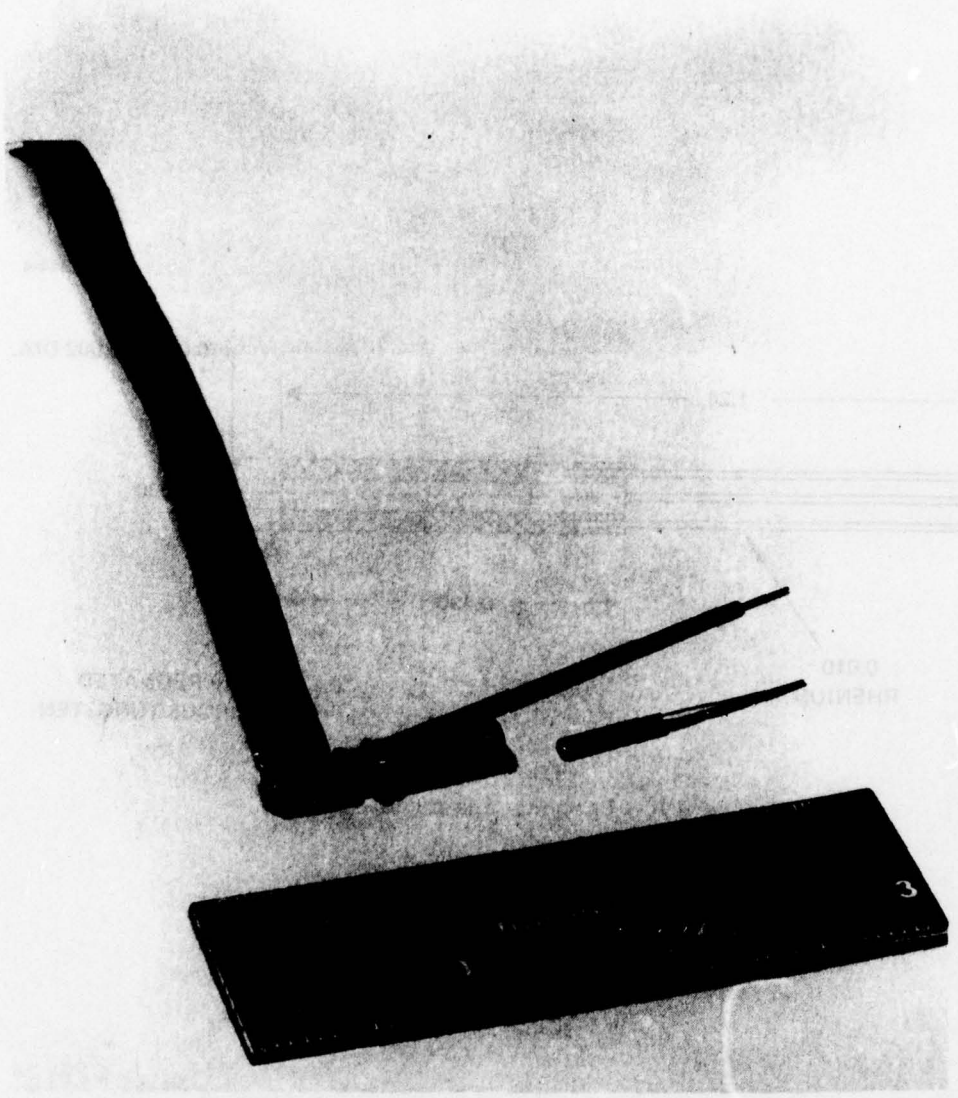

Figure 18. Cathode photograph during assembly.

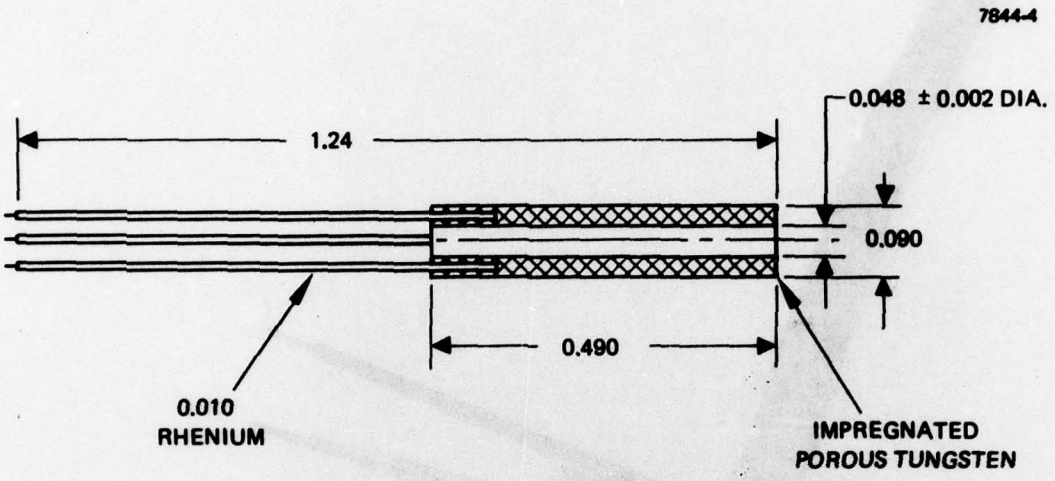

Figure 19. Cathode insert design.

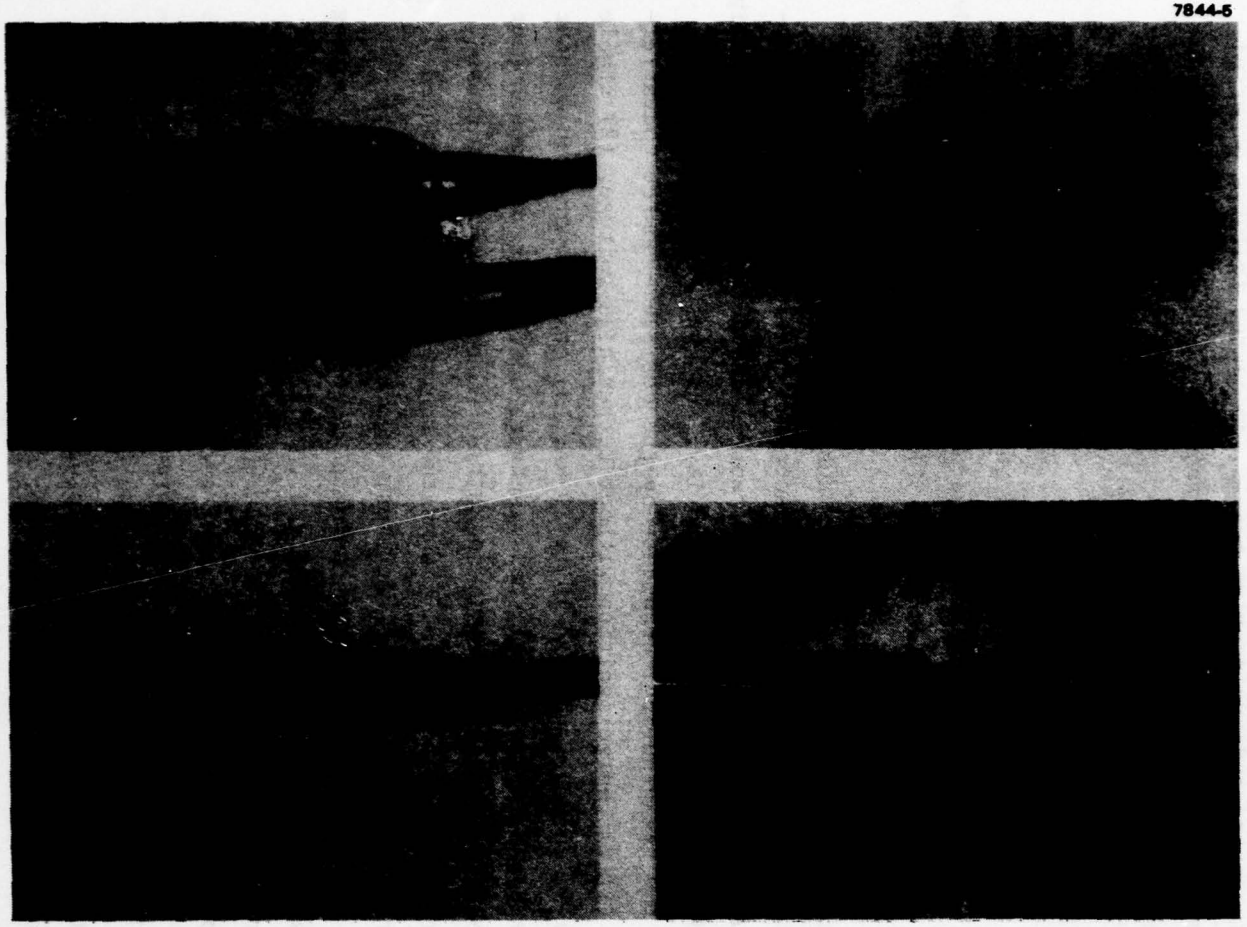

Figure 20. Cathode insert photographs.

During the SPIBS and RM-SPIBS programs, four sources were fabricated. Except for the design deficiencies identified and corrected in the breadboard and engineering models, no source failures occurred due to workmanship. Thus, a reliable procedure was developed for ion source fabrication.

C. ION SOURCE PERFORMANCE

The performance data presented in this section are representative of those obtained with four similar sources (breadboard, EM, flight model, and RM). Specific information on the SPIBS sources is presented in Ref. 1. Rocket model data are discussed in Section 5.

Interpretation and comparison of test results was a significant problem for several reasons. First, source operation, including start-up, discharge stability, and beam-current/discharge-current relationships, was found to depend on "gas system purity." It was generally easy to identify the "high-purity" condition by the desirable source characteristics: (1) discharge ignition without keeper high voltage, (2) stable discharge at currents down to 10 to 20 mA, (3) stable operation without the keeper, and (4) relatively low discharge and keeper voltages. Poor or bad operation was also easily identified by the opposite of these characteristics. Unfortunately, when the source operation produced characteristics between these extremes, the reason was not always obvious, particularly at the beginning of the program. Several testing procedures were eventually established to allow the gas purity factor to be separated from other performance characteristics. Once the "purity problem" was identified, many anomolous results were explained.

The second problem in data interpretation was gas flow rate uncertainty. Initially, a blowdown-type gas system was used for supplying xenon. The breadboard source porous plug required a pressure of 18 to 22 psia to achieve a suitable flowrate. The EM, flight model, and RM sources were designed for about 7 to 8 psia to simplify fabrication. With the blowdown system, flow rates could be estimated after a few

hours of testings. Once regulators (for 7 psia) were obtained, flow rates were not measured, and the pressure was set to produce the desired discharge voltage and beam current.

A third factor in data comparison is source-to-source fabrication differences. Such differences might include screen grid aperture diameter or magnetic field strength. Although care was taken to make each source identical, fabrication tolerances, material variations, and magnet handling introduce some variations.

The fourth factor in data interpretation and comparison was instrumentation. With the current levels involved, voltmeter location in the circuits becomes critical since voltmeters draw current. In addition, tests were performed with both laboratory-type power supplies and metering as well as with SPIBS power processing. Ensuring that the wiring connections were made correctly was a constant concern. In addition, power supply wave forms (60 Hz sinusoidal, or 20 kHz square wave) affect meter response and reading accuracy.

A fifth factor affecting data comparison is the ion source stabilization time. With the relatively low discharge and keeper current levels, cathode activation and ion source thermal time constants are apparently on the order of tens of minutes. Thus, run-to-run comparisons are somewhat dependent on the procedure used to obtain the data.

With these factors in mind, the data scatter observed throughout the test program is not surprising. However, even with these uncertainties, all four sources performed quite similarly. With the technique of adjusting flow rate (i.e., pressure) to obtain the desired discharge voltage, variations due to fabrication tolerances tend to be reduced. Since only a small fraction (1 to 6%) of the gas is converted to ions, minor flow rate variations between sources are not too significant.

1. Ion Optics Performance

Ion optics performance can be characterized by considering perveance and backstreaming. Typical results showing beam current and accelerator current as functions of total extraction voltage are shown

in Figures 21 and 22, respectively. The "perveance limit" line, determined from Figure 22, was taken to be the point at which accelerator current begins to increase as total voltage is decreased. This represents the point at which the beam starts to defocus. The measured perveance was about 4.3×10^{-9} $A/V^{3/2}$, which is in good agreement with the design value.

The curves in Figure 21 are typical of plasma ion sources. As total extraction voltage increases, the electric field at the screen grid penetrates further into the aperture. This penetration increases the area of the plasma sheath at the aperture and provides a larger source of ions for each beamlet. Beam currents below the perveance line are possible but at the sacrifice of higher accelerator current.

Backstreaming results are shown in Figure 23 for two sets of accelerator diameters. The format of beam current versus accelerator voltage is used because backstreaming is indicated by a rise in beam current. For the small aperture diameter (1.02 mm), accelerator voltages from 125 V (1 mA at 1 kV) to 185 V (2 mA at 2 kV) were needed to prevent backstreaming. With the larger aperture (1.52 mm), the minimum voltages increased to about 300 V and 400 V, respectively.

The SPIBS final accelerator aperture diameter was chosen based on tests discussed in Ref. 1. This diameter was determined by grid sputtering considerations. Life tests demonstrated that smaller apertures were "ion machined" to about 1.2 mm. Thus, to avoid depositing the sputtered grid material on the optics, the initial diameter was 1.2 mm.

Accelerator voltage was specified for the power processor design on the basis of Figure 23. To provide for accelerator aperture diameters up to 1.5 mm, the minimum voltage was set at 300 V for a beam voltage of 1 kV. Since the PPA was designed to provide an accelerator voltage directly proportional to beam voltage, an accelerator voltage of about 600 V is obtained with a beam voltage of 2 kV.

2. Ion Chamber Performance

The primary information needed to characterize ion chamber performance is the relationship between beam current and discharge

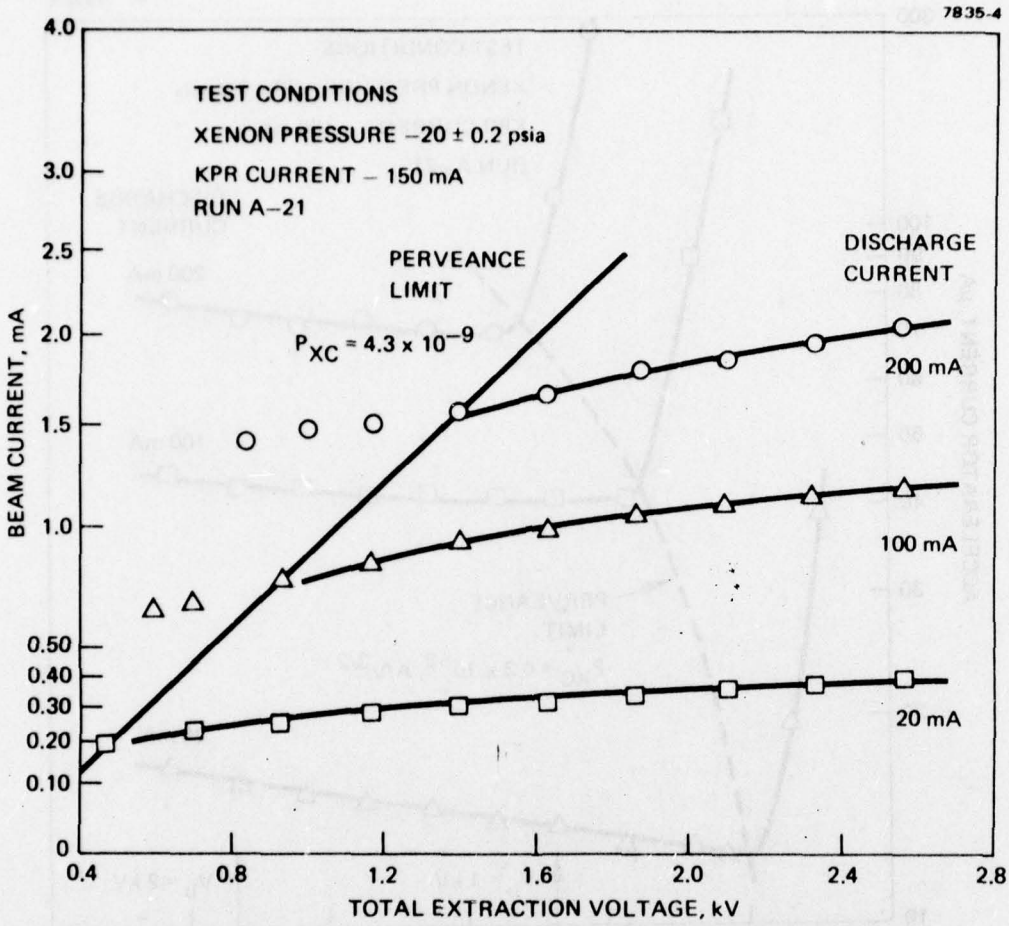

Figure 21. Beam current versus total extraction voltage (typical).

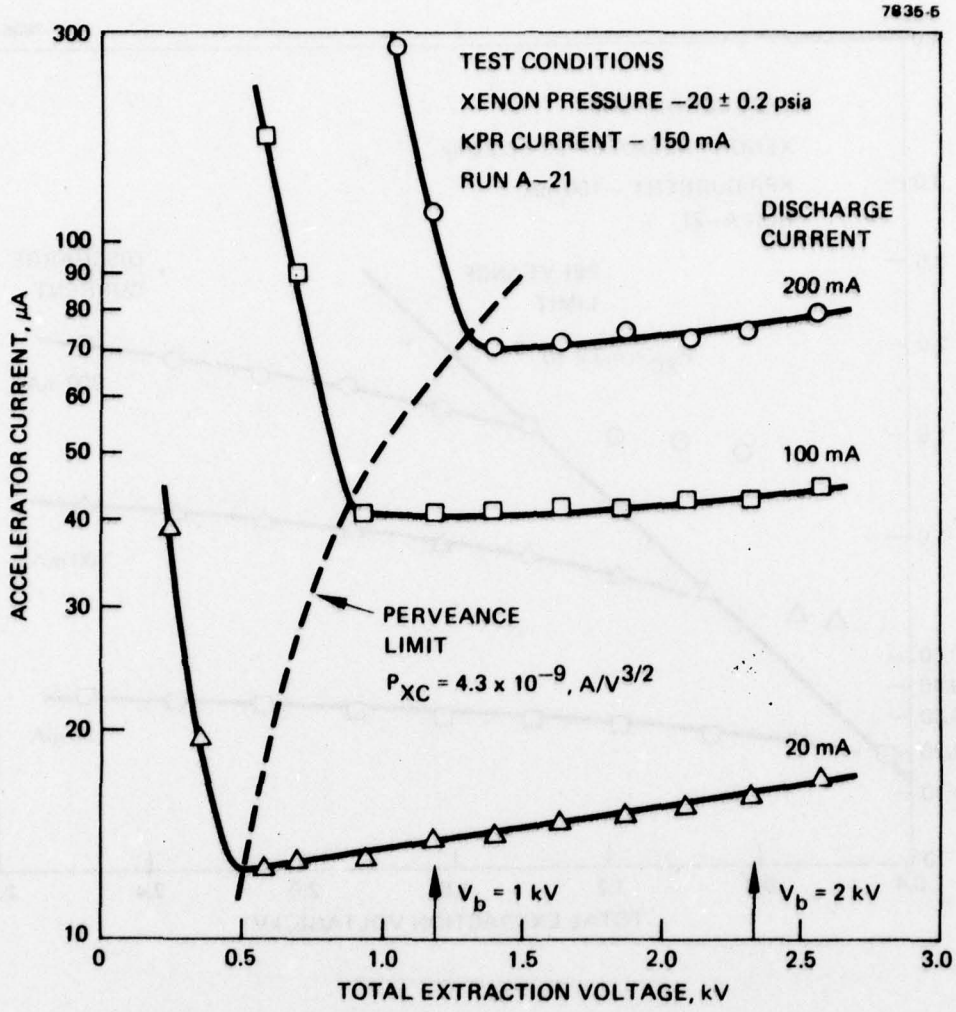

Figure 22. Accelerator current versus total extraction voltage (typical).

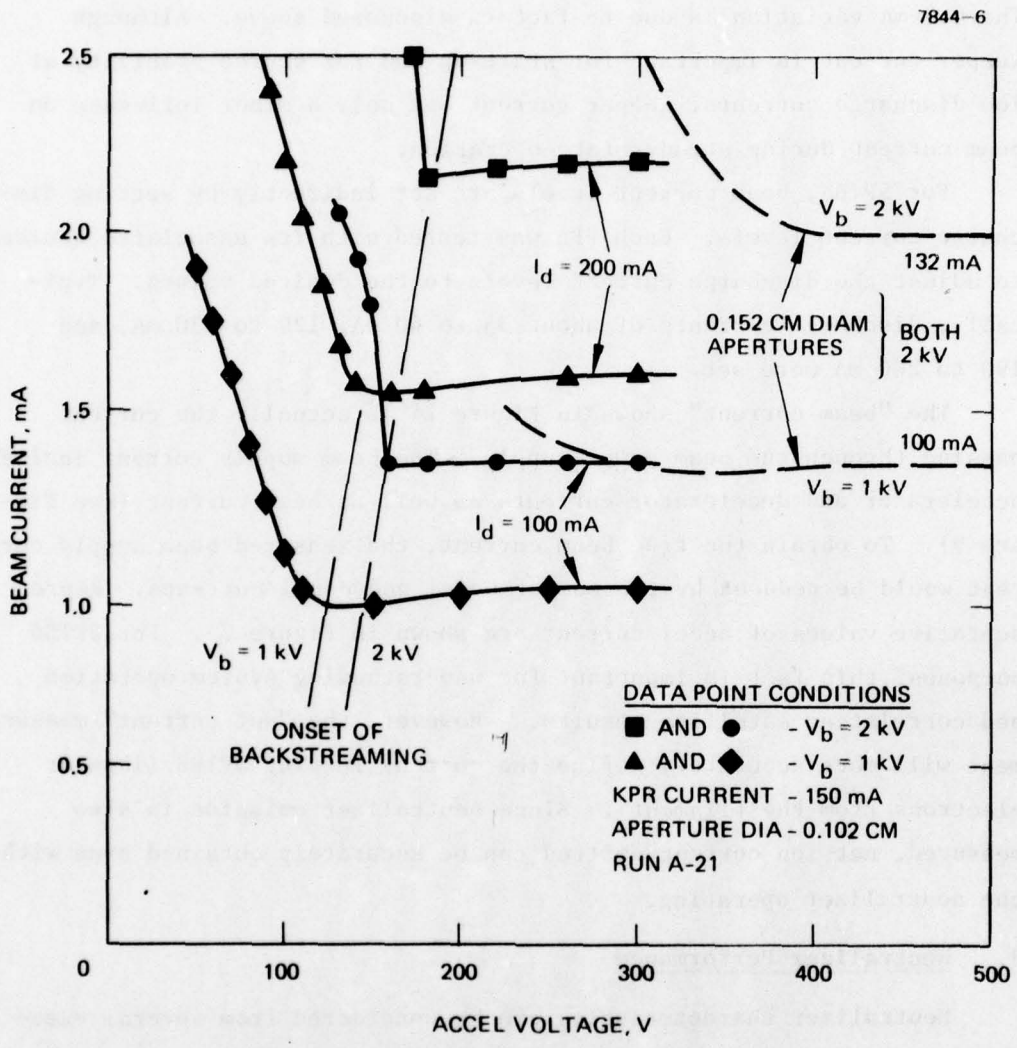

Figure 23. Electron backstreaming characteristics (typical).

current as shown in Figure 24. These data are representative of the four sources tested. Typically, a beam current of 2.0 ±0.2 mA is obtained with a discharge current of 200 mA and a beam voltage of 2 kV. The 0.2-mA variation is due to factors discussed above. Although keeper current is important for start-up and for source stability at low discharge currents, keeper current has only a minor influence on beam current during steady-state operation.

For SPIBS, beam current levels are set indirectly by setting discharge current levels. Each PPA was tested with its associated source to adjust the discharge current levels to the desired values. Typically, discharge currents of about 35 to 40 mA, 120 to 130 mA, and 190 to 200 mA were set.

The "beam current" shown in Figure 24 is actually the current passing through the beam power supply. The beam supply current includes accelerator and decelerator currents as well as beam current (see Figure 9). To obtain the true beam current, the measured beam supply current would be reduced by the sum of accel and decel currents. Representative values of accel current are shown in Figure 25. For SPIBS purposes, this fact is important for understanding system operation and correlating satellite results. However, the "net current" measurement will more accurately define the current leaving SPIBS (ions or electrons from the filament). Since neutralizer emission is also measured, net ion current emitted can be accurately obtained even with the neutralizer operating.

3. Neutralizer Performance

Neutralizer characteristics can be considered from several viewpoints. On the satellite, the primary goal is to provide the ability to eject a positive or neutral (in terms of space charge) beam. Since the beam is coupled to the neutralizer filament when it emits electrons, an additional objective is to bias the satellite relative to space plasma potential by biasing the filament. Without the ion beam it may be possible to eject electrons using the bias supply alone.

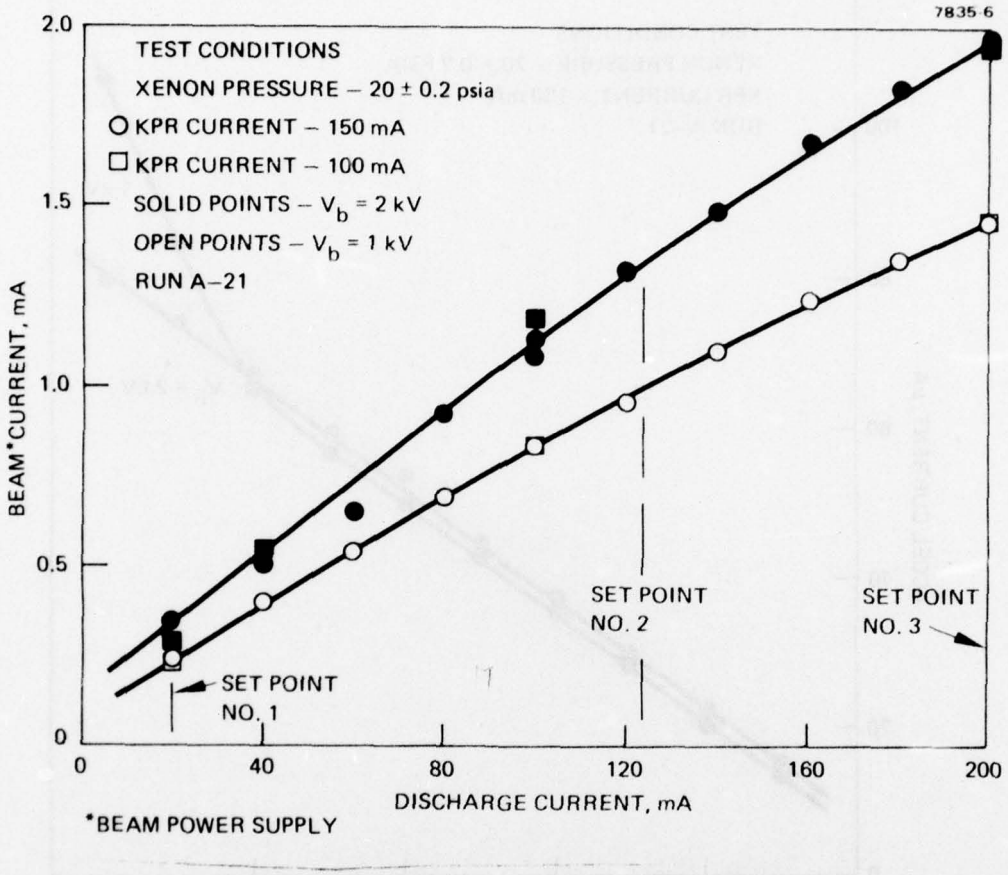

Figure 24. Beam current versus discharge current (typical).

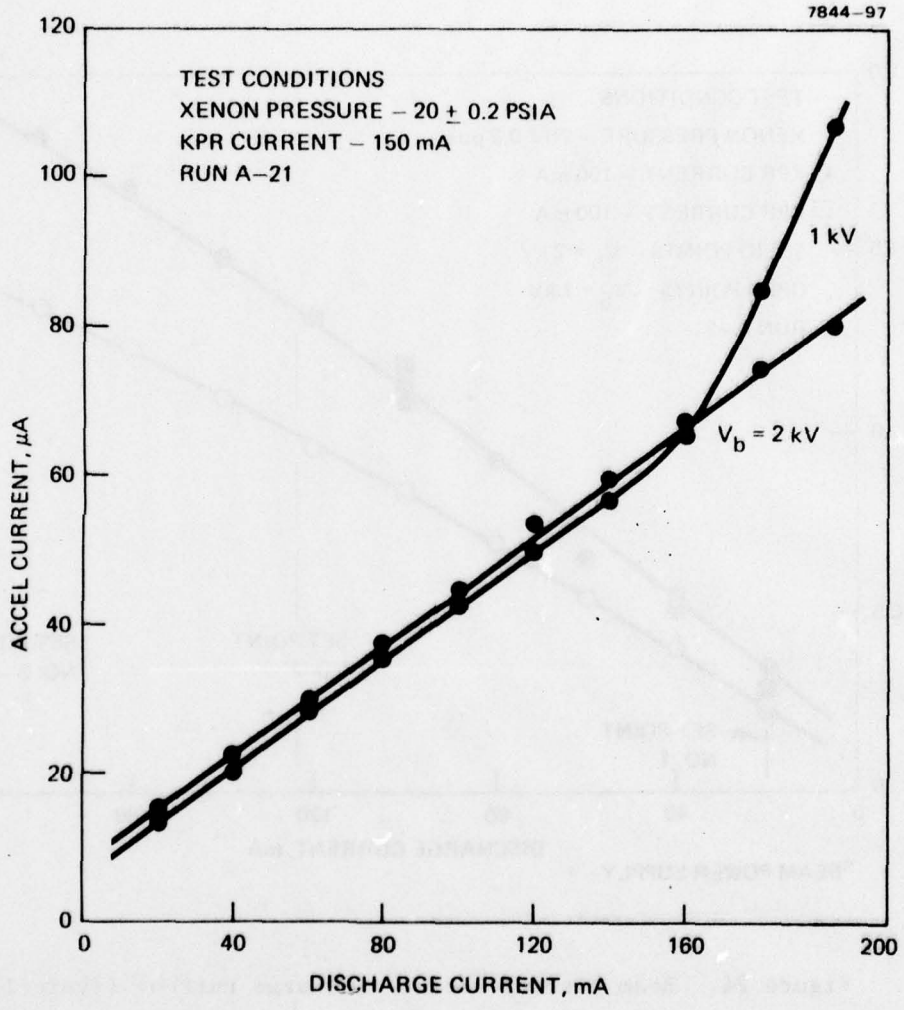

Figure 25. Variation of accel current with discharge current.

Ground tests, without relatively elaborate vacuum facilities, limit the extent to which these various objectives can be tested. The main neutralizer related goal during the SPIBS development was to set current levels to assure full neutralization when desired (i.e., more electrons available from the filament than required for one-to-one neutralization). Electrons not demanded by the ion beam would either not leave the filament or would go to the decel or other local surfaces. Neutralizer emission was not controlled to equal beam current because, in the "neutralizer only" mode, a different control scheme would be needed. In most ground tests, neutralizer emission levels greater than the beam current were commonly obtained with filament to beam potential differences of 10 to 20 V. With the net current electrometer connected (see Figure 9), the filament and the ion beam are tied to ground. In this case, the filament biasing was provided by the bias supply.

The neutralizer heater and emission control loop characteristic is shown in Figure 26. The heater power supply is current limited at a safe level (filaments will operate for short periods at 3 A) that provides adequate emission. Without emission (e.g., if the beam is off) the heater goes to full current. Three emission current set points are set by command along with discharge current levels; two lower neutralizer emissions levels are set separately. When emission reaches the set value, the heater current feedback loop controls to maintain the set emission. For the example shown in Figure 26, the filament provided adequate emission for the four lowest current levels without biasing. However, emission above 1.5 mA was not possible without a few volts of negative bias.

Once the filament was coupled (i.e., with the heater controlling emission), biasing had a range of effects. For the three highest current levels, biasing caused only small reductions in heater power. However, at the lowest emission levels, negative biasing was apparently effective in attracting sufficient ion current to satisfy the emission loop, and the heater turned off. The ion current may have originated in the beam or in the vacuum chamber plasma near the source.

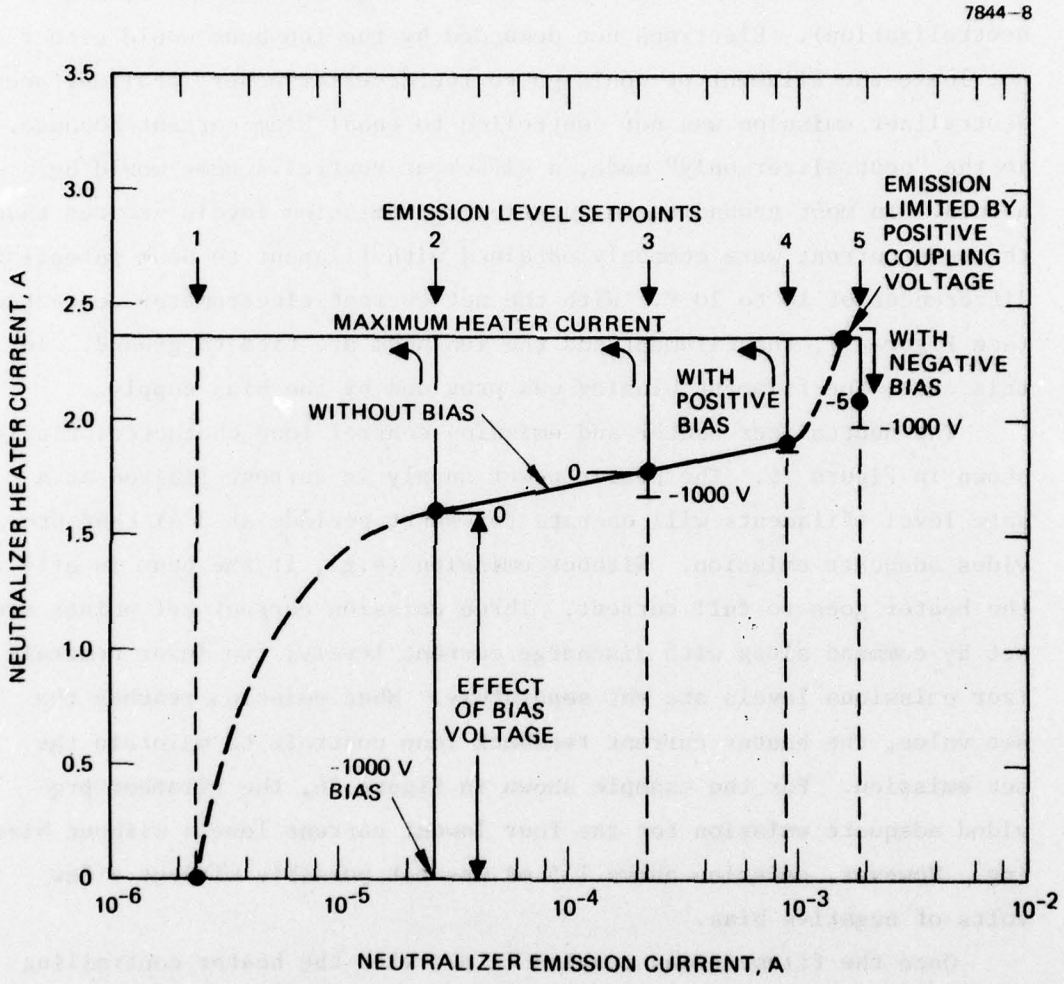

Figure 26. Neutralizer control loop characteristics.

Other examples of neutralizer operation are discussed in Ref. 1. For instance, tests to establish filament position, neutralization capability, and biasing characteristics were performed with a floating power supply arrangement that provided self-biasing. Through manual control of the neutralizer heater, characteristics of the type shown in Figure 27 were generated. A movable collector was placed in front of the source to provide a relative measure of beam potential. When sufficient electron emission is provided, both the power supply floating potential and the collector potential are reduced to near zero. Tests of this type were helpful in optimizing filament position. Endurance tests were later used to verify that the neutralizer position was satisfactory.

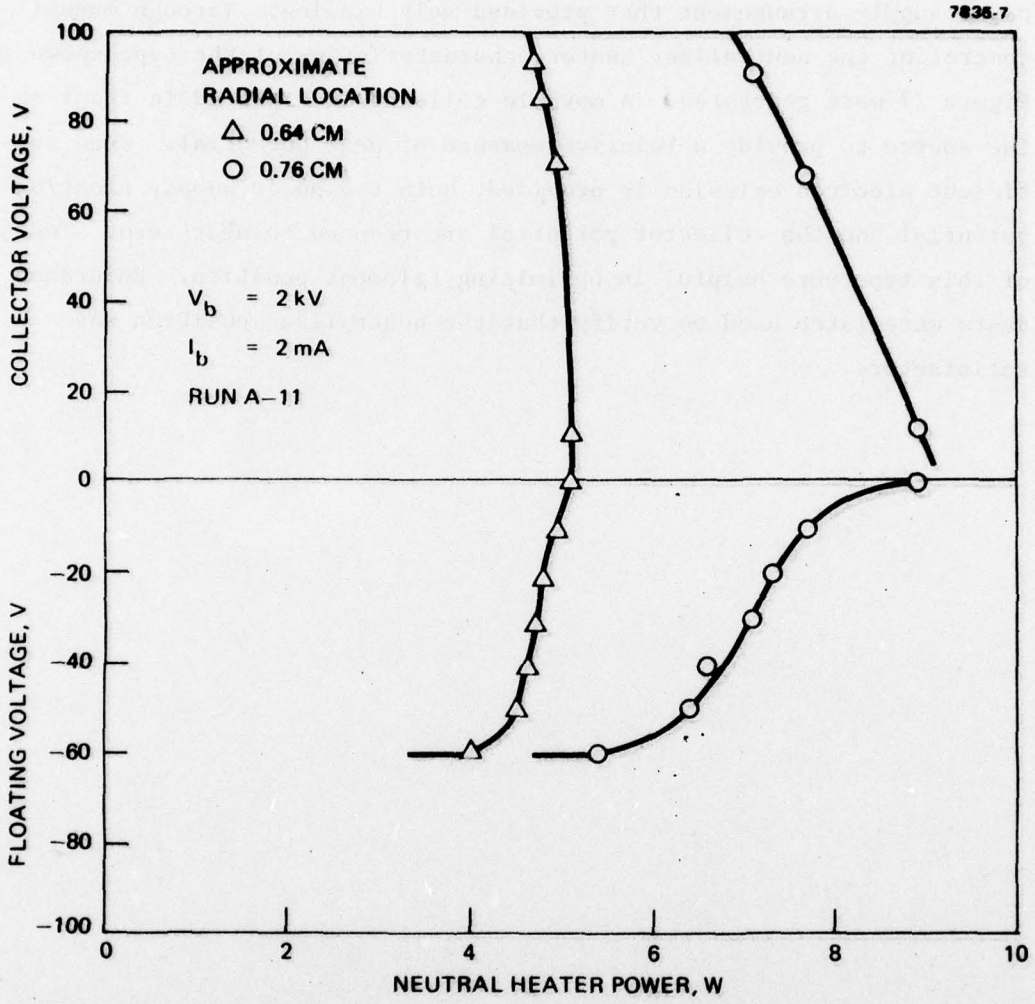

Figure 27. Example of neutralizer coupling using self-biasing.

SECTION 3

EXPELLANT ASSEMBLY

The SPIBS expellant assembly (EA) provides xenon storage, pressure regulation, and pressure monitoring. An assembly drawing is shown in Figure 28. The components in this assembly were selected on the basis of availability, flight qualifiability, and cost. Several options were considered but were generally more expensive and/or required development.

A photograph of a typical EA is presented in Figure 29; another view is shown in Figure 6. The EA is mounted to the system structure with clamps around the reservoir and over the regulator. The regulator outlet is connected to the source with 1.5-mm-diameter stainless-steel tubing and Swagelock fittings.

A. RESERVOIR SUBASSEMBLY

The reservoir is a Department of Transportation (DOT) rated commercial aircraft part. When filled to 800 psi, this reservoir contains about 50 standard liters of xenon. At the design flow rate, this will provide about 1500 hr of source operation. As seen in Figures 28 and 29, a fitting is attached to the reservoir. This fitting contains a fill valve (Schrader type) and a pressure transducer. For xenon filling, the reservoir, fill fitting, and latching valve are shipped as a unit to the gas supplier.

B. RESERVOIR

The reservoir is manufactured using AISI 4130 steel and a spinning process. Although a significant fraction of the SPIBS mass is associated with the reservoir (about 9% empty, 12% filled), the availability of a rated pressure vessel was the main factor in its selection. Other vessels or a lightened version of the existing part could have been obtained but only at a significant cost for DOT rating.

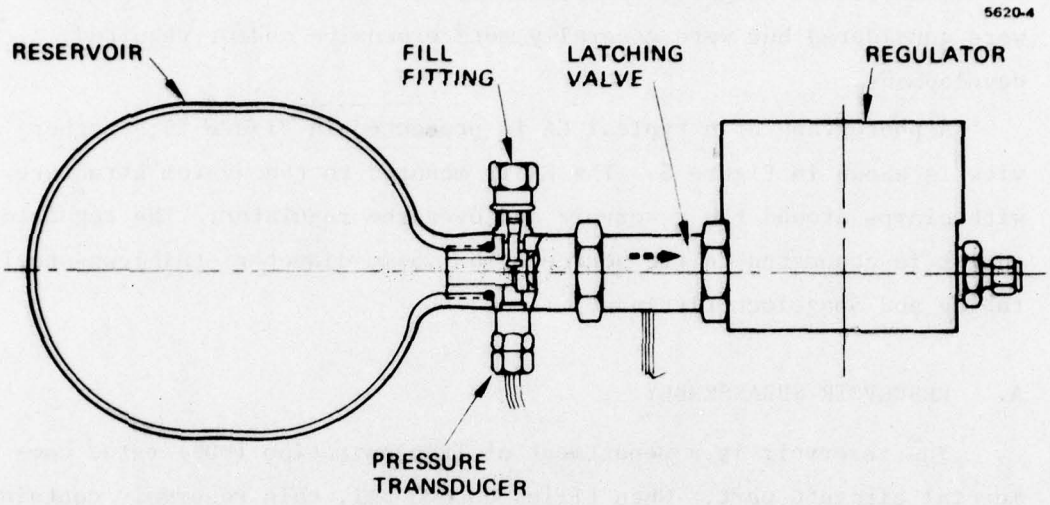

Figure 28. Expellant assembly layout drawing.

M11951

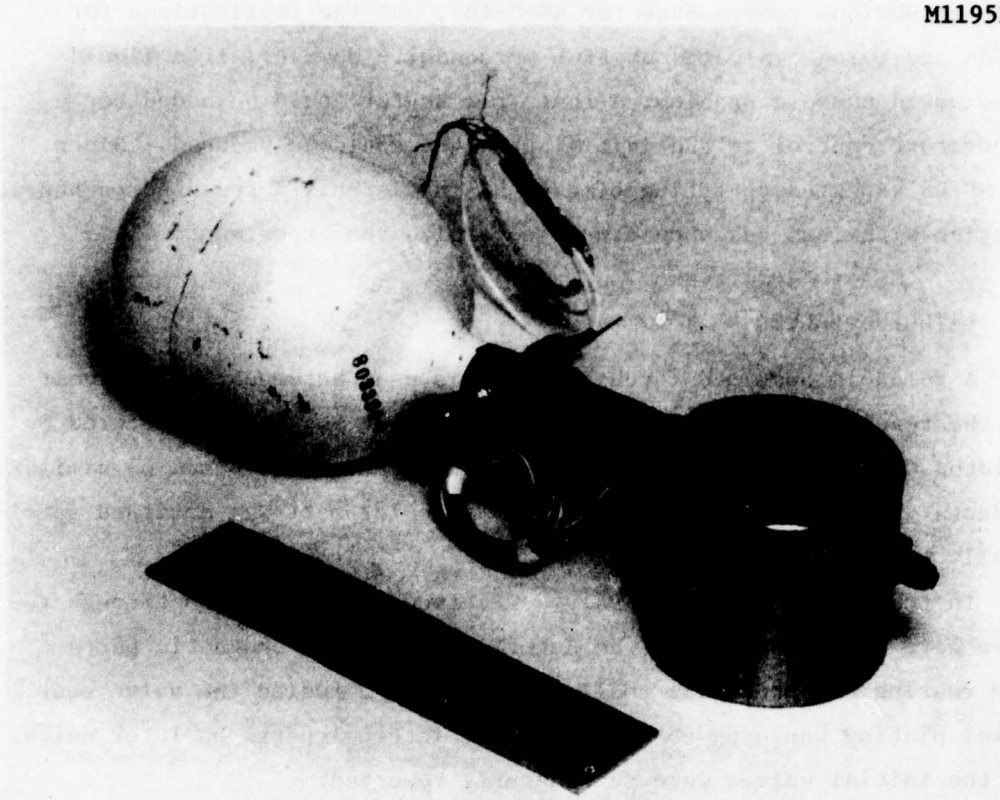

Figure 29. Expellant assembly photograph.

Xenon compressibility characteristics do not obey the ideal gas law. At the design pressure of 800 psi, a fraction of the xenon will be a liquid at temperatures below about 17°C. This characteristic is of no serious consequence for RM-SPIBS, but the implications for SCATHA are being evaluated by AFGL personnel. However, if a liquid phase would cause a problem, a reservoir heater could be added for temperature control or the initial pressure could be reduced. Since the SPIBS expected operating time on SCATHA is only a few hundred hours, starting with less gas should not jeopardize the experiment.

C. LATCHING VALVE

A solenoid-operated latching valve is used between the reservoir and the regulator. This valve, shown in Figure 30, is manufactured by Carleton Controls Corp. Although the valve design was based on similar products developed by Carleton, this particular part was designed specifically for the SPIBS applications.

In tests with the first valves received, several leaks through the valve were experienced. It was determined that ferromagnetic parts were rusting and producing small particles that fouled the valve seat. Nickel plating was used to protect these internal parts on later units, and the initial valves were subsequently reworked.

Valve operation requires a 100 ms current pulse of about 1 A at 28 V to open and about 0.1 A to close. The higher opening power is required to overcome launch load restraints on the pintle. A single solenoid winding is used and the current directions are simply reversed between opening and closing.

D. PRESSURE REGULATOR

A photograph of the Carleton Controls regulator is shown in Figure 31. This is an aneroid-type regulator using a sealed bellows movement. Outlet pressure can be adjusted simply over a range of about 5 to 10 psia to match the flow impedance characteristics of the ion source porous plug. Once adjusted, accurate regulation is obtained

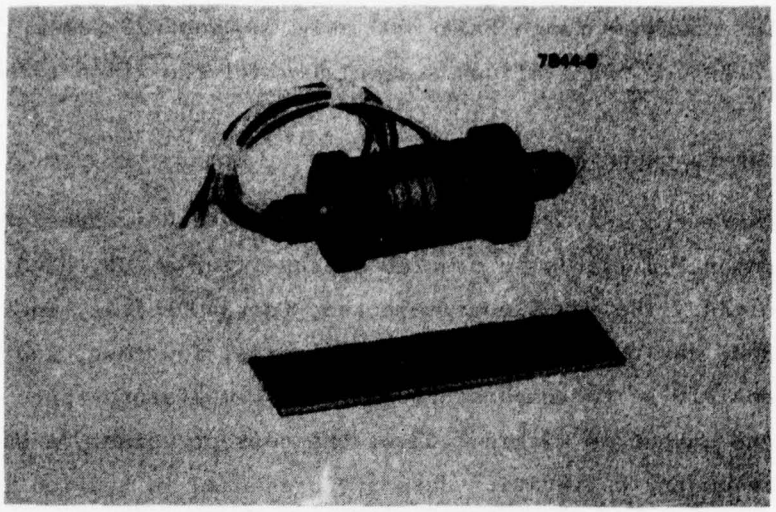

Figure 30. Latching valve photograph.

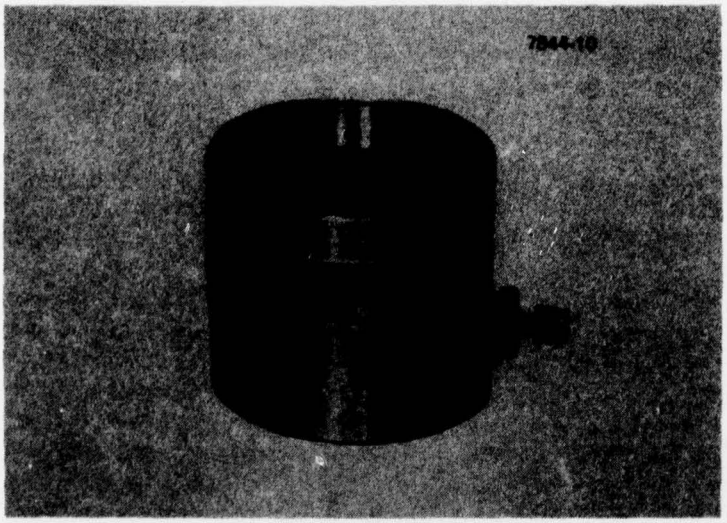

Figure 31. Pressure regulator photograph.

over an inlet pressure range from 1000 psig to about 20 psia. This wide inlet pressure range allows essentially all the xenon to be used.

E. PRESSURE TRANSDUCER

A pressure transducer is used to monitor reservoir pressure. Since this measurement is mainly to provide status information, high accuracy is not required. The transducer selected, Entran Devices, Inc., P/N EPS-1032-1500, has the advantages of small size, low cost, and reasonably low sensitivity to temperature. Over a temperature range of -40 to +80°C, the output is within ±10% of the correct value. A calibration curve and telemetry calibration data are presented in Section 7.

SECTION 4

POWER PROCESSOR ASSEMBLY

The function of the PPA is to supply power to and control the ion source, operate the expellant valve, provide telemetry data, and accept commands. This section describes the design implemented to meet the requirements discussed in previous sections.

A. ELECTRICAL DESIGN

A functional block diagram of the PPA, shown in Figure 32, indicates the general power processing technique. Input power is first regulated at 21 Vdc. A 20 to 25 kHz square wave free running inverter then produces 42 Vac rms for each power supply. Saturable reaction-type power supplies are generally used.

A major feature of this design is the achievement of electrical isolation between the input power lines, the command lines, telemetry, and the outputs of the various supplies. The isolation of the command lines is obtained by using relays. The relay coils provide electrical isolation, and magnetic latching provides nonvolatile storage of the received commands. The isolation between input, output, and the telemetry lines is achieved by using transformer isolation. Each individual supply has an output transformer and, where required, includes isolated voltage sense windings and a current transformer on the primary for voltage and current telemetry, respectively.

The discharge, neutralizer heater, cathode keeper, and accelerator supplies are fixed setpoint supplies and are saturable reactor current limited for short-circuit protection. The beam and cathode heater supplies use saturable reactors for both controllability and current limiting. The neutralizer bias supply is transistor regulated. The line regulator is a "buck" switching regulator that converts the unregulated 24 to 32 V input to a regulated 21 Vdc output. An input filter is

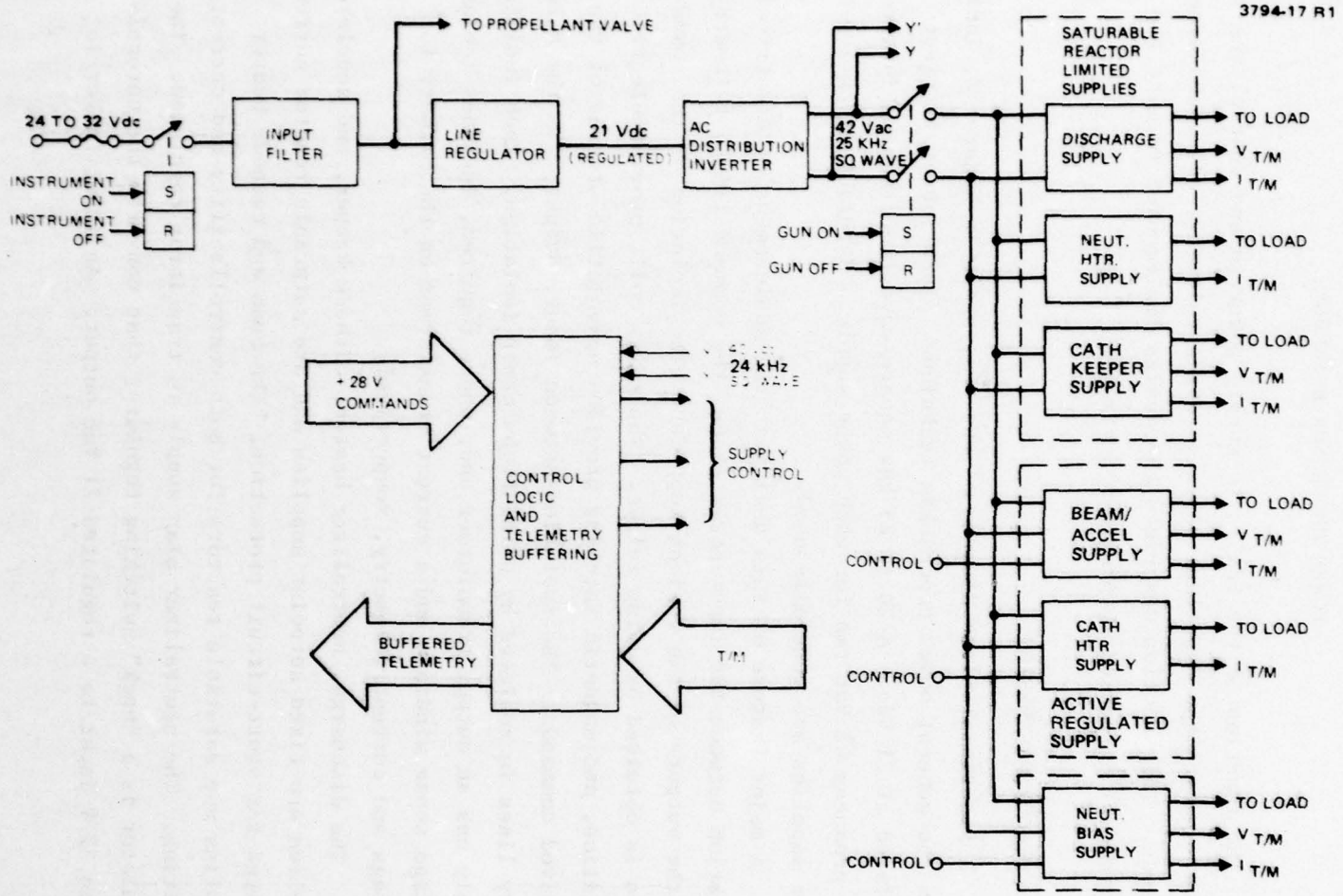

Figure 32. PPA functional block diagram.

required to prevent the ripple current generated by the line regulator from appearing on the input power bus lines.

1. Line Regulator and AC Inverter

A block diagram of the line regulator is shown in Figure 33. A switching regulator was chosen for this application to achieve the desired regulation with maximum efficiency. This regulator operates over an input range of 24 to 32 Vdc and provides a regulated 21 Vdc power output for the ac distribution inverter. Preregulation of the bus power assures that the ac inverter output will be a constant amplitude square wave as required by the power supply saturable reactors.

The line filter will attenuate the ripple current produced by the switching regulator. The main requirements for the input filter are to be stable when a negative resistance device is connected to its output and to adequately reduce the ripple current returning to the power source.

An error amplifier compares the 21 V output with a reference and furnishes an error signal to the comparator. The comparator compares the output of the error amplifier with a ramp voltage supplied by the ramp generator. The comparator output is a pulse width modulated wave that turns on and off the drive to the NPN power transistor switch. The input of the ramp generator is fed back from the output of the ac distribution inverter. Hence, the switching regulator and ac distribution inverter operate at the same frequency.

The ac distribution inverter receives regulated 21 Vdc from the line regulator and converts it to a square wave, 42 Vac rms for use by the power supplies. The block diagram for the ac distribution inverter is shown in Figure 34. The 21 Vdc is sent to the primary center tap of the output power auto transformer. A pair of push-pull power transistors are connected to the two legs of the primary of the output power transformer and are driven by a square wave oscillator.

The schematic of the line regulator and ac inverter is shown in Figure 35 (drawing 1028500). The error amplifier AR2 compares the reference voltage created by Zener diode VR1 to a voltage on a resistor R40,

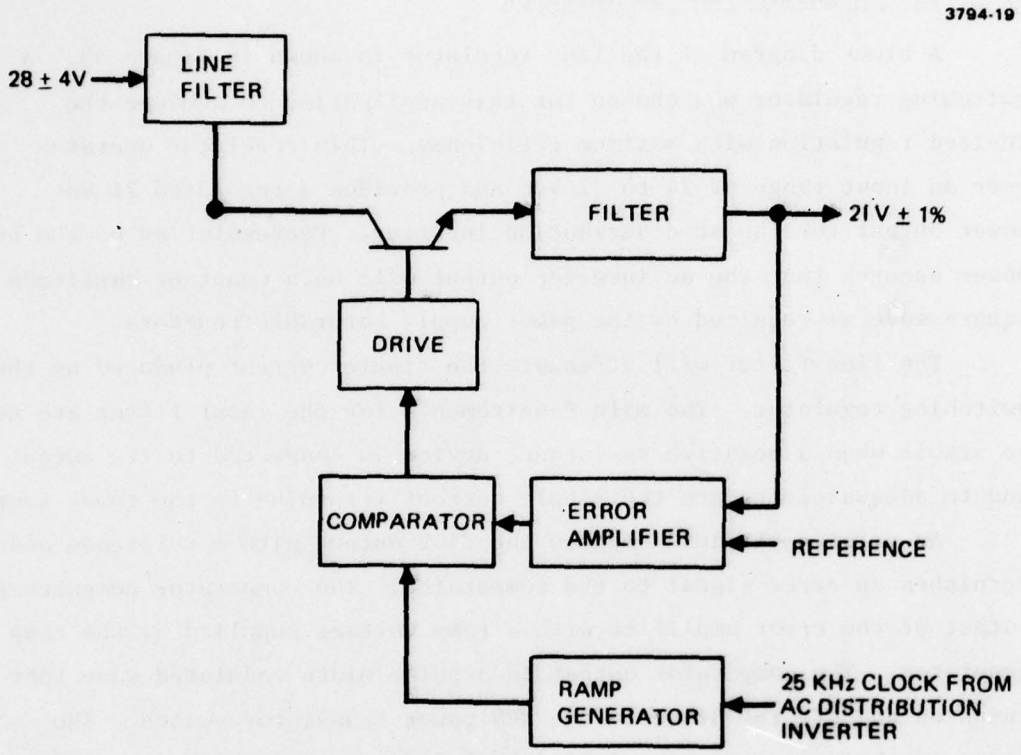

Figure 33. Line regulator block diagram.

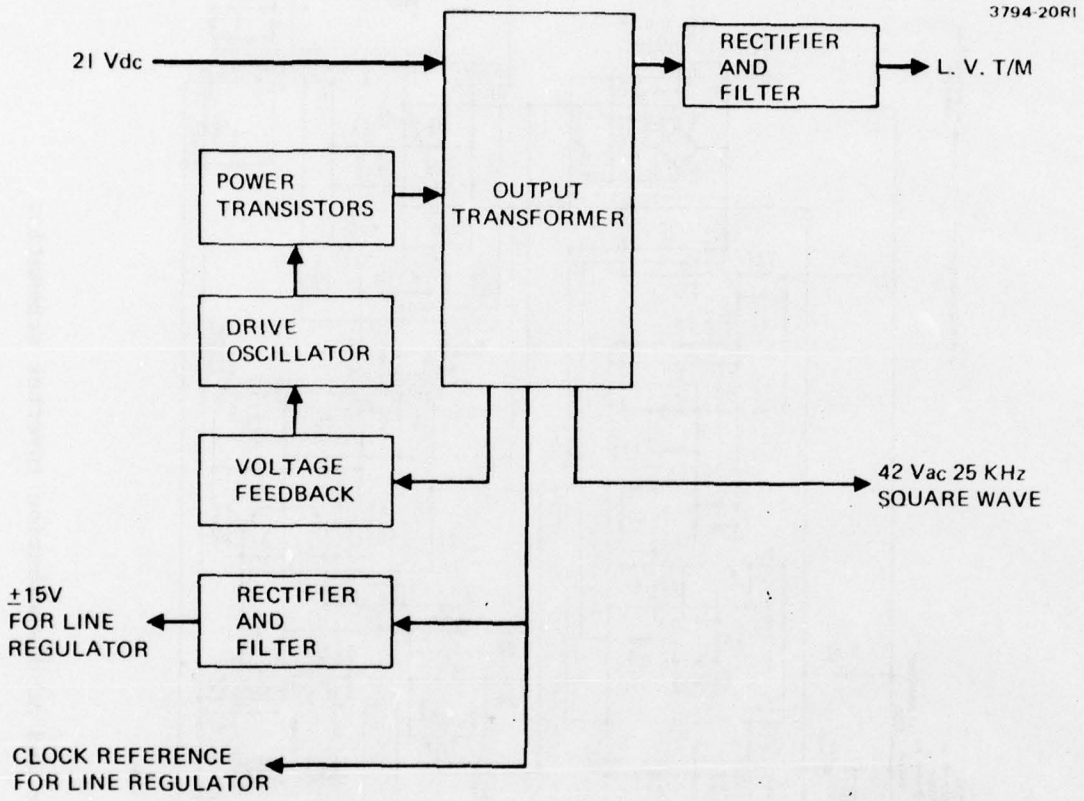

Figure 34. AC distribution inverter block diagram.

THIS PAGE IS BEST QUALITY PRACTICABLE
FROM COPY FURNISHED TO DDC

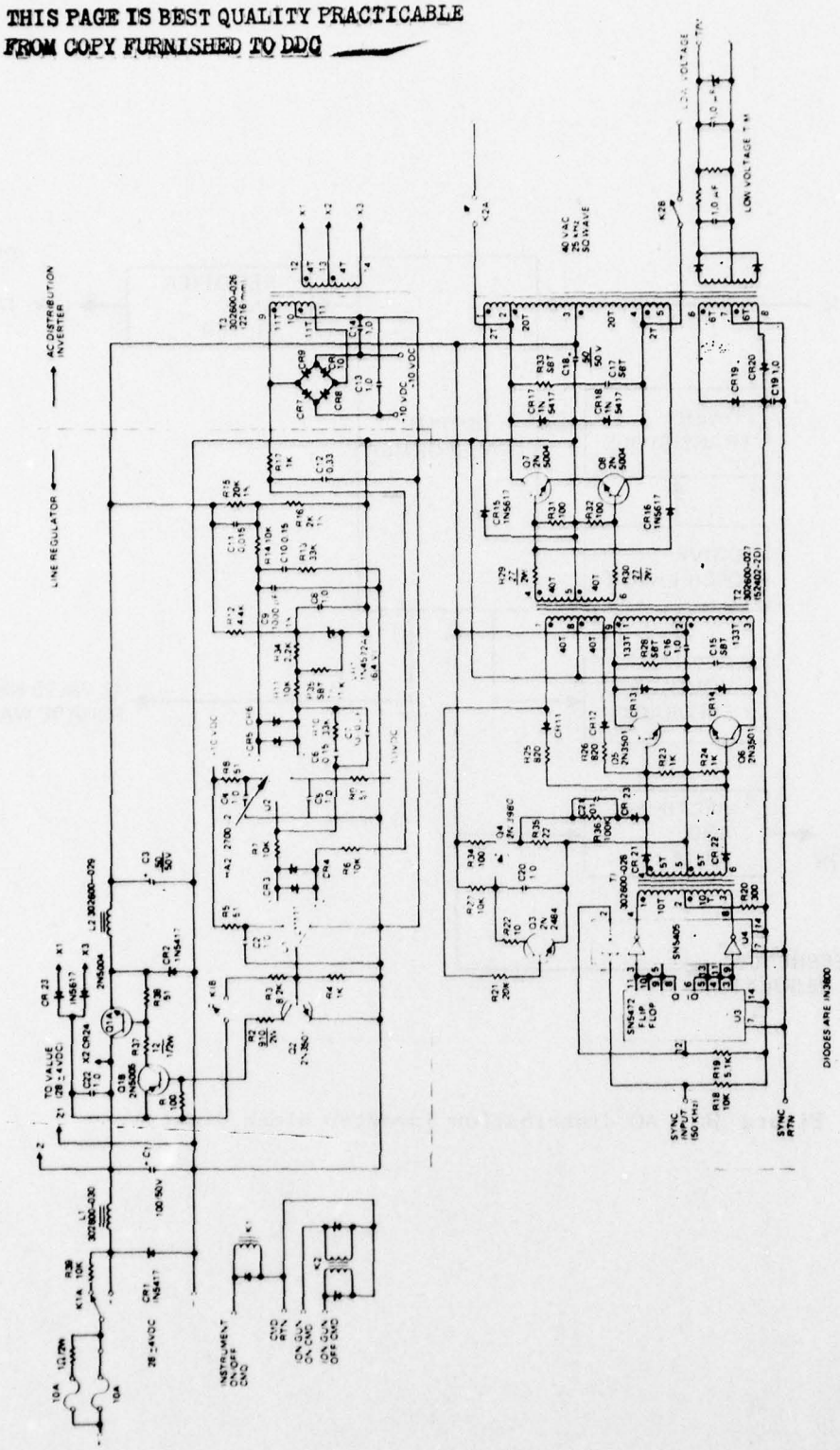

Figure 35. Line regulator and AC distribution inverter schematic.

which is a function of the output voltage. The ramp generator is comprised of resistor R41 and capacitor C16. This network produces a ramp voltage by integrating the clock reference square wave which is supplied from the ac distribution inverter. The comparator AR1 compares the output of the error amplifier AR2 to the voltage ramp on capacitor C16. The comparator turns transistor Q2 on and off which, in turn, turns transistors Q9 and Q1 on and off in a pulse width controlled fashion.

The connections of Q9 and Q1 shown in Figure 35 allow Q1 to saturate. Inductor L2 and capacitors C6 and C19 comprise the filter which averages the pulsewidth controlled output of Q1 to obtain 21 Vdc. Diode CR10 is a commutating diode which furnishes a path for the current in inductor L2 when transistor Q1 turns off.

Resistor R5 is the oscillator starting resistor. It causes current to flow into the base of transistor Q5 or Q6. For example, the resistor could cause current to flow into the base of transistor Q5 causing it to turn on. Transistor Q5 will remain on because transformer T2 is phased so that positive feedback will occur. After several volt-seconds, as determined by the windings on T2, T2 will saturate, Q5 will turn off, and Q6 will turn on. This type of oscillator is basically a Royer circuit.

2. Screen/Accel Supply

The block diagram for the combined screen and accel supplies is shown in Figure 36. Since the output windings of screen and accel supplies are common to one output transformer, the output T/M winding (also on the same transformer) is representative of either the screen or accel output voltages. Output current T/M for both supplies is isolated by individual output transformers.

The block labeled "control electronics" accepts level I or level II command pulses which set the screen and accel output levels at +1000 or +2000 Vdc and -300 or -600 Vac, respectively. The relay shown in the primary winding of the output transformer turns both supplies off when receiving *screen/accel off* command.

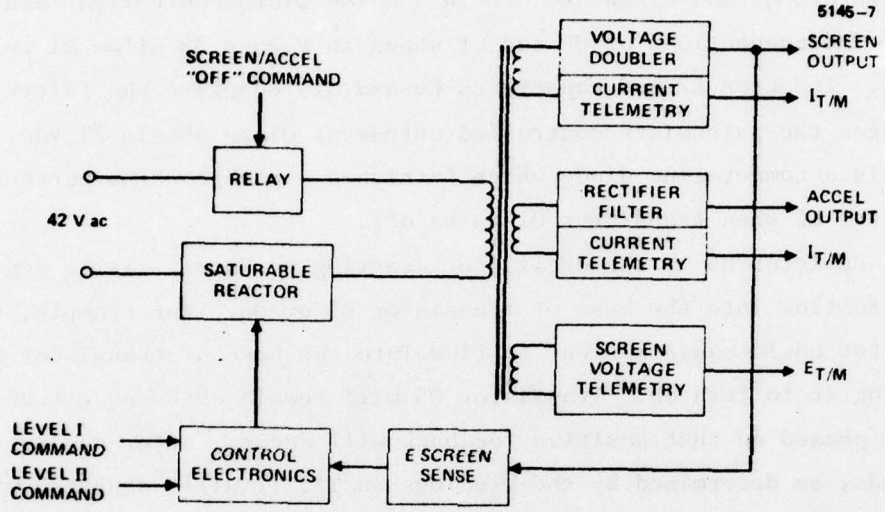

Figure 36. Screen/accel supply block diagram.

A schematic of the combined screen and accel supplies is shown in Figure 37 (drawing 1028190). The output voltages of the screen and accel supply are derived from two isolated windings of output transformer T-1. In this configuration, the screen and accel output voltages both vary as the primary input voltage of T1 is varied.

A full wave voltage doubler consisting of CR3, CR6, C3, and C4 constitutes the output circuit of the screen supply. An identical voltage doubler circuit, consisting of CR8, CR10, C5, and C7, is employed in the accel supply. The output voltage of the screen supply is sensed through a voltage divider (R13 through R33) and compared with a reference voltage established by Zener diode VR2 at the inputs of error amplifier AR1. The output of AR1 provides base drive for transistor Q1 which sets the control current level of MA1 (saturable reactor 1). MA1 provides series current regulation to the primary winding of T1. The amount of primary current flowing in each half cycle of the input wave is limited by the conduction level of Q1 and the turns ratio between the gate and control windings of MA1. This type of control regulation has the advantage of current limiting during short circuit conditions.

The two output levels of screen and accel supplies are controlled by relay K1 (magnetic latching). Level I command (screen:1000 Vdc; accel:-300 Vdc) initiates contact closure of K1, which completes the circuit of the reference voltage divider R7 and R53 and reduces the reference voltage to AR1. Level II command (screen:2000 Vdc; accel: -600 Vdc) restores the reference to the Zener voltage level.

Voltage telemetry is provided by an auxiliary winding on transformer T1. The output is full wave rectified by CR12, CR13, filtered by C20 and C6, and scaled with voltage divider R9 and R11 to provide 0 to 5 Vdc. Zener diode VR5 is used to limit the T/M output to 6.2 Vdc.

Current telemetry for the screen and accel supplies is implemented with identical circuits, each of which provides 0 to 5 Vdc floating outputs. Because the circuits are identical, only the screen current T/M will be discussed. The gain of amplifier AR2 is adjusted to provide a 0 to 5 Vdc output from an input voltage signal developed across current

THIS PAGE IS BEST QUALITY PRACTICABLE
FROM COPY FURNISHED TO DDC

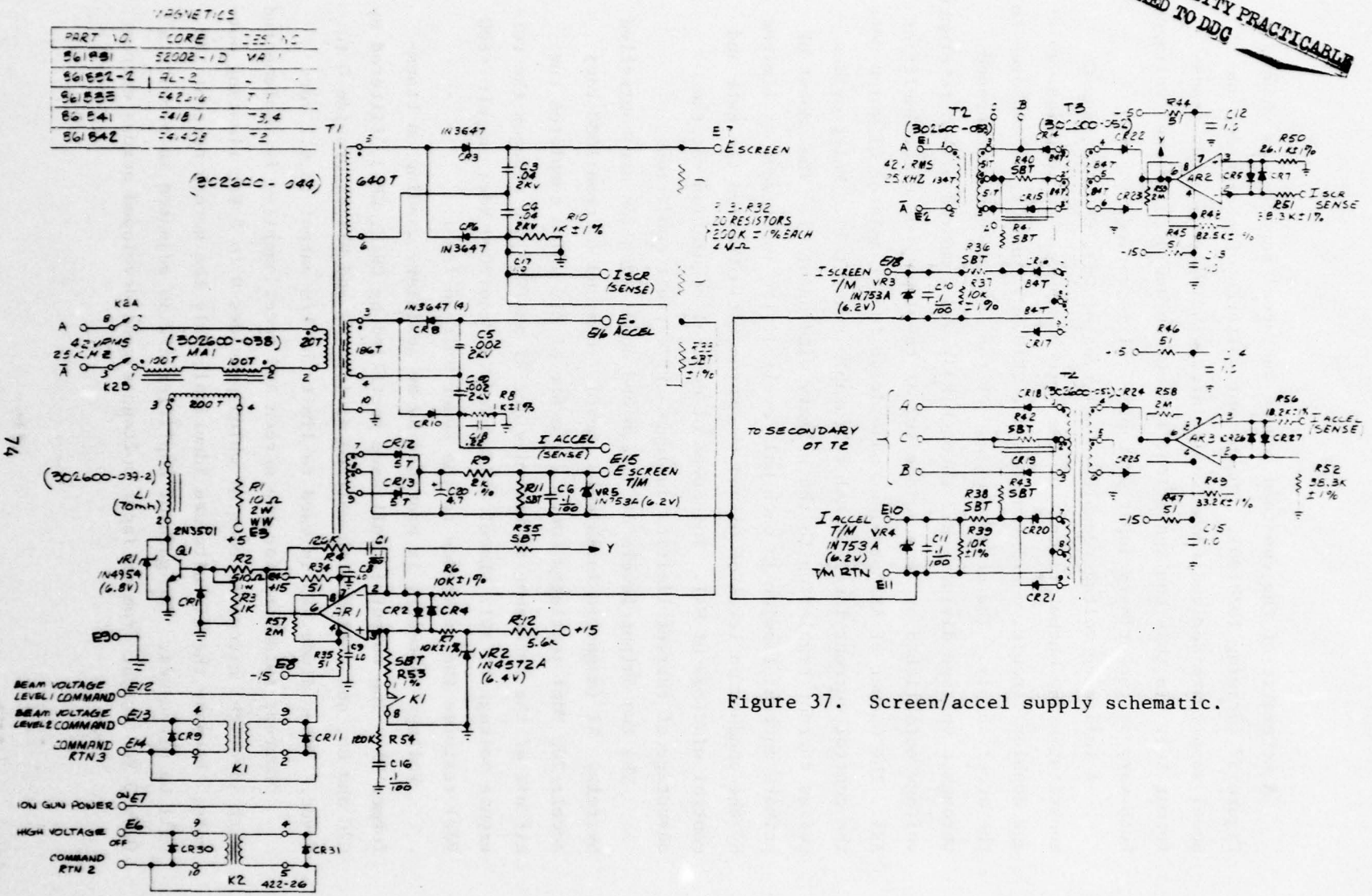

Figure 37. Screen/accel supply schematic.

sensing resistor R10. The output of AR2 provides a current sink to the output winding and rectifiers CR22, and CR23 of transformer T3. Any voltage level generated at the output of CR22 and CR23 is duplicated at the output of rectifiers CR16, CR17. R40 in the primary winding of T3 determines the current sink requirements of AR2 and establishes the available output power to the T/M output circuit. R41 provides a forward bias current for CR16, CR17 at low-level T/M outputs.

3. Cathode Heater and Discharge Supplies

The block diagram for the cathode heater and discharge supplies is shown in Figure 38. A control loop is used between the "voltage sensing" block of the discharge supply and the "saturable reactor and control electronics" block of the cathode heater supply. Before discharge ignition takes place, the maximum cathode heater output current is established by current-limiting resistors in the saturable reactor control winding. After discharge ignition, the feedback voltage from the discharge supply will suddenly decrease to a value less than the reference voltage in the heater control electronics. At this time, the cathode heater supply will be cutback to virtually zero output.

The output current levels of the discharge supply are 35, 125, and 250 mA and are set by level I, II, and III command signal to latching relays in the "discharge output current" block. Voltage and current T/M signals for both supplies are transformer isolated.

The cathode heater and discharge supplies circuit schematics are presented in Figure 39 (drawing 1028191). The discharge supply is a constant current supply in which output voltage is sensed to control the cathode heater current. As in the screen supply, a current limiting feature is designed into both output transformer control magnetics.

The output current level is selected by latching relays K1 and K2, which are operated by the discharge level commands. A voltage sense winding on the discharge supply output transformer T3 furnishes a voltage proportional to the output voltage and is used to control the electronics in the heater supply. Operational amplifier AR1 compares this voltage

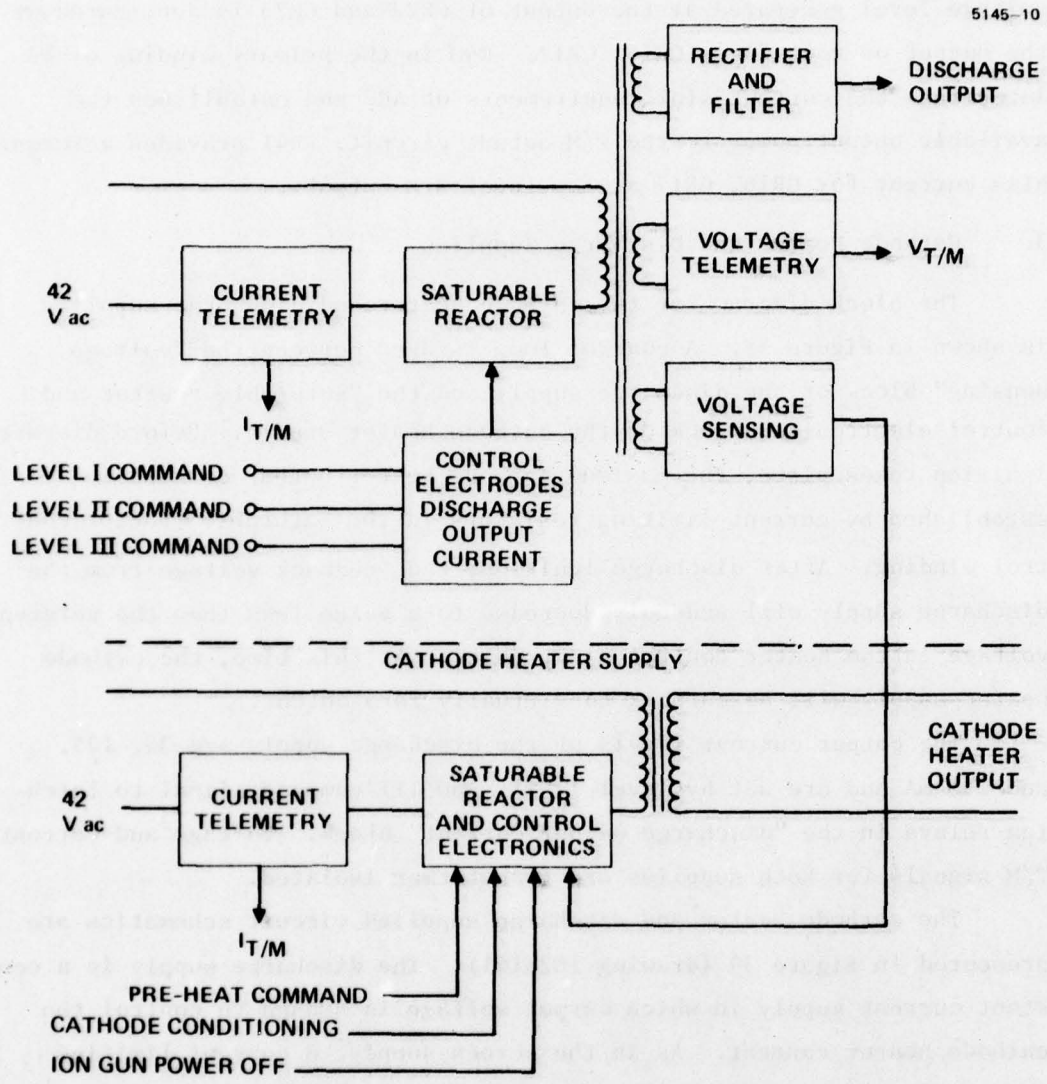

Figure 38. Cathode heater and discharge supplies block diagram.

THIS PAGE IS BEST QUALITY PRACTICABLE
FROM COPY FURNISHED TO DDC

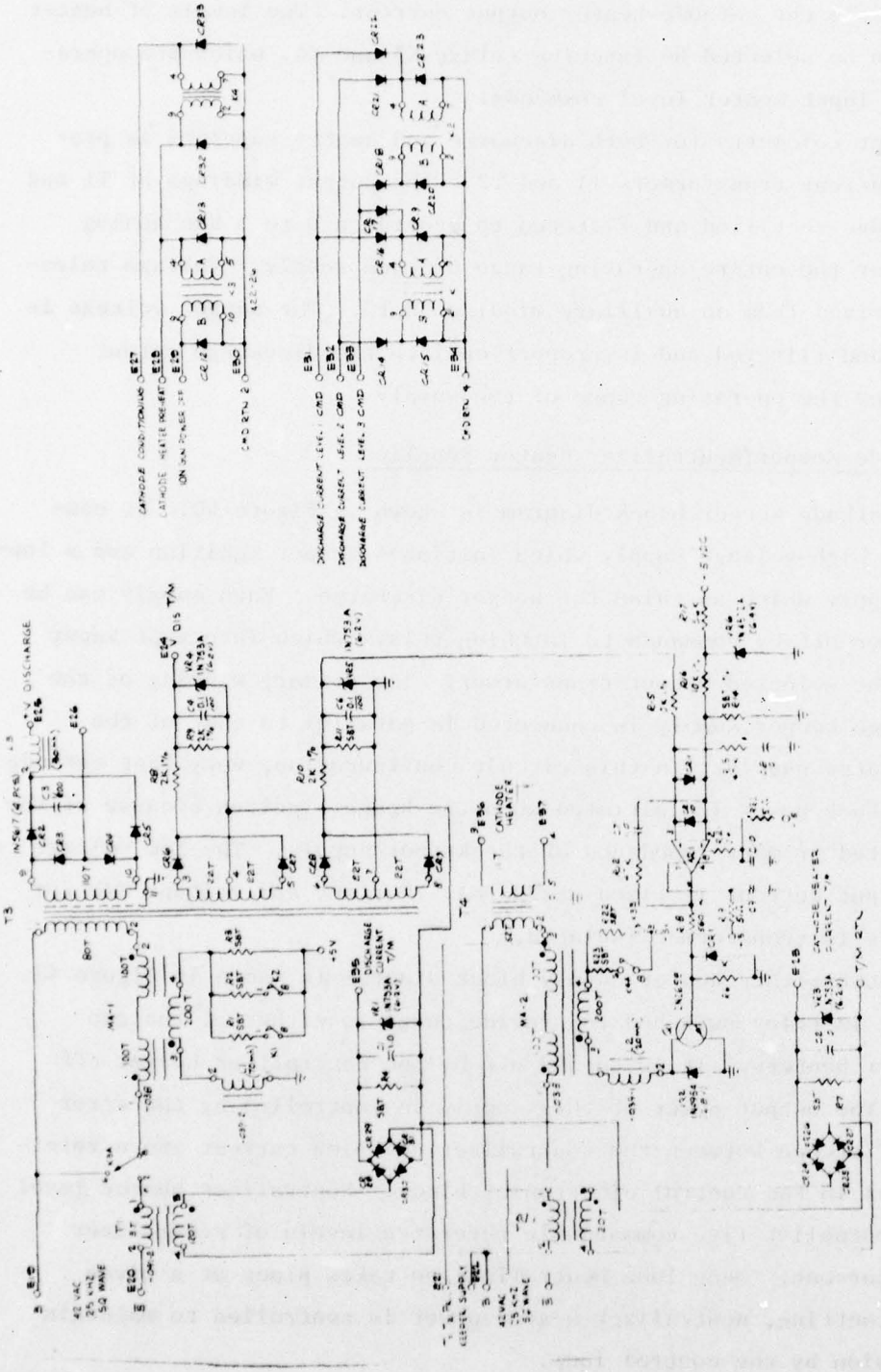

Figure 39. Cathode heater and discharge supplies schematic.

with a reference voltage and varies the base drive to transistor Q1, which controls the cathode heater output current. Two levels of heater current can be selected by latching relays K3 and K4, which are operated by the input heater level commands.

Current telemetry for both discharge and heater supplies is provided by current transformers T1 and T2. The output windings of T1 and T2 are bridge rectified and filtered to provide a 0 to 5 Vdc analog voltage over the entire operating range of each supply. Voltage telemetry is derived from an auxiliary winding on T3. The output voltage is rectified and filtered and is proportional to the discharge output voltage over the operating range of the supply.

4. Cathode Keeper/Neutralizer Heater Supplies

The cathode keeper block diagram is shown in Figure 40. It consists of a high-voltage supply which initiates keeper ignition and a low-voltage supply which sustains the keeper discharge. Each supply can be turned on or off by commands to latching relays which interrupt input power to the selected output transformer. The primary winding of the high-voltage keeper supply is connected in parallel to that of the cathode heater supply. In this circuit configuration, very fast cathode heater cutback power is initiated when the keeper ignites because of the low reflected primary impedance of the keeper supply. The low voltage keeper output current is fixed at 235 mA. Current and voltage T/M for this supply is transformer isolated.

The neutralizer heater supply block diagram is shown in Figure 41. Its output is relay switched to provide power to either of the two neutralizer heaters. It is turned off by the neutralizer heater off command. The output power of this supply is controlled by the error signal difference between the neutralizer emission current and a reference signal in the control electronics block. Neutralizer heater level commands establish five commandable reference levels of neutralizer emission current. Once 100% neutralization takes place at a given reference setting, neutralizer heater power is controlled to maintain this emission by the control loop.

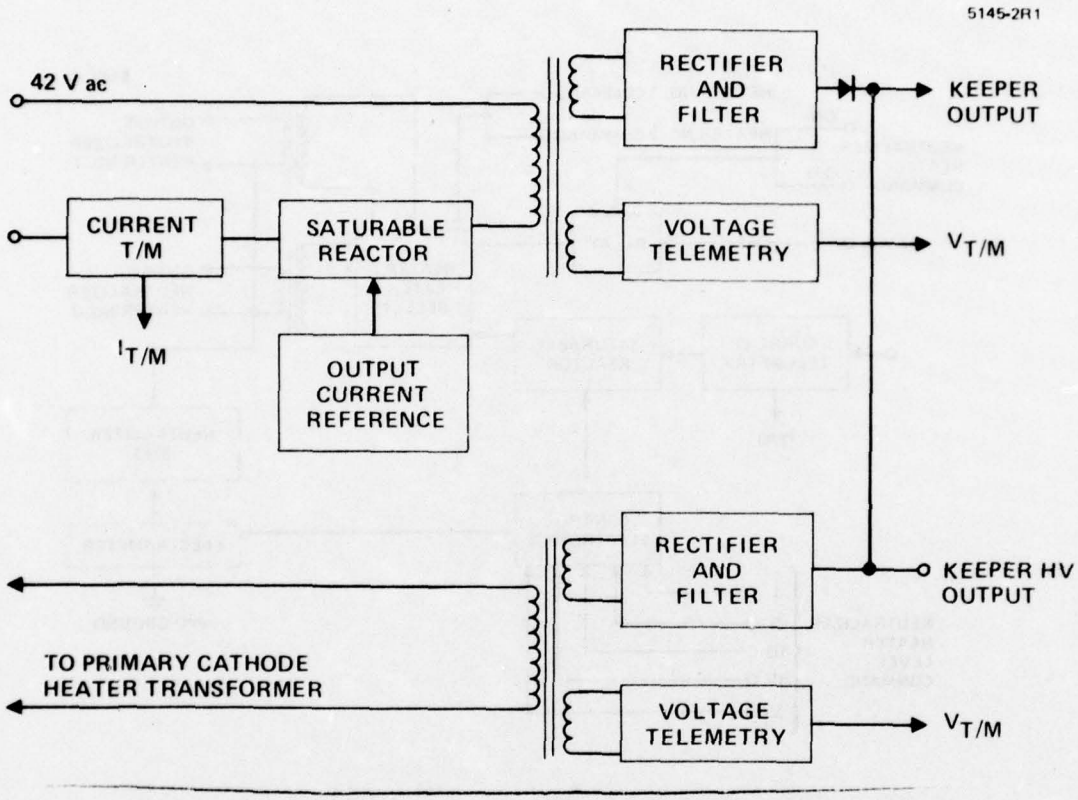

Figure 40. Cathode keeper supply block diagram.

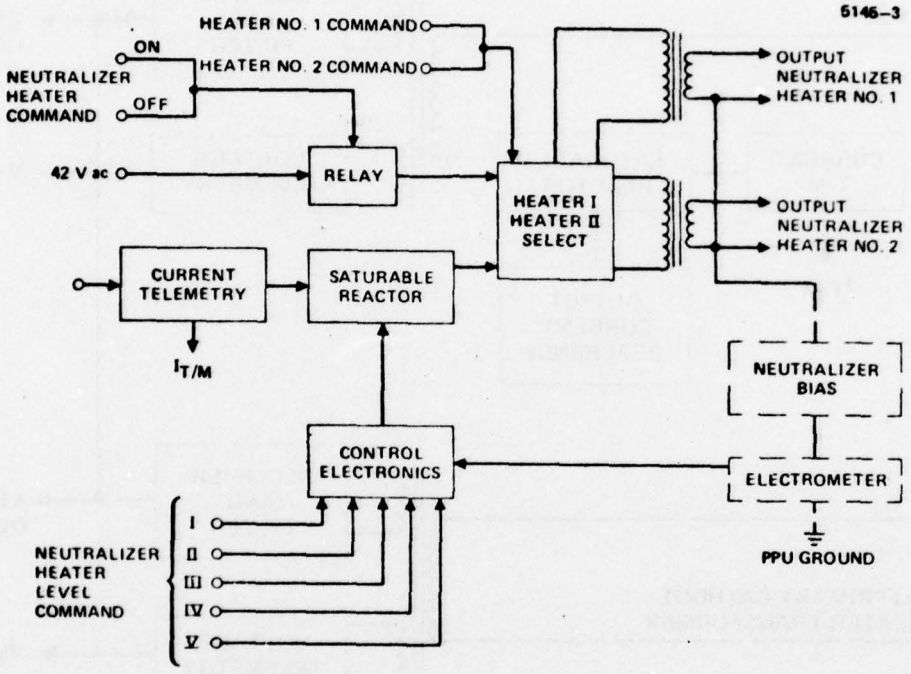

Figure 41. Neutralizer heater supply block diagram.

Current T/M for the neutralizer heater supply is transformer isolated. Neutralizer emission current T/M is furnished by the electrometer.

The cathode keeper supply schematic is shown in Figure 42 (drawing 1028192). The supply includes a high-voltage module for keeper ignition and a low-voltage module to sustain the keeper discharge in normal operation. The high-voltage winding on T2 provides 1000 Vdc after being rectified by CR12 through CR15. The output current is limited to 20 mA because T2 derives its power from the magnetic amplifier in the cathode heater supply. At the 1000 Vdc output level, a telemetry voltage winding on T2 provides a 5 Vdc signal at the output of CR10, CR11 and R-C filter circuit.

The low-voltage output is derived from T3 with its output full wave rectified by CR16 and CR17. CR18 is a high-voltage diode which protects the output circuit of T3 from high-voltage stresses before ignition takes place. Current limiting is accomplished by the action of saturable reactor MA1. The output of the keeper supply is turned on and off by latching relay K7.

Current telemetry is implemented with transformer T1 and its associated rectifier-filter output circuit. This provides a 0 to 5 Vdc analog signal proportional to the keeper load current.

The circuit of the neutralizer heater supply is identical to that of the cathode heater supply with the exception that the neutralizer heater current is controlled by the neutralizer emission current. Five level commands which operate latching relays K3, K4, K5, and K6 change the reference signal on amplifier AR1. An increase in the reference level at the input of AR1 corresponds to an increase in heater current which results in an increase in neutralizer emission current. The current supplied to the heater becomes stabilized when the emission current signal reaches the level of the reference voltage at the inputs of AR1. The option of selecting either one of two neutralizer heaters is implemented by latching relay K2. Neutralizer heater current telemetry is derived from transformer T4. The output, which is rectified and

THIS PAGE IS BEST QUALITY PRACTICABLE
FROM COPY FURNISHED TO DDC

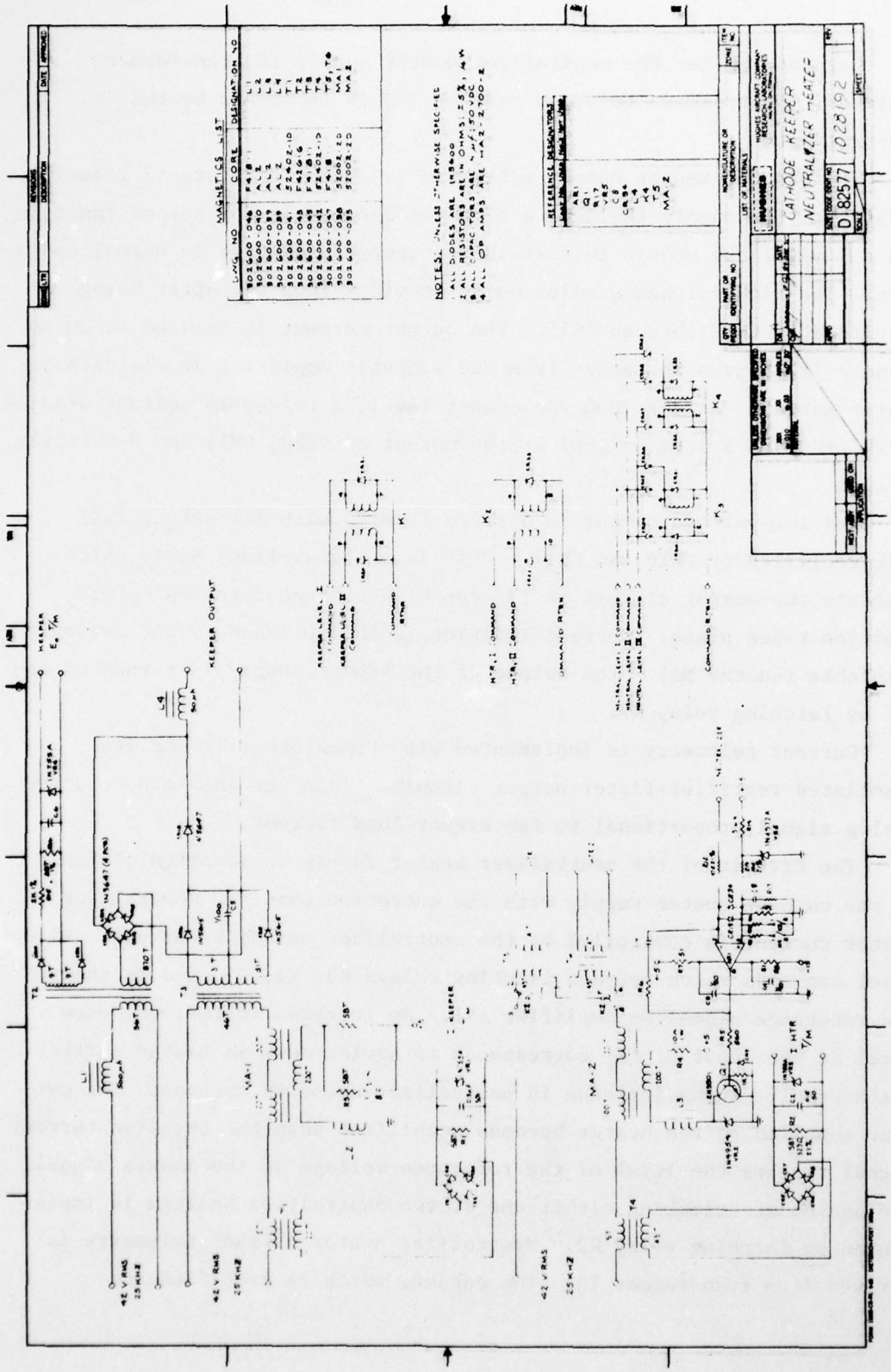

Figure 42. Cathode keeper and neutralizer heater schematic.

filtered, provides a 0 to 5 Vdc signal which corresponds to the applied heater current.

5. Neutralizer Bias Supply

A block diagram of the neutralizer bias supply is shown in Figure 43. The 42 Vac input passes through an isolation transformer and goes to two similar series-regulated supplies. Each supply (one for positive bias and one for negative) consists of a series pass transistor which has current limiting, a step-up transformer, a voltage doubler, and an error amplifier. The zener reference is common to both supplies. On receiving a polarity command, a relay selects the desired supply.

The neutralizer bias supply design is shown schematically in Figures 44 and 45 (drawing 1028406). The basic design consists of positive and negative voltage-regulated supplies and a commandable relay (K6) that selects the desired supply. The negative supply consists of an output transformer T3 and a full-wave voltage doubler CR17, CR18, C19, and C20. The output voltage is sensed by operational amplifier AR1 through resistors R27 through R31 and compares this voltage to the reference provided by zener diode VR2. The operational amplifier linearly drives Q4, which varies the voltage on the primary of transformer T3 to close the regulation loop. Transistor Q3 and resistor R5 are included to provide current limiting. The positive supply is similar in design to the negative supply but has a series string of 3 mA constant current diodes CR21 through CR32 across the output. These diodes provide a path for the current that the supply must sink. The different output levels are obtained by commands which activate relays K2, K3, K4, and K5. Amplifier AR3 and a magnetic telemetry isolator will generate a telemetry signal that corresponds to the absolute output voltage. A polarity flag is used to indicate the polarity of the output.

6. Electrometers

The SPIBS system requires accurate telemetry measurements for the neutralizer emission current (I_{NE}) and SPIBS net current (I_{NET}) (i.e.,

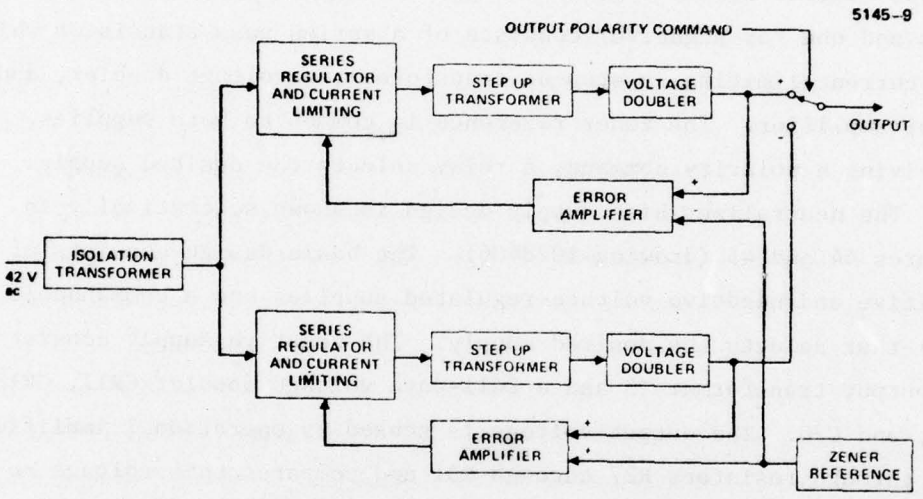

Figure 43. Neutralizer bias supply block diagram.

THIS PAGE IS BEST QUALITY PRACTICABLE
FROM COPY FURNISHED TO DDC

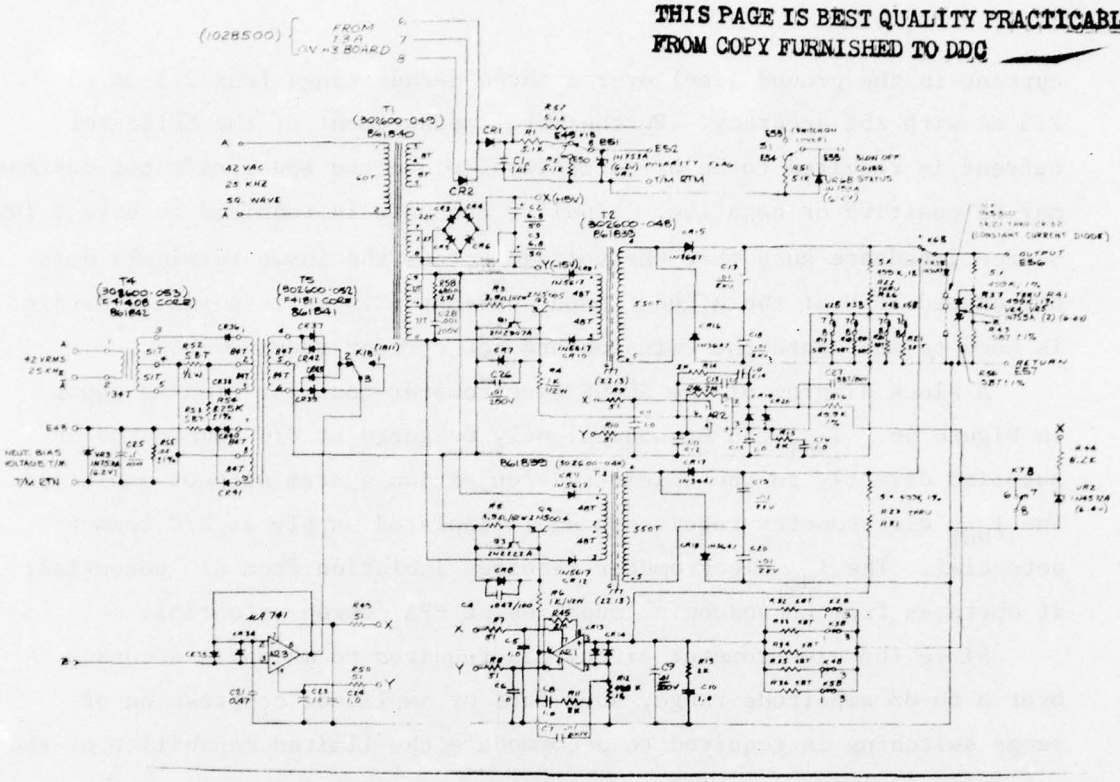

Figure 44. Neutralizer bias supply schematic.

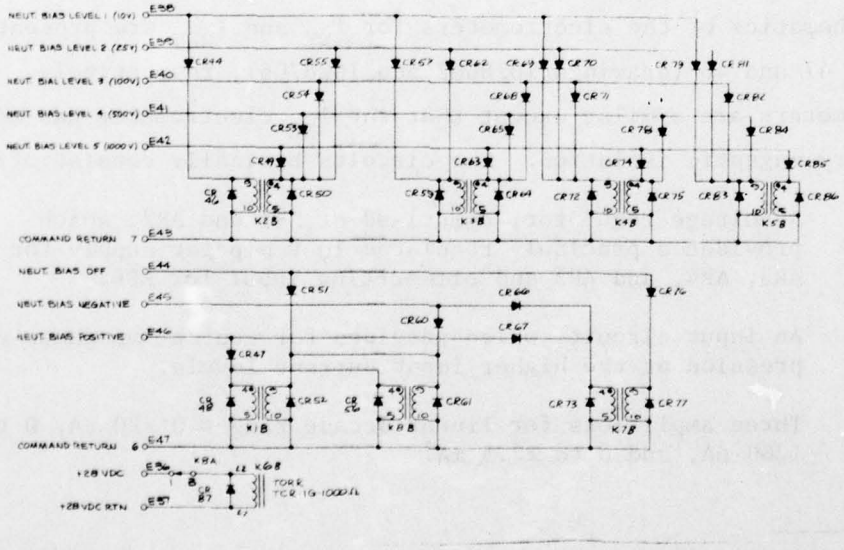

Figure 45. Neutralizer bias supply schematic.

current in the ground line) over a three decade range from 2.5 μA to 2.5 mA with ±5% accuracy. Furthermore, measurement of the SPIBS net current is required to be bi-directional since the spacecraft net current may be positive or negative. Finally, the unit is required to have a low source impedance such that the voltage across the input terminals does not exceed ±2 V at the highest input current (2.5 mA). A single design is used to meet both the emission and net current requirements.

A block diagram of the SPIBS electrometer configuration is shown in Figure 46. I_{NET} can be conveniently measured at S/C common and be supplied directly to the telemetry acquisition system without isolation. The I_{NET} electrometer requires a small isolated supply at S/C common potential. The I_{NE} electrometer requires isolation from S/C potential; it operates from housekeeping supplies at PPA common potential.

Since the electrometer circuit is required to maintain accuracy over a 60-dB amplitude range, some form of amplitude compression or range switching is required to accommodate the limited capability of the telemetry isolation amplifiers and telemetry acquisition systems. Amplitude compression was selected since the need for relays or switches for range switching and the need for extra bits to define the measurement range are eliminated.

Schematics of the electrometers for I_{NE} and I_{NET} are presented in Figures 47 and 48 (drawings 1028602 and 1028706), respectively. The electrometers are similar except that the I_{NE} electrometer has additional telemetry magnetic isolation. The circuits basically consist of:

- A voltage regulator, comprised of AR1 and AR2, which provides a precisely regulated 10 V bipolar supply for AR3, AR4, and AR5 and off-setting input for AR6.
- An input circuit, which provides for source impedance compression at the higher input current levels.
- Three amplifiers for linear decade ranges 0 ±20 μA, 0 to ±200 μA, and 0 to ±2.5 mA*.

*The amplifiers each operate over a ±10 V output range and are designed to provide a precise supply voltage and a 0 to ±100 MV input range clamp when the input range for that amplifier is exceeded.

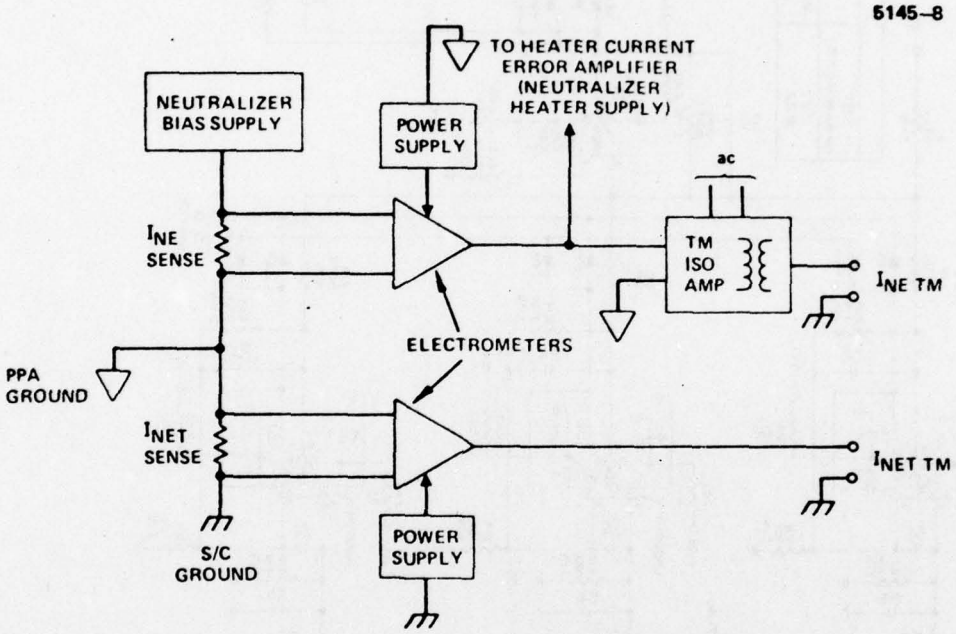

Figure 46. Block diagram of the SPIBS electrometer configuration.

THIS PAGE IS BEST QUALITY PRACTICABLE
FROM COPY FURNISHED TO DDC

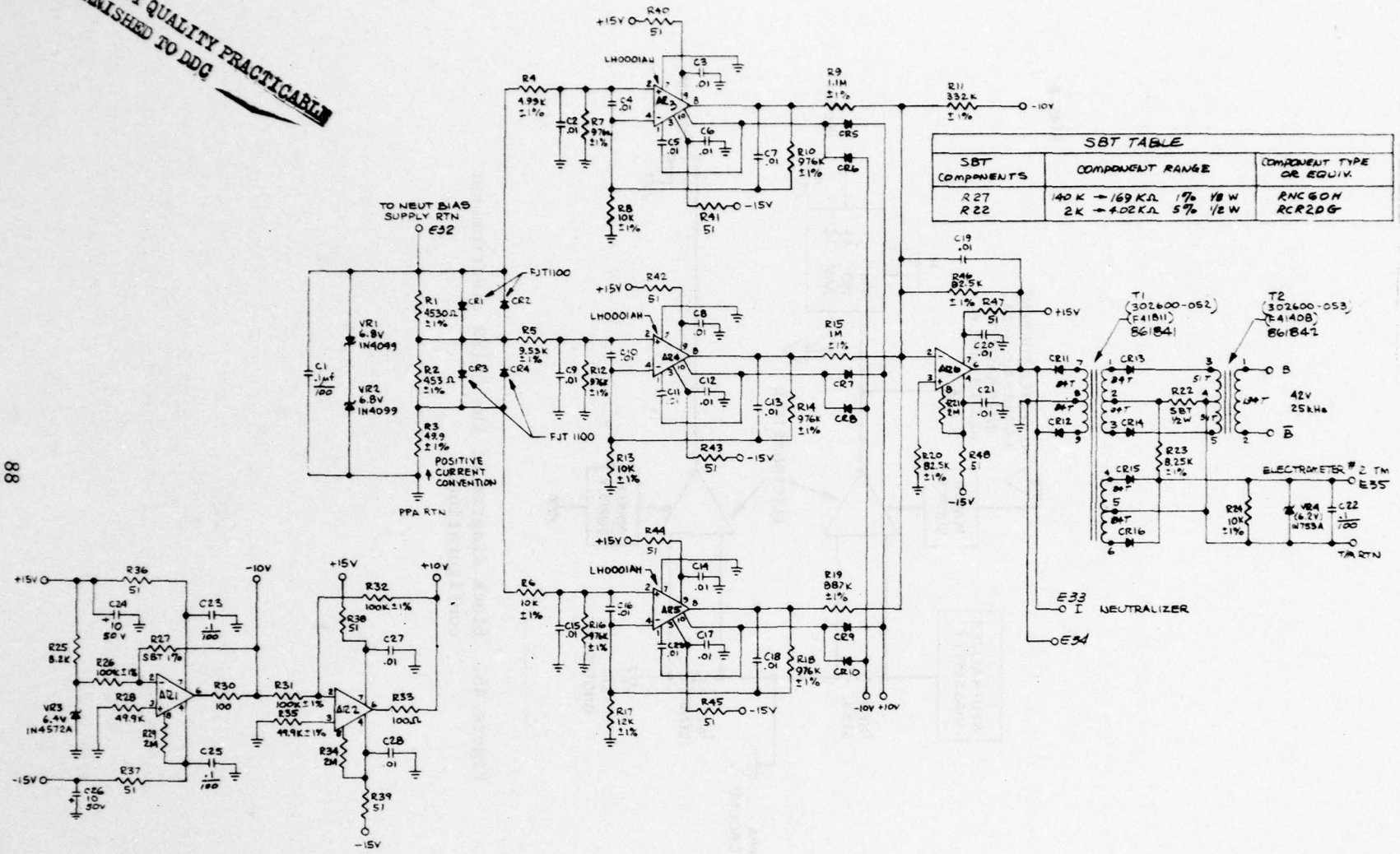

Figure 47. Neutralizer emission electrometer schematic.

THIS PAGE IS BEST QUALITY PRACTICABLE
FROM COPY FURNISHED TO DDC

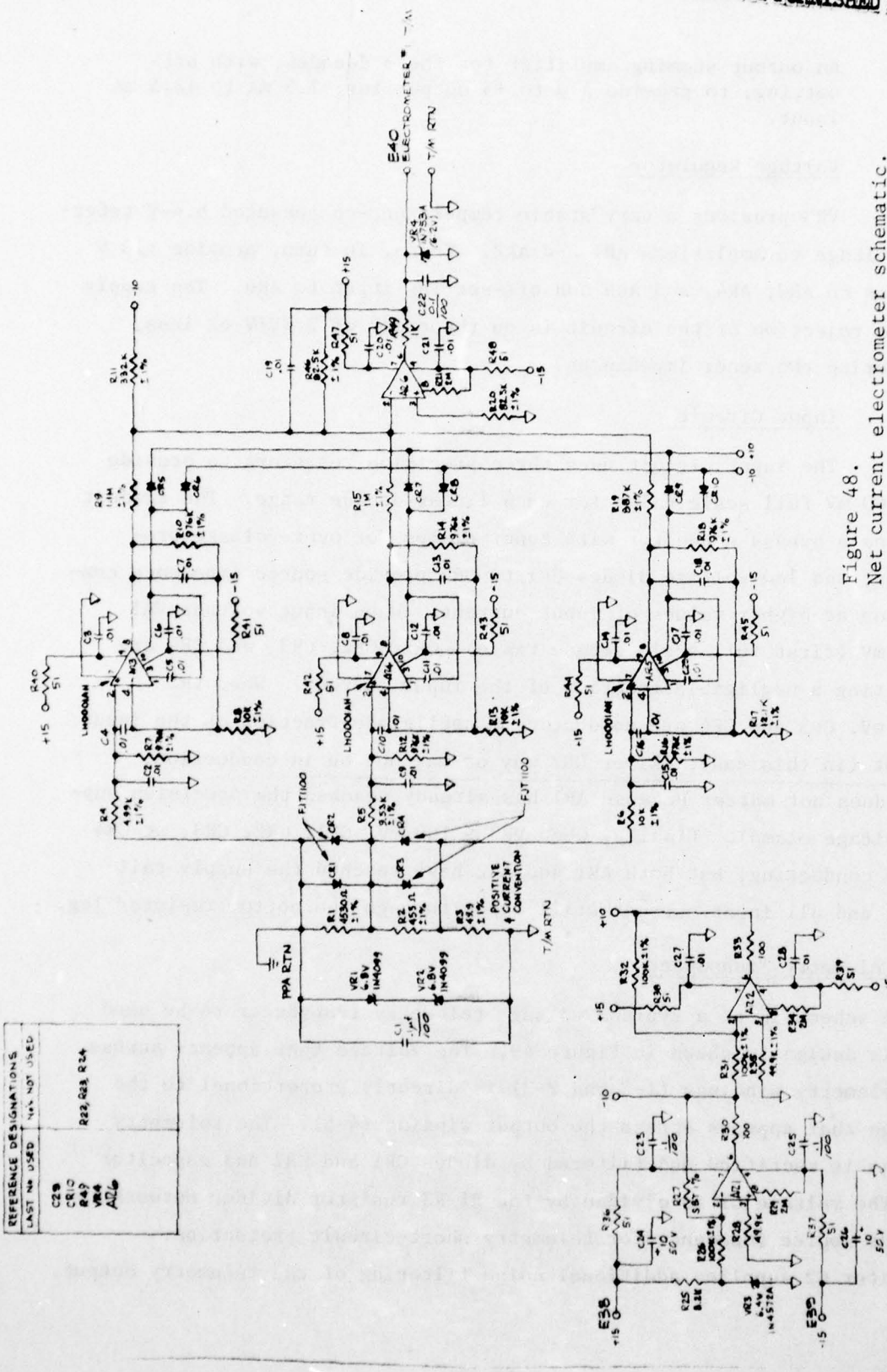

Figure 48.
Net current electrometer schematic.

- An output summing amplifier for the 3 decades, with off-setting, to provide a 0 to +5 output for -2.5 mA to +2.5 mA input.

a. Voltage Regulator

VR3 provides a very stable temperature-compensated 6.4-V reference voltage to amplifiers AR1 and AR2. These, in turn, provide ±10 V voltages to AR3, AR4, and AR5 and off-setting input to AR6. The supply voltage rejection of the circuit is on the order of 2 mV/V or less, considering the zener impedances.

b. Input Circuit

The input circuit uses three precision resistors to provide 0 to 100 mV full scale value for each linear decade range. The circuit contains a bypass capacitor with zener clamps for over-voltage protection, and low-voltage diodes CR1 to CR4 provide source impedance compression at higher values of input current. When input voltage VR1 $\leq$ 100 mV (first full scale decade range), CR1, CR2, CR3, and CR4 are conducting a negligible fraction of the input current. When VR2 $\leq$ 100 mV, CR3 and CR4 are conducting a negligible fraction of the input current (in this case, CR1 or CR2 may or may not be in conduction, which does not matter because AR1 has already reached the precision supply voltage clamp). Finally, when VR3 $\leq$ 100 mV, CR1, CR2, CR3, or CR4 may be conducting, but both AR1 and AR2 have reached the supply rail clamp, and all input current still flows through the bottom resistor leg.

7. Telemetry Transducers

A schematic of a typical voltage telemetry transducer to be used in this design is shown in Figure 49. The voltage that appears across the telemetry windings (1-2 and 2-3) is directly proportional to the voltage that appears across the output winding (4-5). The telemetry voltage is rectified and filtered by diodes CR1 and CR2 and capacitor C1. The voltage C1 is divided by the R1-R2 resistor divider network to provide source impedance for telemetry short-circuit protection. Capacitor C2 supplies additional noise filtering of the telemetry output.

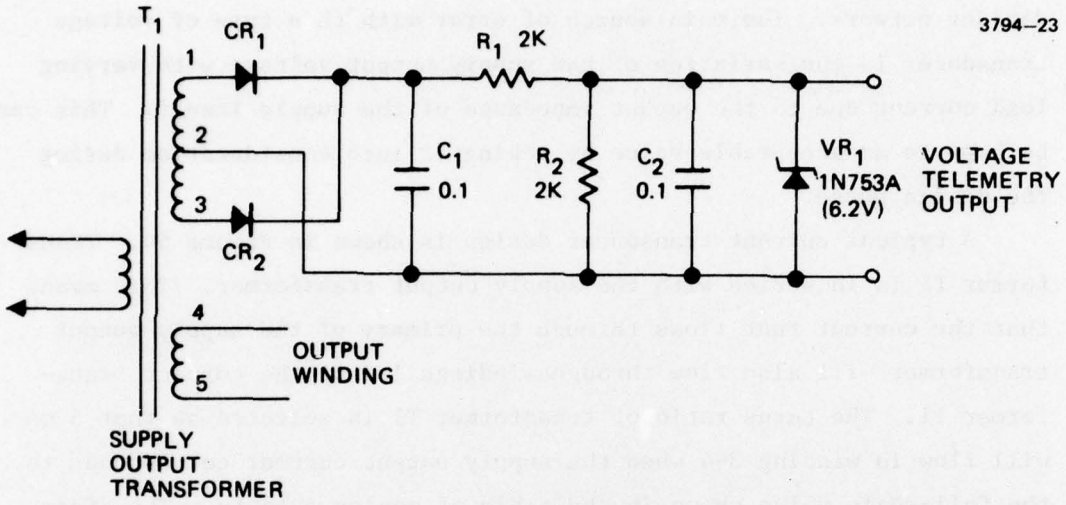

Figure 49. Typical voltage telemetry transducer schematic.

Zener diode VR1 is included to prevent the telemetry output voltage from rising too high and possibly damaging the telemetry multiplexer. The analog telemetry voltage can be adjusted to the various full-scale values shown by proper selection of the turns ratio of the output transformer between the output windings and the adjustment of the R1-R2 resistor divider network. The main source of error with this type of voltage transducer is the variation of the supply output voltage with varying load current due to the output impedance of the supply itself. This can be kept to an acceptable value by taking it into consideration during the design phase.

A typical current transducer design is shown in Figure 50. Transformer T1 is in series with the supply output transformer. This means that the current that flows through the primary of the supply output transformer will also flow through windings 1-2 of the current transformer T1. The turns ratio of transformer T1 is selected so that 5 mA will flow in winding 3-4 when the supply output current corresponds to the full-scale value shown in the table of analog outputs. The diode bridge, CR1-CR4, rectifies the winding 3-4 current which will flow through resistor R1. Capacitor C1 is included to filter the telemetry output voltage. Zener diode VR1 will prevent the telemetry voltage from rising too high and damaging the telemetry multiplexer.

The transducer output can be scaled by adjusting the turns ratio of the current transformer T1 and selecting the value of resistor R1. The main source of error encountered with this type of transducer arises from the fact that, in this design, it is placed in series with the primary of the output transformer. This is done so that the current transformer will not require high-voltage insulation. Therefore, any additional loading on the secondary side of the output transformer, such as voltage telemetry, will be reflected on the current telemetry output. In most cases, this will appear as a "zero" offset and can be taken into consideration when the current telemetry channels are calibrated. One feature common to both the voltage and current transducers proposed is that the telemetry output is isolated electrically from the rest of the

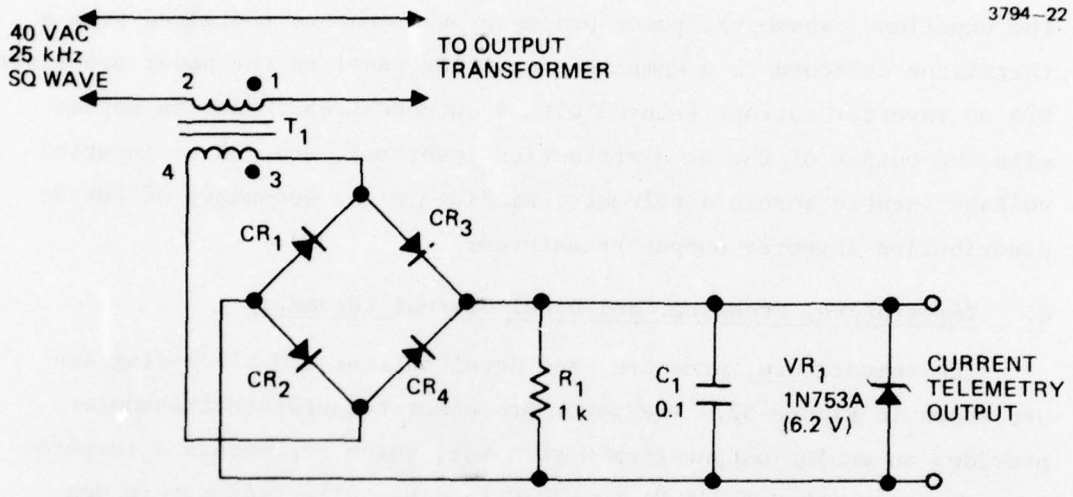

Figure 50. Typical current telemetry transducer schematic.

power processor electronics by utilizing the inherent isolation of magnetic devices.

Eighteen channels of telemetry are provided for monitoring the performance of the SPIBS system as shown in Table 2. The sensing locations for 14 of these quantities are shown in Figure 51. The other four telemetry channels are: tank pressure (obtained from a transducer in the expellant assembly), power processor temperature (obtained from a thermistor attached to a component mounting panel in the power processor), PPA ac inverter current (sensed with a current transformer in series with the output of the ac distribution inverter), and PPA ac inverter voltage (sensed across a telemetry winding in the secondary of the ac distribution inverter output transformer).

8. Temperature, Pressure, and Decel Current Telemetry

The temperature, pressure, and decel current T/M block diagrams are shown in Figure 52. The power processor temperature transducer provides an analog output from 0 to 5 Vdc, which represents a temperature range of +60°C (1.25 V) to -20°C (4.4 V). The temperature measuring device is a conventional type thermistor operated from a constant current source. The output is amplified and buffered to provide the T/M output.

The Entran semiconductor type pressure transducer is operated from regulated 4 Vdc and provides an analog signal from about 0 to 120 mV for a reservoir pressure from 0 to 1500 psi. This signal is amplified to provide a 0 to 5 Vdc T/M signal.

The decel current amplifier provides a T/M signal of 0 to 5 Vdc over a range of -2.5 mA to +2.5 mA of decel current. All of these circuits are operated from an isolated ±15 Vdc supply and are referenced to vehicle telemetry ground.

Schematics of these telemetry circuits are shown in Figure 53 (drawing 1028636). The pressure transducer, described previously, provides a low-level pressure analog voltage to buffer amplifier AR3. The output of the buffer amplifier is combined with a dc offset by

Table 2. Analog Outputs

Channel No.	Description	Actual Value for 5 V Output, ±5%
1	Beam current	2.5 mA (±2%)
2	Beam voltage	2500 V
3	Discharge current	250 mA
4	Discharge voltage	50 V
5	Keeper current	250 mA
6	Keeper high voltage	1000 V
7	Keeper low voltage	50 V
8	Cathode heater current	5 A
9	Accel current[a]	2.5 mA
10	Decel current[a]	2.5 mA
11	Neutralizer heater current	5 A
12	Neutralizer bias voltage	1000 V
13	Neutralizer emission[b]	2.5 mA (±10%)
14	SPIBS net current[b]	2.5 mA (±10%)
15	Tank pressure	1500 psia
16	Power processor temperature	See calibration curve
17	PPA ac inverter current	1.5 A
18	PPA ac inverter voltage	50 V

[a] To indicate anomolous condition.

[b] In three ranges: 2.5 to 25 μA; 25 μA to 250 μA to 2.5 mA.

AD-A063 253 HUGHES RESEARCH LABS MALIBU CALIF F/G 20/3
ROCKET MODEL SATELLITE POSITIVE ION BEAM SYSTEM.(U)
OCT 78 T MASEK F19628-76-C-0272
UNCLASSIFIED AFGL-TR-78-0179 NL

2 OF 2
AD
A063253

END
DATE
FILMED
3-79
DDC

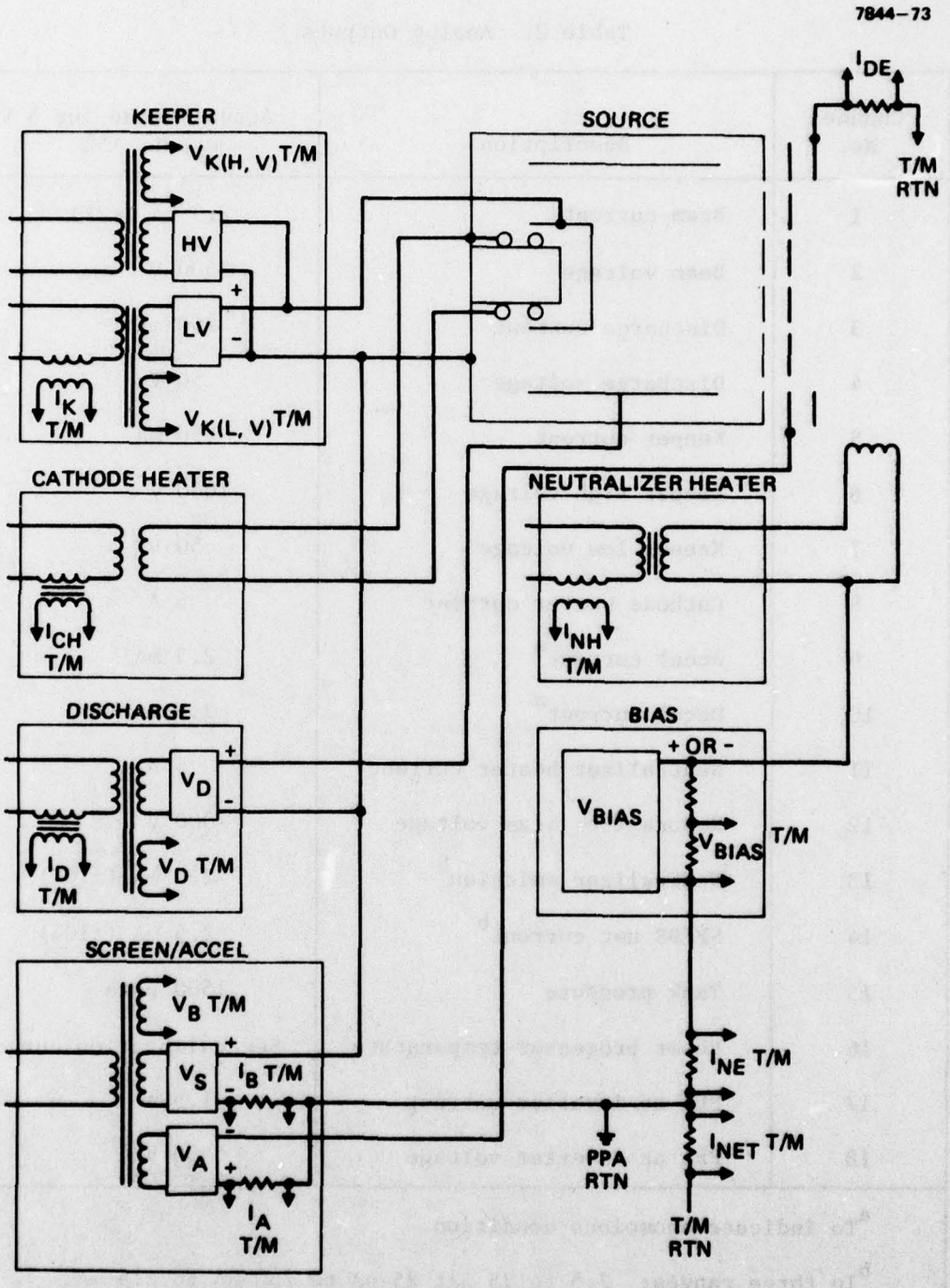

Figure 51. Telemetry sensing locations.

THIS PAGE IS BEST QUALITY PRACTICABLE
FROM COPY FURNISHED TO DDC

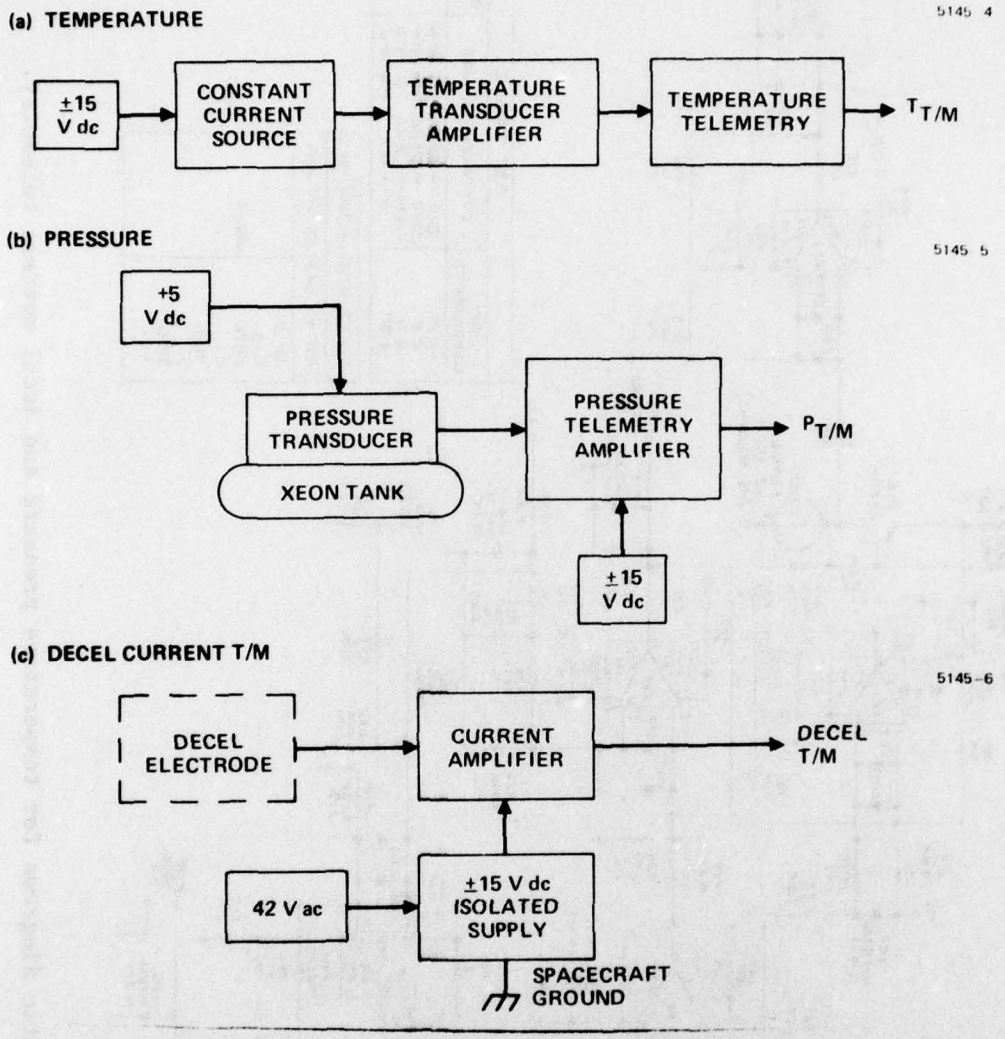

Figure 52. Block diagrams for temperature, pressure, and decel current telemetry.

THIS PAGE IS BEST QUALITY PRACTICABLE
FROM COPY FURNISHED TO DDC

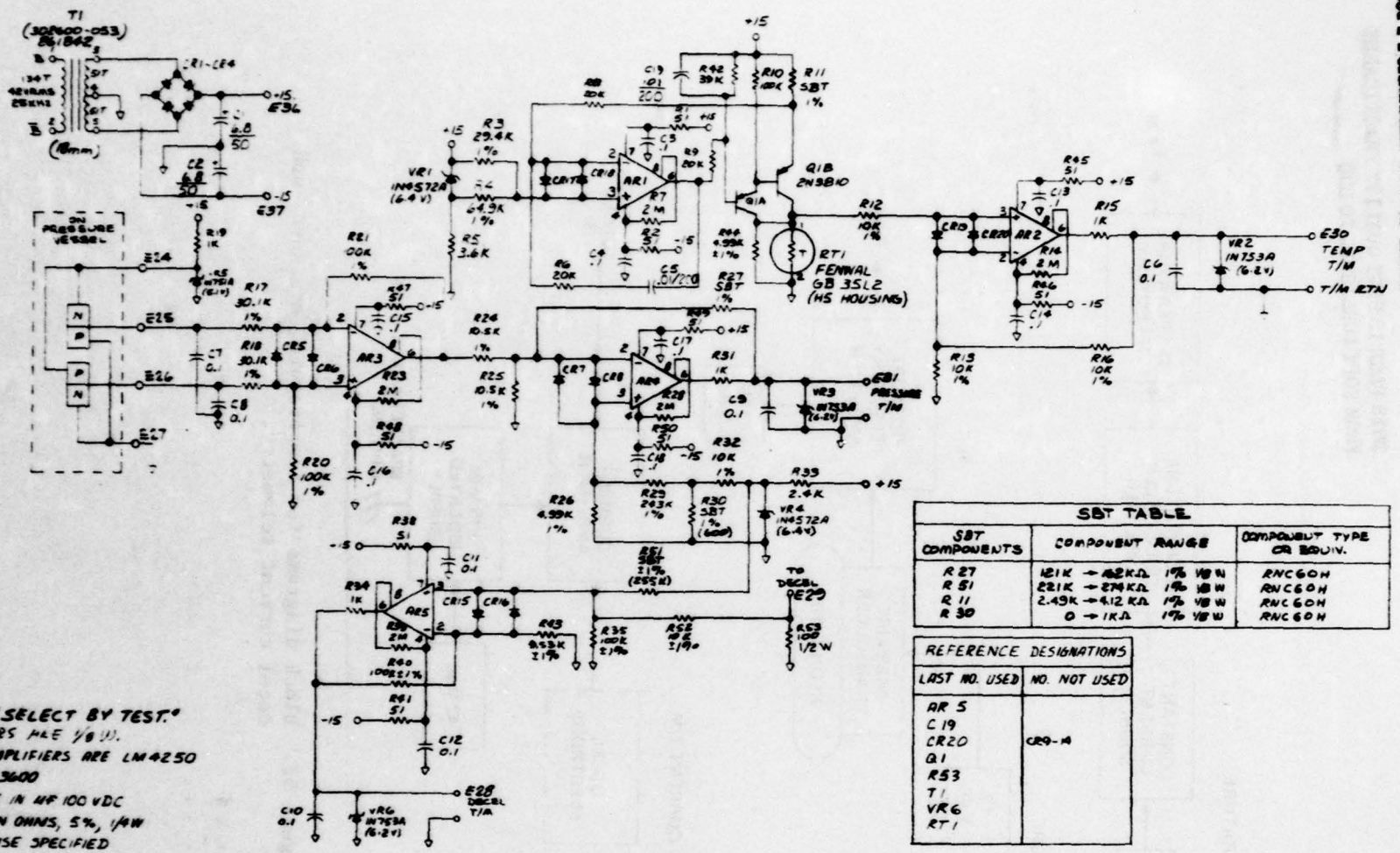

6. S.B.T. MEANS "SELECT BY TEST."
5. ±1% RESISTORS ARE 1/8 W.
4. OPERATIONAL AMPLIFIERS ARE LM4250
3. DIODES ARE IN3600
2. CAPACITORS ARE IN MF 100 VDC
1. RESISTORS ARE IN OHMS, 5%, 1/4W

NOTES- UNLESS OTHERWISE SPECIFIED

SBT TABLE		
SBT COMPONENTS	COMPONENT RANGE	COMPONENT TYPE OR EQUIV.
R 27	121K → 182K Ω 1% 1/8 W	RNC60H
R 51	221K → 274K Ω 1% 1/8 W	RNC60H
R 11	2.49K → 4.12 K Ω 1% 1/8 W	RNC60H
R 30	0 → 1K Ω 1% 1/8 W	RNC60H

REFERENCE DESIGNATIONS	
LAST NO. USED	NO. NOT USED
AR 5	
C 19	
CR20	CR9-19
Q 1	
R53	
T 1	
VR6	
RT 1	

Figure 53. Schematic diagrams for temperature pressure and decel current telemetry.

amplifier AR4 to provide a 0 to 5 Vdc output, which corresponds to a reservoir pressure of 0 to 1500 psi.

For the temperature measurement, a constant current is supplied to the thermistor by the Q1-AR1 circuitry. The voltage that appears across the thermistor will be representative of the temperature of the surface to which the thermistor is mounted (in this case, the baseplate of the power processor). Amplifier AR2 amplifies and buffers the thermistor voltage to obtain the required telemetry voltage. A calibration curve of telemetry voltage versus power processor temperature is used since the thermistor resistance versus temperature is characteristically a non-linear function.

As shown in the schematic, the pressure, temperature, and decel telemetry circuitry derives power from the output of transformer T1. This allows the pressure, temperature, and decel telemetry to be isolated from the power-processing circuitry. The accuracy of pressure and temperature measurements will primarily be determined by the accuracy with which the initial calibration curves are generated. The decel current which flows through R53 (decel current sense resistor) is detected by amplifier AR5. When properly scaled, the output of AR5 will produce a 0 to 5 Vdc T/M signal.

9. Commands

A total of 29 ground commands are available in SPIBS, as indicated in Table 3. The command function schematic presented in Figure 54 shows how the commands to the SPIBS accomplish their intended functions. All commands, except the expellant valve open and close commands, control the operation of one or more of the power processor supplies. The commands to the power processor, with one exception, can be grouped into two types: those that apply or remove ac input power to supplies and those that adjust the level of control signals. Examples of the former are *Ion gun power on* and *High voltage off*; examples of the latter are *Neutralizer bias Levels 1 through 5* and *Beam voltage Levels 1 and 2*. The one exception to the functions described above is the reversing of the polarity of the bias supply output voltage.

Table 3. Command Capability

Command	Function
1. *Instrument on*[a]	Turns on instrument power
2. *Instrument off*[a]	Turns off all instrument power
3. *Expellant valve open*	Opens solenoid valve
4. *Expellant valve closed*	Closes solenoid valve
5. *Cathode heater preheat*	Turns on the cathode heater to Level 1 and turns on discharge supply
6. *Ion gun power on*	Turns on the ion gun power
7. *Ion gun power off*	Turns off the ion gun power
8. *Beam voltage Level 1*	Sets the beam power supply to 1000 V
9. *Beam voltage Level 2*	Sets the beam power supply to 2000 V
10. *Keeper off*	Turns the keeper supply off
11. *Discharge current and neutralizer emission Level 1*	Sets the discharge current reference to achieve 20 mA current; sets neutralizer emission level to 0.4 mA
12. *Discharge current and neutralizer emission Level 2*	Sets the discharge current reference to achieve 125 mA current; sets neutralizer emission level to 1.2 mA
13. *Discharge current and neutralizer emission Level 3*	Sets the discharge current reference to achieve 200 mA current; sets neutralizer emission level to 2.2 mA
14. *Neutralizer emission Level 4*	Sets neutralizer emission level to 2 μA
15. *Neutralizer emission Level 5*	Sets neutralizer emission level to 20 μA

Table 3. Command Capability (cont)

Command		Function
16.	*Neutralizer No. 1*	Selects neutralizer filament No. 1
17.	*Neutralizer No. 2*	Selects neutralizer filament No. 2
18.	*Neutralizer heater on*	Turns on the neutralizer cathode heater on
19.	*Neutralizer heater off*	Turns off the neutralizer heater
20.	*Neutralizer bias off*	Turns off the neutralizer bias power supply
21.	*Neutralizer bias positive*	Sets the neutralizer bias for positive polarity
22.	*Neutralizer bias negative*	Sets the neutralizer bias for negative polarity
23.	*Neutralizer bias Level 1*	Turns on the neutralizer bias to 10 V
24.	*Neutralizer bias Level 2*	Turns on the neutralizer bias to 25 V
25.	*Neutralizer bias Level 3*	Turns on the neutralizer bias to 100 V
26.	*Neutralizer bias Level 4*	Turns on the neutralizer bias to 500 V
27.	*Neutralizer bias Level 5*	Turns on the neutralizer bias to 1000 V
28.	*High voltage off*	Turns off the beam and accel power supplies
29.	*Cathode conditioning*	Turns on the cathode heater to Level 2

[a]In the SPIBS instrument, *instrument on/off* is implemented by connecting or disconnecting 28 V input power.

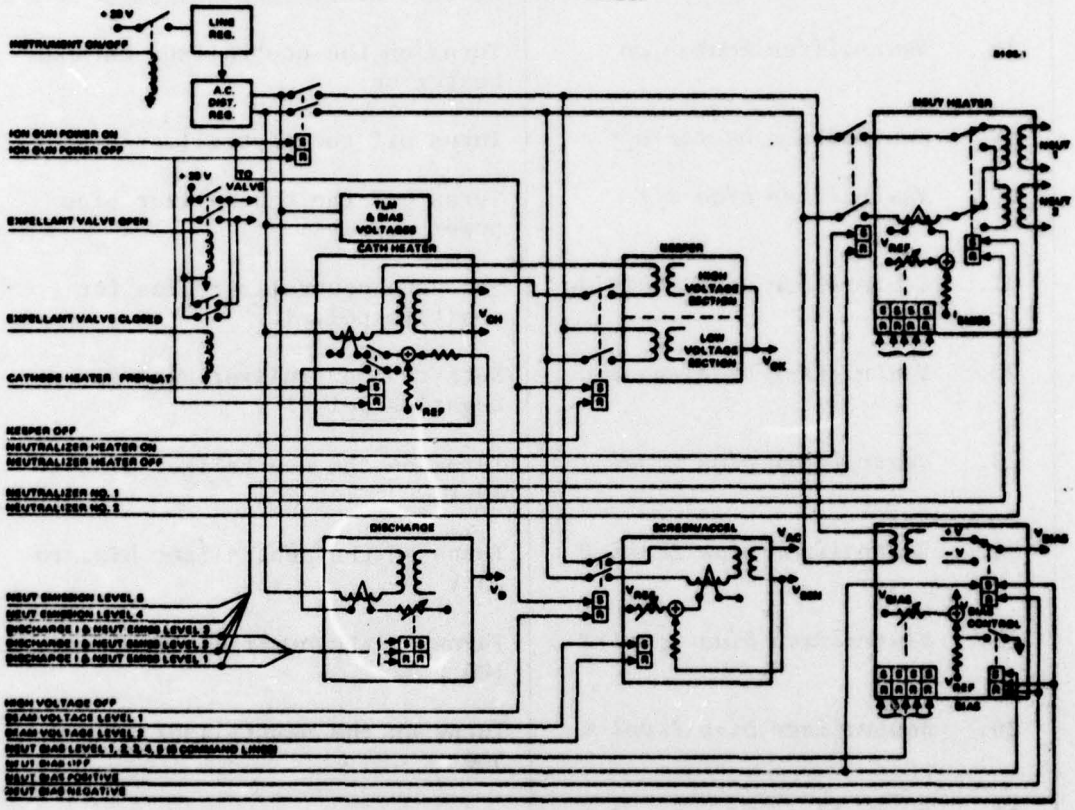

Figure 54. Command function schematic.

All commands received by the SPIBS, except the *Instrument on/off* command, are momentary pulse commands. Therefore, the SPIBS must possess the necessary "memory" to maintain a commanded mode of operation until commanded to change. Memory is provided by magnetic latching relays, which remain in the set (S) or reset (R) condition until the opposite command is received. All command functions except *Instrument on/off* are achieved with latching relays.

As shown in Figure 54, most level-setting commands adjust the current through the control winding of a saturable reactor. The one exception is the bias supply where two series regulators are used, one in the positive supply and one in the negative supply. Also shown are the internal control functions that (1) turn off the cathode heater when the discharge voltage drops below a selected level and (2) turn off the keeper high voltage output when the cathode heater is turned off.

10. SPIBS Command Unit

Ground tests require a method for issuing commands to SPIBS and monitoring telemetry. The SPIBS command unit, shown in Figure 55, contains the necessary circuitry to provide the following functions: (1) supply +28 V bus power to the power processor; (2) supply a continuous +28 V *Instrument on* command; (3) generate any of the additional 26 commands described in the command list presented above; and (4) provide a front panel read out of the bus voltage, bus current, and the 18 telemetry inputs listed above. A schematic of the command unit is presented in Figure 56.

The power-processor bus voltage is regulated by sensing the bus voltage at the input to the power processor to compensate for the line drop in the cable between the command unit and the power processor. The sensed bus voltage is used as the feedback signal in the voltage control loop of a commercial power supply capable of 0.05% regulation. The same sensed bus voltage is displayed when the VOLTS position is selected on the DVM input selector switch. When the AMPS position is selected, the output current of the bus supply is displayed.

Figure 55.
Command unit photograph.

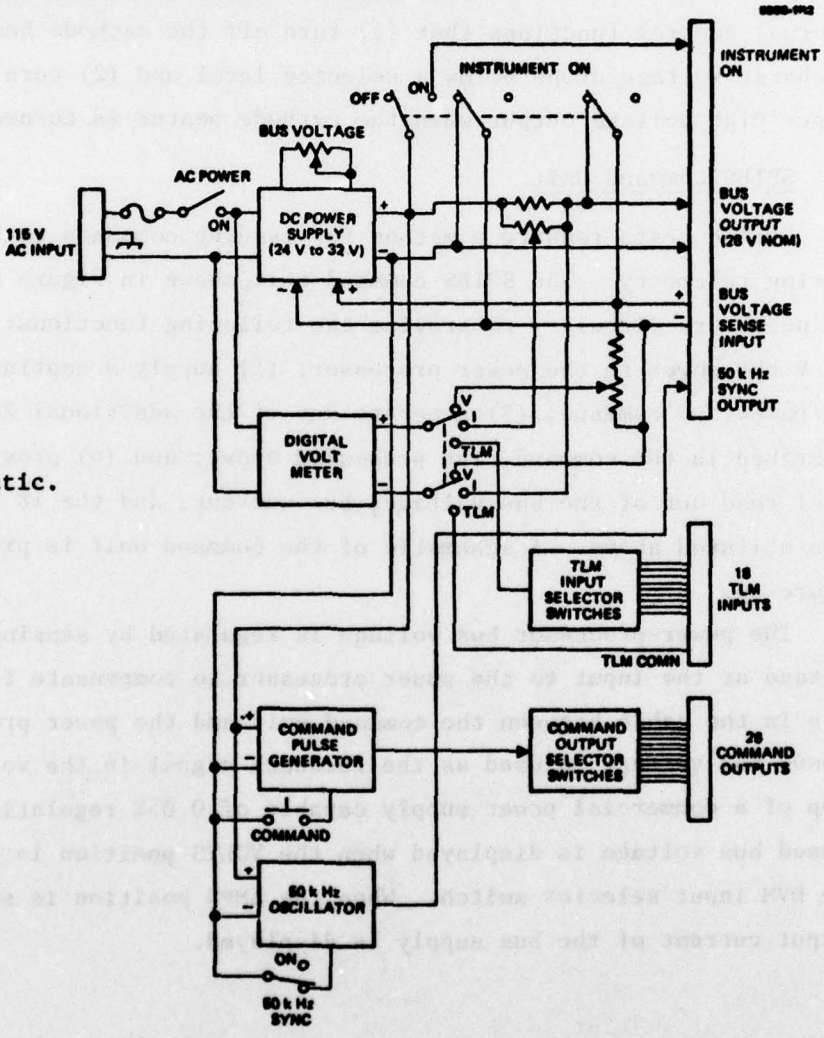

Figure 56.
Command unit schematic.

The output of the command pulse generator is one +28 V 100-ms pulse for each depression of the front panel COMMAND button. The command pulse is routed to the proper output lead by setting the two COMMAND SELECT rotary switches to the desired command number.

B. PPA FABRICATION

The PPA fabrication process was tailored to the quality requirements of each SPIBS instrument model. The breadboard model PPA was assembled at HRL without detailed specifications. Various design difficulties and design adjustments needed to match ion source characteristics were worked out with the breadboard. The breadboard PPA did not include full command capability and provided only limited telemetry data.

The EM PPA fabrication process provided the first opportunity to evaluate the electronic packaging design. Several problems were encountered in fitting the parts and circuits onto three circuit cards and in fitting the harnessed cards into the structural enclosure. To fit the circuitry into the structural package defined for SCATHA, most magnetic components were bonded to the circuit cards rather than using a stud attachment. During the EM phase, shake tests were performed by AFGL on simulated PPA cards to prove that the bonding technique was acceptable.

RM-SPIBS model PPU circuit cards were assembled at the Hughes Culver City plant by personnel familiar with flight electronics assembly in a clean room environment. Harness design and pin-to-pin wiring lists were prepared at Culver City from HRL schematics and parts layouts. The SPIBS EM- and RM-SPIBS were assembled concurrently. Magnetics were fabricated by the Hughes Culver City Components and Materials Laboratory; other PPA parts were purchased or fabricated by HRL. The quality assurance level applied to the RM-SPIBS PPA was primarily in terms of craftsmanship; complete inspection was not applied.

The RM-SPIBS circuit card designs and assembly process notes are shown in Figures 57 through 59 (drawings 1095560, 1095561, and 1095562). The structure of the circuit is machined out of magnesium stock for light weight. The terminal strips and magnetic components are bonded to the cards using Hughes process specification HP 16-103, Type 6. The electrical components are mounted between the terminal strips and hard-wired

THIS PAGE IS BEST QUALITY PRACTICABLE
FROM COPY FURNISHED TO DDC

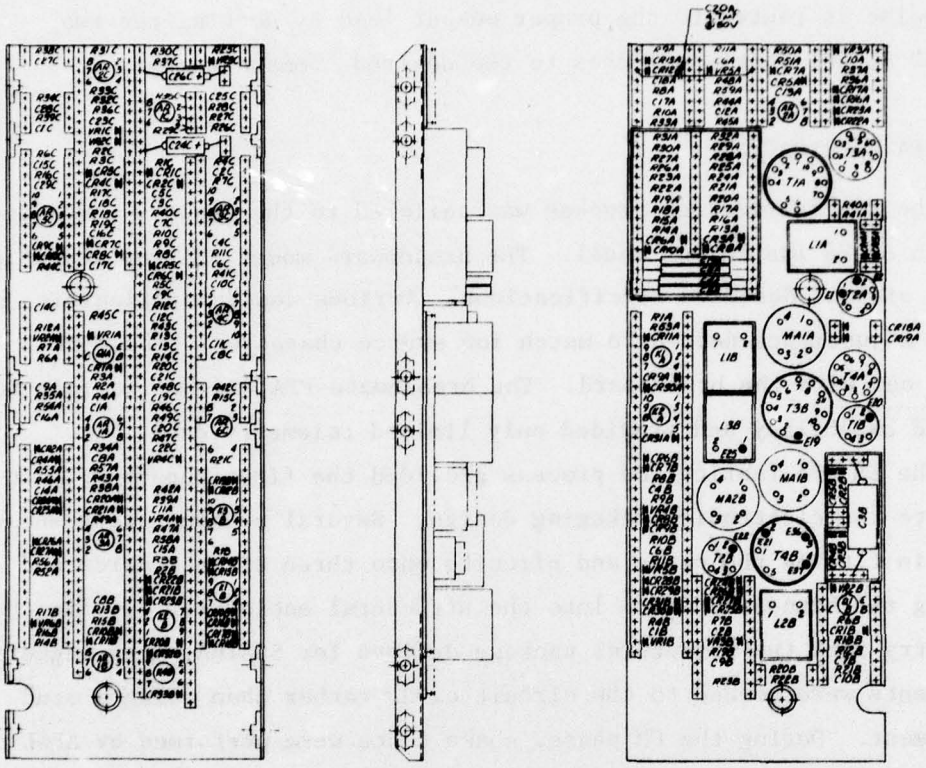

NOTES-UNLESS OTHERWISE SPECIFIED

1. INSTALL PER HP15-38.
2. BOND ALL FAYING SURFACES OF TERMINAL STRIPS MAGNETIC COMPONENTS AND SHEET PLASTIC LAMINATE PARTS, ITEMS 3,4,7 & 8, TO CKT BOARD AND EACH OTHER WHERE APPLICABLE PER HP16-103, TYPE G.
3. FOR SCHEMATIC DIAGRAMS SEE DWGS 1028190 (SCREEN ACCEL), 1028191 (CATHODE HTR AND DISCHARGE SUPPLY), 1028706 (ELECTROMETER #1).
4. ASSEMBLE PER HP11-53.
5. IDENTIFY PER HP8-5, TYPE II.
6. LETTER "A" OR "B" OR "C" ADDED TO COMPONENT REF DESIGNATOR FOR SCREEN ACCEL ("A" CKT), CATHODE HTR AND DISCHARGE SUPPLY ("B" CKT) AND ELECTROMETER #1 ("C" CKT).
7. "E" NO. DESIGNATIONS CODED ⓔ.
8. FOR H.V. AREAS WITH URALANE PER HP16-87 USING ALUMINUM OXIDE FILLER MMS 20-1795, TYPE I.
9. CONFORMAL COAT PER HP16-66, TYPE 1, CLASS 2.
10. PERFORM PICKLING PROCESS PER HP4-65 PRIOL TO INSTALLATION OF NUT PLATES ON MAGNESIUM CIRCUIT BOARD (1095571).
11. APPLY MARKER DESIGNATORS PER HP8-5 TYPE I, CLS, GRADE A, FORM 2 USING LETTRASET TRANSFER MARKINGS OVERCOAT MARKING DESIGNATORS PER HP8-56 TYPE I, CL 1 OR 2 USING HYSOL PC 18 OR PC 15 RESIN. MARK EVERY STD TERMINAL.
12. AFTER TESTING, FILLET BOND C7B, C8B, C7A, C8A C11B & R8A PER HP16-103 TYPE II, CLASS B.
13. BOND ITEMS 1,2,5 & 6, PER HP-25 TYPE 12.

Figure 57. Circuit card part layout drawing.

THIS PAGE IS BEST QUALITY PRACTICABLE
FROM COPY FURNISHED TO DDC

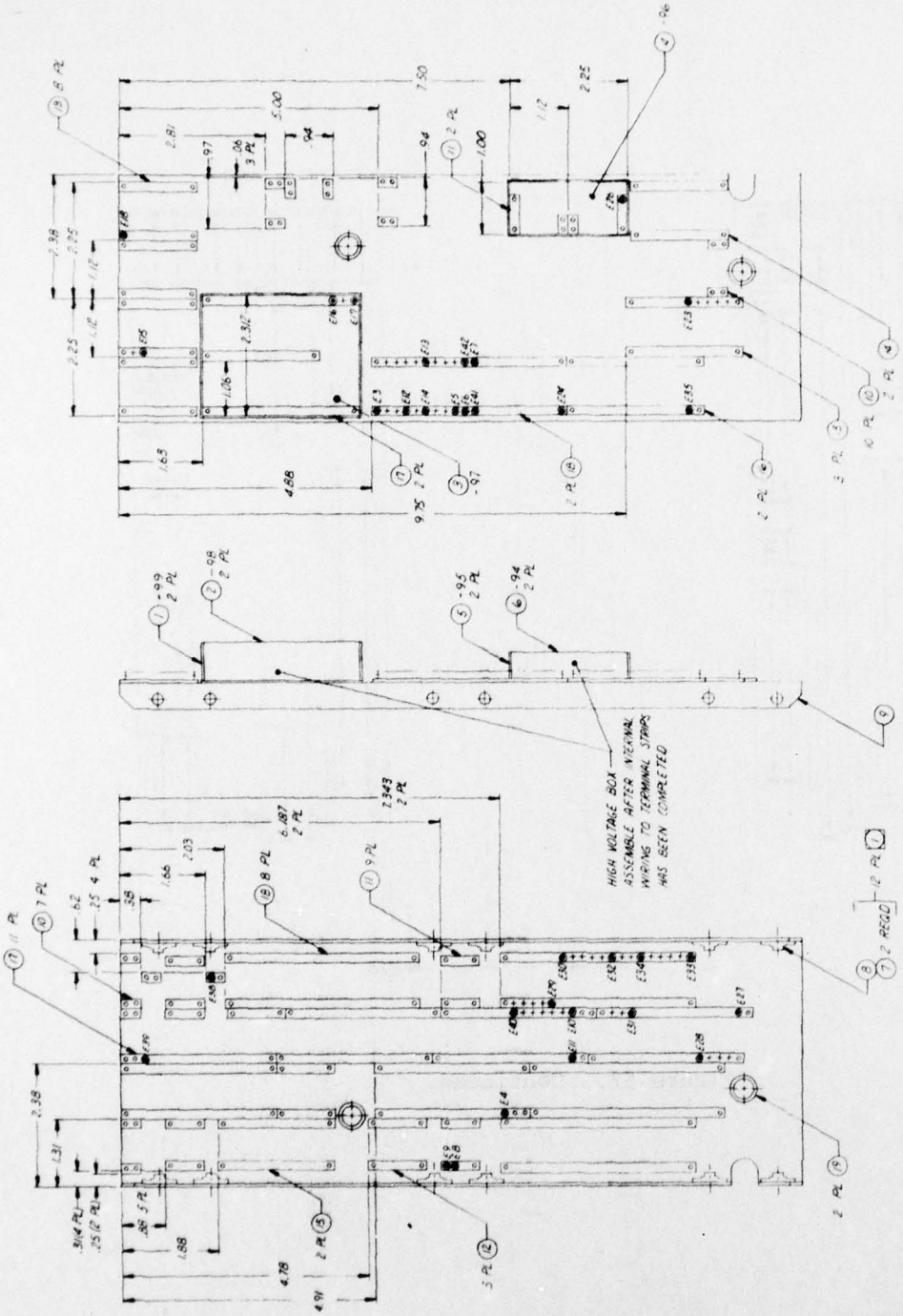

Figure 57. Continued.

THIS PAGE IS BEST QUALITY PRACTICABLE
FROM COPY FURNISHED TO DDC

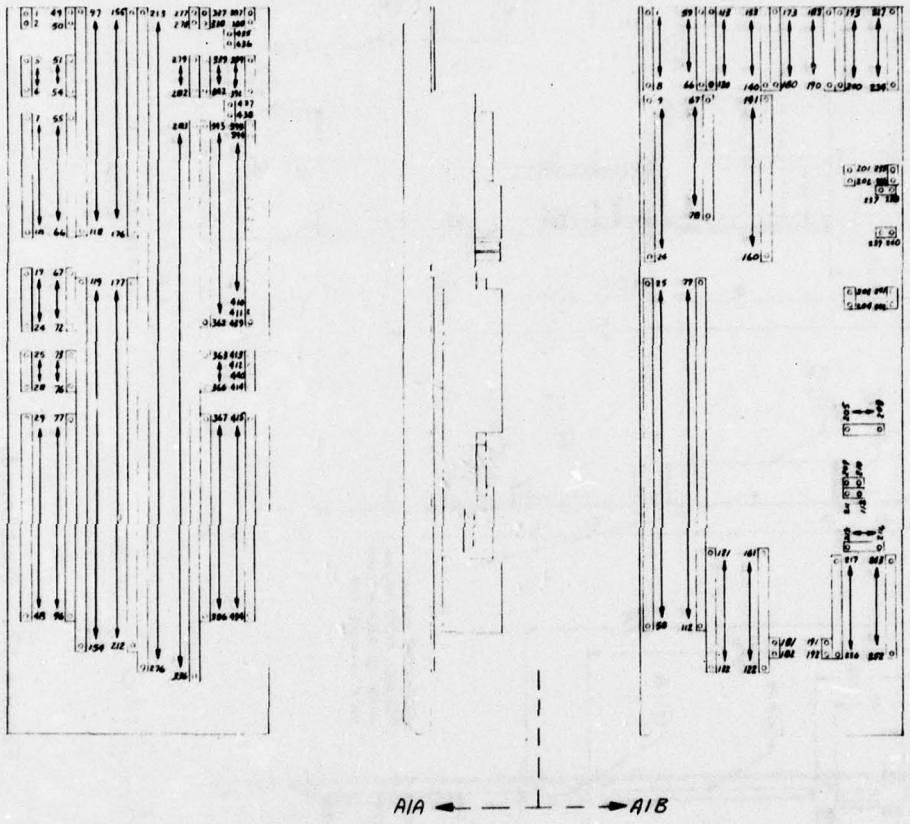

Figure 57. Continued.

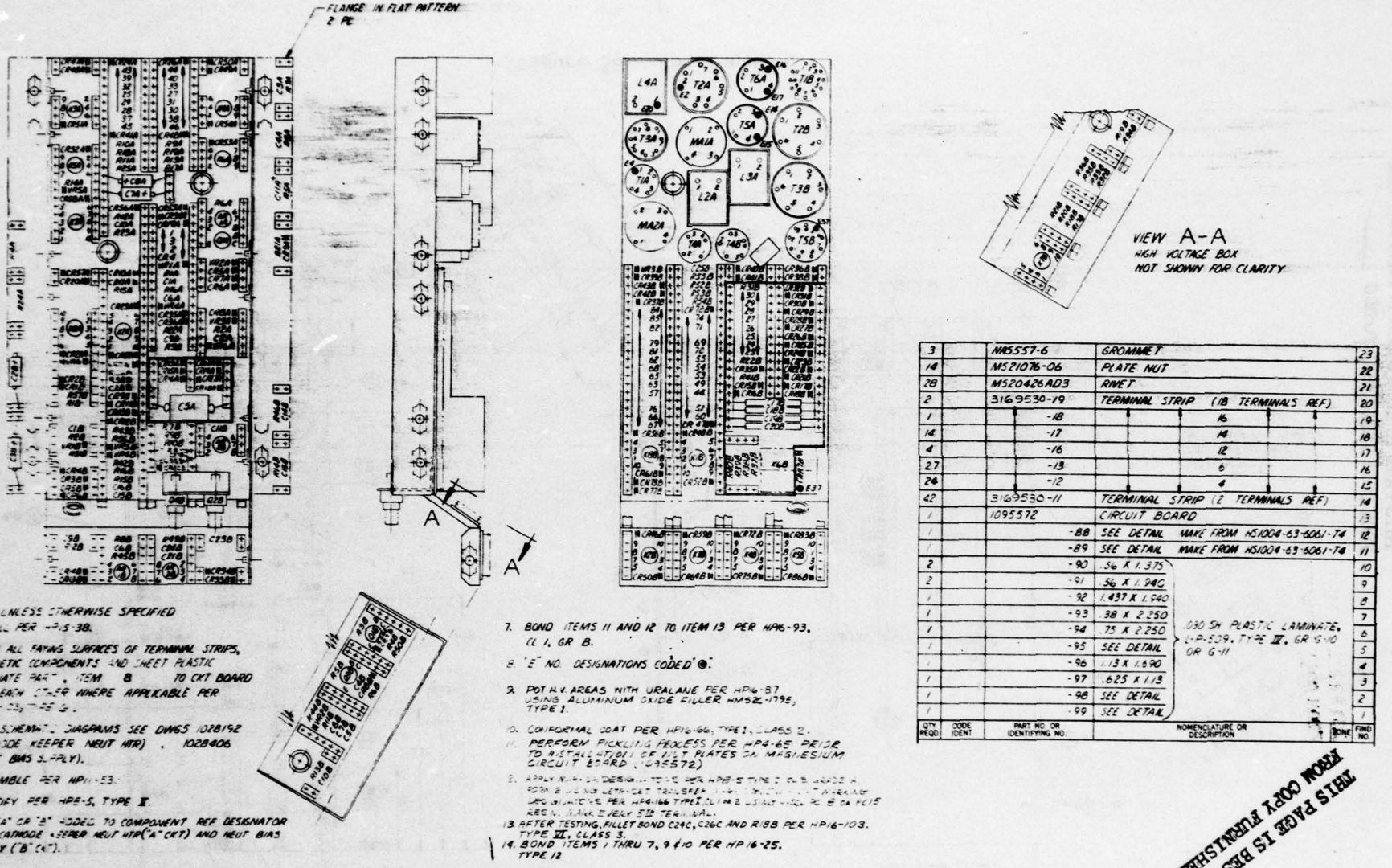

QTY REQD	CODE IDENT	PART NO. OR IDENTIFYING NO.	NOMENCLATURE OR DESCRIPTION	DONE	FIND NO.
3		NAS557-6	GROMMET		23
14		MS21076-06	PLATE NUT		22
28		MS20426AD3	RIVET		21
2		3169530-19	TERMINAL STRIP (18 TERMINALS REF)		20
1		-18	16		19
14		-17	14		18
4		-16	12		17
27		-13	6		16
24		-12	4		15
42		3169530-11	TERMINAL STRIP (2 TERMINALS REF)		14
1		1095572	CIRCUIT BOARD		13
1		-88	SEE DETAIL MAKE FROM HS1004-63-6061-T4		12
1		-89	SEE DETAIL MAKE FROM HS1004-63-6061-T4		11
2		-90	.56 X 1.375		10
2		-91	.56 X 1.940		9
1		-92	1.437 X 1.940		8
1		-93	.38 X 2.250		7
1		-94	.75 X 2.250		6
1		-95	SEE DETAIL		5
1		-96	1.13 X 1.690		4
1		-97	.625 X 1.13		3
1		-98	SEE DETAIL		2
1		-99	SEE DETAIL		1

.030 SH PLASTIC LAMINATE, L-P-509, TYPE II, GR G-10 OR G-11

NOTES - UNLESS OTHERWISE SPECIFIED

1. INSTALL PER HP16-38.
2. BOND ALL FAYING SURFACES OF TERMINAL STRIPS, MAGNETIC COMPONENTS AND SHEET PLASTIC LAMINATE PART, ITEM 8 TO CKT BOARD AND EACH OTHER WHERE APPLICABLE PER HP16-93, TYPE G.
3. FOR SCHEMATIC DIAGRAMS SEE DWGS 1028192 (CATHODE KEEPER NEUT HTR), 1028406 (NEUT BIAS SUPPLY).
4. ASSEMBLE PER HP16-53.
5. IDENTIFY PER HPE-5, TYPE II.
6. "A" OR "B" ADDED TO COMPONENT REF DESIGNATOR FOR CATHODE KEEPER NEUT HTR("A" CKT) AND NEUT BIAS SUPPLY ("B" CKT).
7. BOND ITEMS 11 AND 12 TO ITEM 13 PER HP16-93, CL 1, GR B.
8. "E" NO. DESIGNATIONS CODED ●.
9. POT H.V. AREAS WITH URALANE PER HP16-87 USING ALUMINUM OXIDE FILLER HMS2L-1795, TYPE 1.
10. CONFORMAL COAT PER HP16-66, TYPE 1, CLASS 2.
11. PERFORM PICKLING PROCESS PER HP4-65 PRIOR TO INSTALLATION OF ALL PLATES ON MAGNESIUM CIRCUIT BOARD (1095572)
12. APPLY NAMEPLATE DESIGNATING PER HP8-5 TYPE I CLB GRADE A FOR B OR METHOD TRUSSED [illegible] PER HP4-166 TYPE ALUM 2 USING ADHESIVE PER HP4-65 RESIN. BOND EVERY SIX TERMINAL.
13. AFTER TESTING, FILLET BOND C24C, C26C AND R18B PER HP16-103, TYPE II, CLASS 3.
14. BOND ITEMS 1 THRU 7, 9 & 10 PER HP16-25, TYPE 12

Figure 58. Circuit card part layout drawing.

THIS PAGE IS BEST QUALITY PRACTICABLE
FROM COPY FURNISHED TO DDC

THIS PAGE IS BEST QUALITY PRACTICABLE
FROM COPY FURNISHED TO DDC

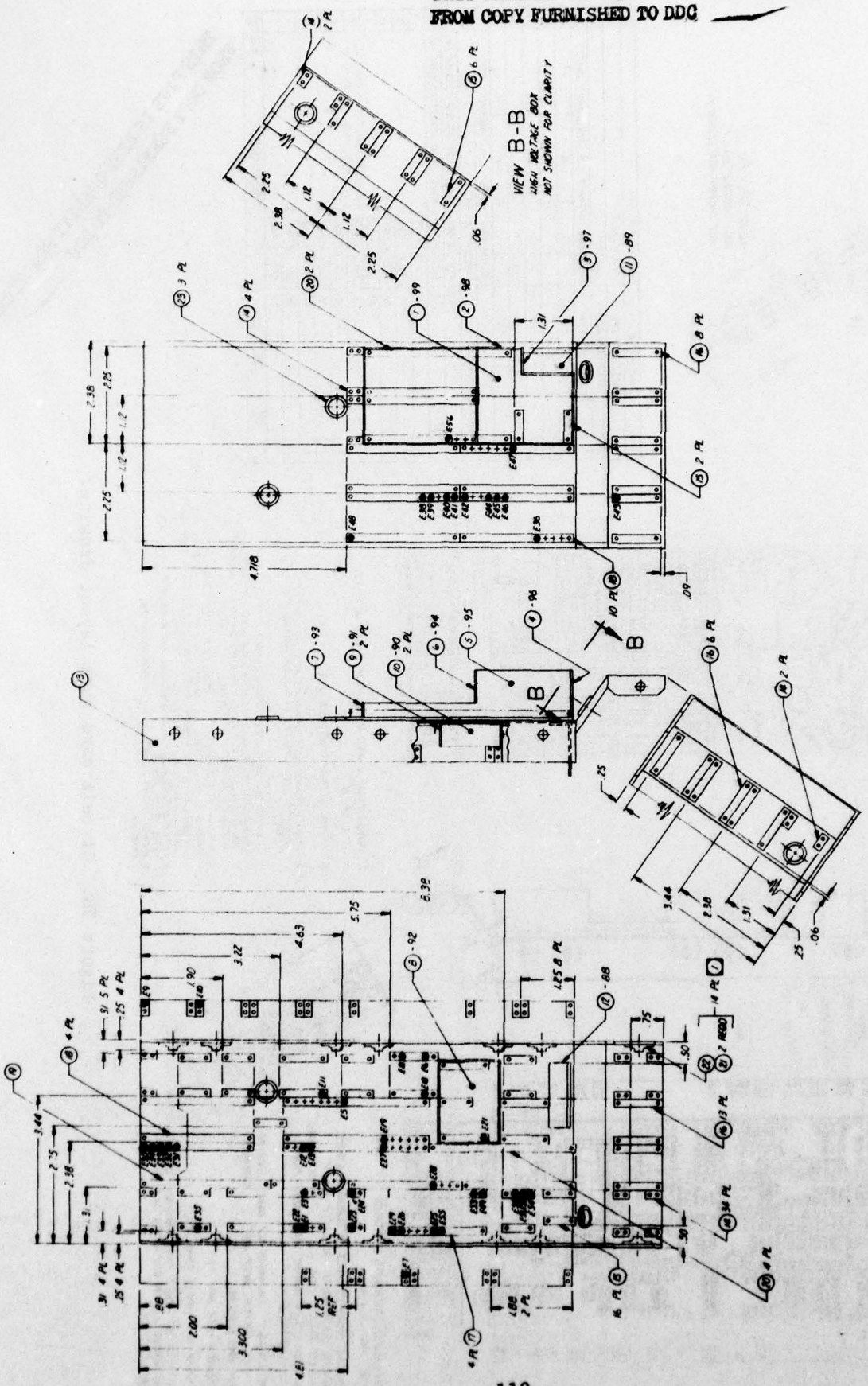

Figure 58. Continued.

THIS PAGE IS BEST QUALITY PRACTICABLE
FROM COPY FURNISHED TO DDC

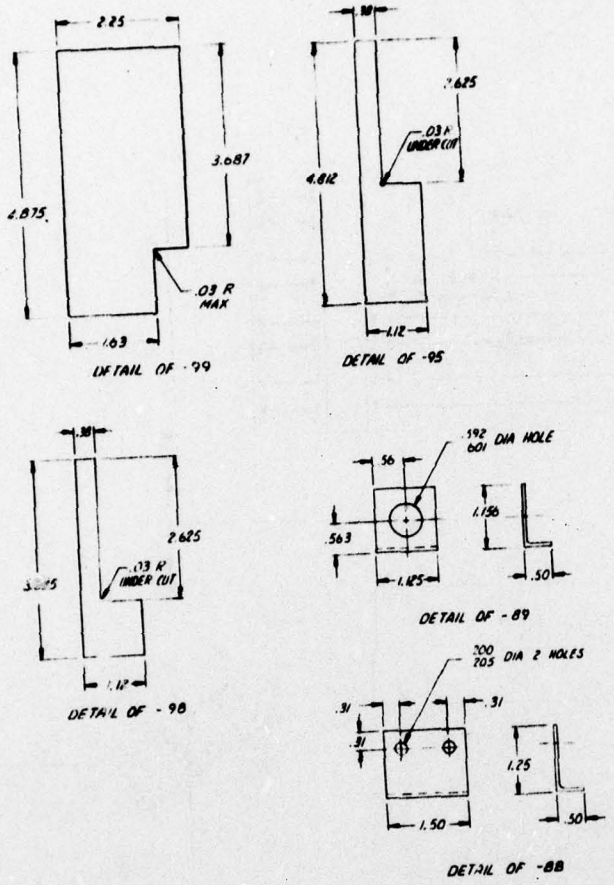

Figure 58. Continued.

THIS PAGE IS BEST QUALITY PRACTICABLE
FROM COPY FURNISHED TO DDC

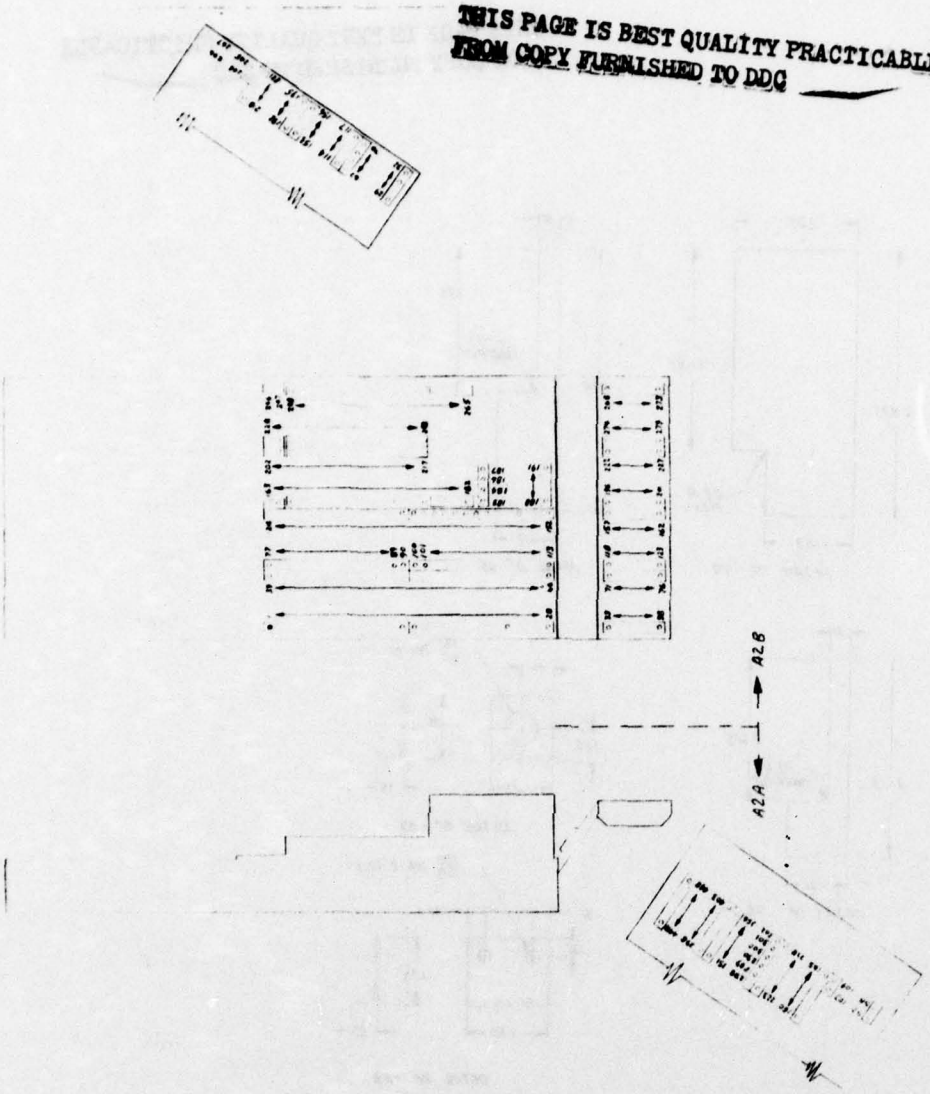

Figure 58. Continued.

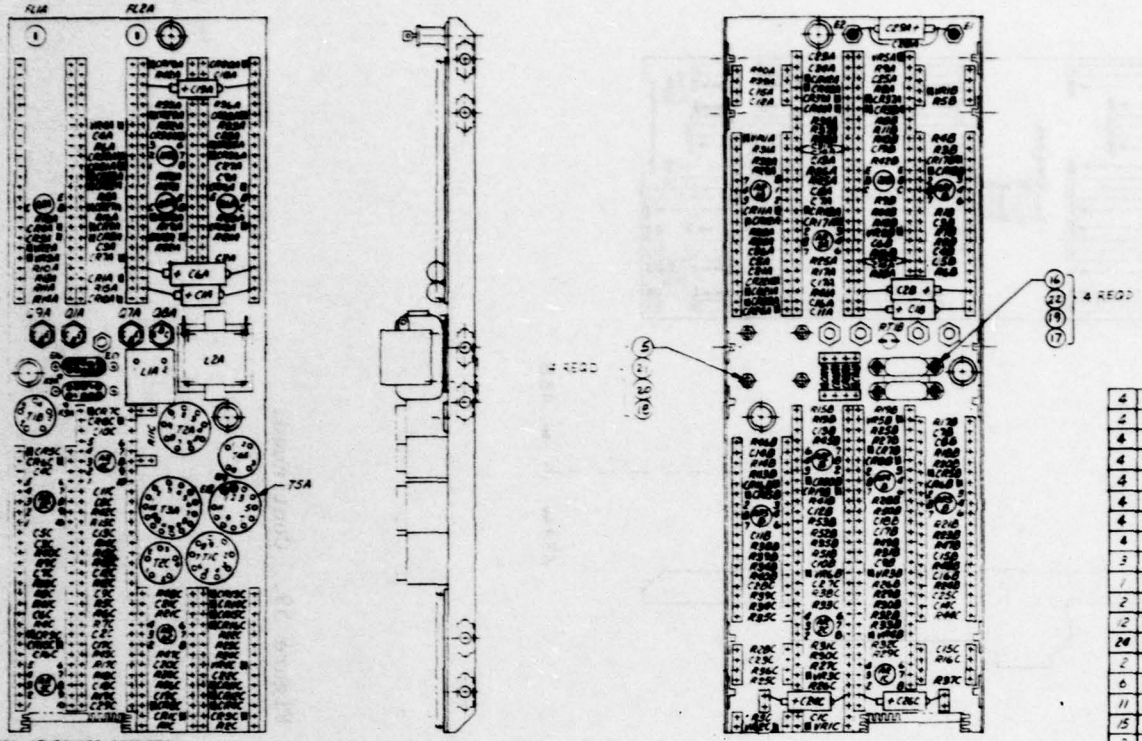

QTY REQD	CODE IDENT	PART NO. OR IDENTIFYING NO.	NOMENCLATURE OR DESCRIPTION	ZONE	FIND NO.
4		NAS 620 C2	FLAT WASHER		22
4		NAS 620 C6	FLAT WASHER		21
4		NAS 671 C6	NUT		20
4		NAS 671 C2	NUT		19
4		MS35338-136	LOCK WASHER		18
4		MS35338-134	LOCK WASHER		17
4		NAS 1635-02-4	SCREW		16
4		NAS 1635-06-5	SCREW		15
3		NAS557-8	GROMMET		14
1		MS21266-1N	GROMMET .687 LONG		13
2		MS21266-4N	GROMMET .312 LONG		12
12		MS21076-06	PLATE NUT		11
28		MS20426 AD3	RIVET		10
2		3169530-20	TERMINAL STRIP (20 TERMINALS REF)		9
6		-19	18		8
11		-18	16		7
15		-17	14		6
2		-16	12		5
10		-14	8		4
10		-12	4		3
9		3169530-11	TERMINAL STRIP (2 TERMINAL REF)		2
1		1095573	CIRCUIT BOARD		1

NOTES - UNLESS OTHERWISE SPECIFIED

1. INSTALL PER NPI5-38.
2. BOND ALL FAYING SURFACES OF TERMINAL STRIPS, MAGNETIC COMPONENTS AND STRIP GROMMETS TO CKT BOARD PER NPI6-103, TYPE G.
3. FOR SCHEMATIC DIAGRAMS SEE DWGS 1028500 (LINE REG AND AC DISTRIBUTION INVERTER), 1028636 (PRESS TEM TM), 1028602 (ELECTROMETER ⌀2)
4. ASSEMBLE PER NPII-53.
5. IDENTIFY PER NPB-5, TYPE II.
6. LETTER 'A' OR 'B' OR 'C' ADDED TO COMPONENT REF DESIGNATOR FOR LINE REG AND AC DISTRIBUTION INVERTER ('A' CKT), PRESS TEM TM ('B' CKT) AND ELECTROMETER ⌀2 ('C' CKT).
7. 'E' NO. DESIGNATIONS CODED ●.
8. CONFORMAL COAT PER NPI6-66, TYPE 1, CLASS 2.
9. PERFORM PICKLING PROCESS PER NP4-65 PRIOR TO INSTALLATION OF NUT PLATES ON MAGNESIUM CIRCUIT BOARD (1095573)
10. APPLY MARKER DESIGNATORS PER NPB-5 TYPE I, CL B, GRADE A, FORM E USING LETRASET TRANSFER MARKING. OVERCOAT MARKING DESIGNATORS PER NP4-166 TYPE I, CL 1 OR 2 USING HYSOL PC15 OR PC18 RESIN. MARK EVERY 5TH TERMINAL.
11. AFTER TESTING, FILLET BOND C1A, C6A, C9A, C18, C28, C29C, C26C & C29A PER NPI6-103, TYPE III, CLASS B.
12. AFTER TESTING, BOND Q2A, Q5A AND Q6A PER NPI6-99, TYPE B.

Figure 59. Circuit card part layout drawing.

THIS PAGE IS BEST QUALITY PRACTICABLE
FROM COPY FURNISHED TO DDC

THIS PAGE IS BEST QUALITY PRACTICABLE
FROM COPY FURNISHED TO DDC

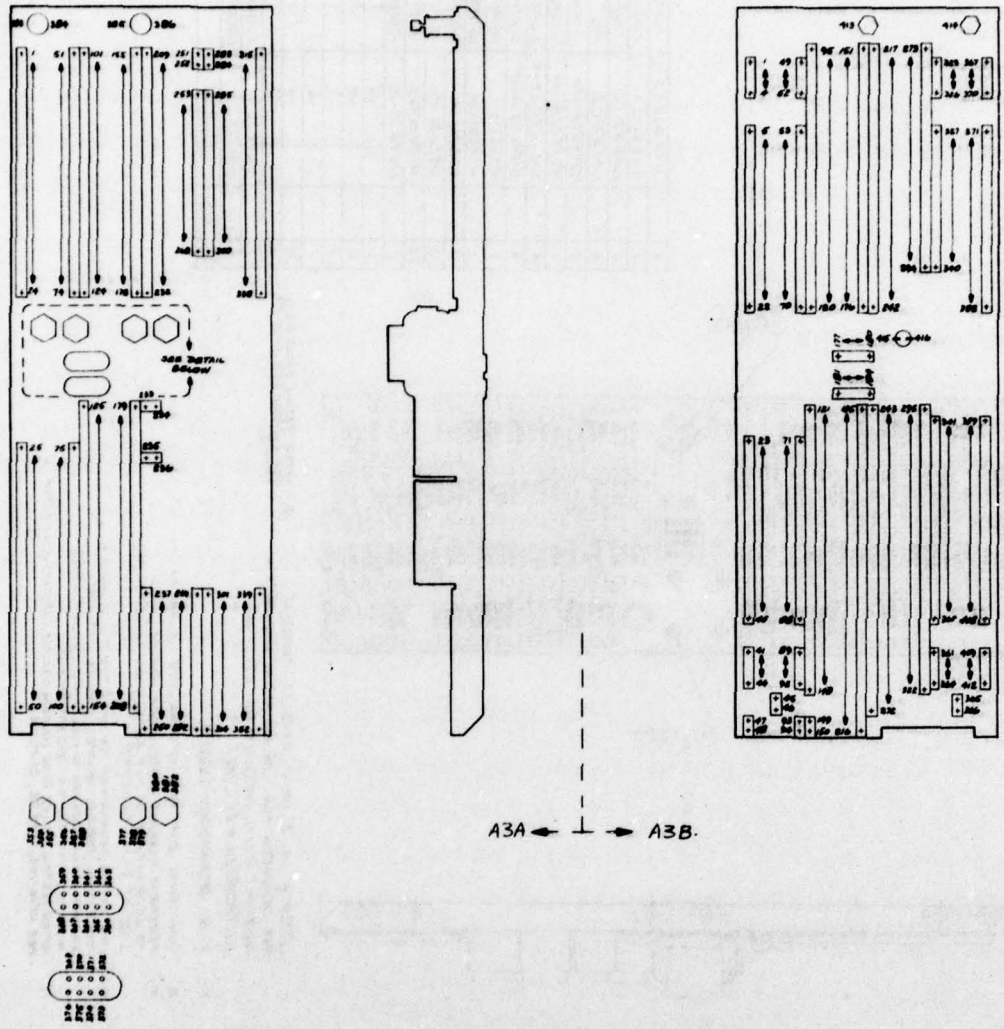

Figure 59. Continued.

THIS PAGE IS BEST QUALITY PRACTICABLE
FROM COPY FURNISHED TO DDC

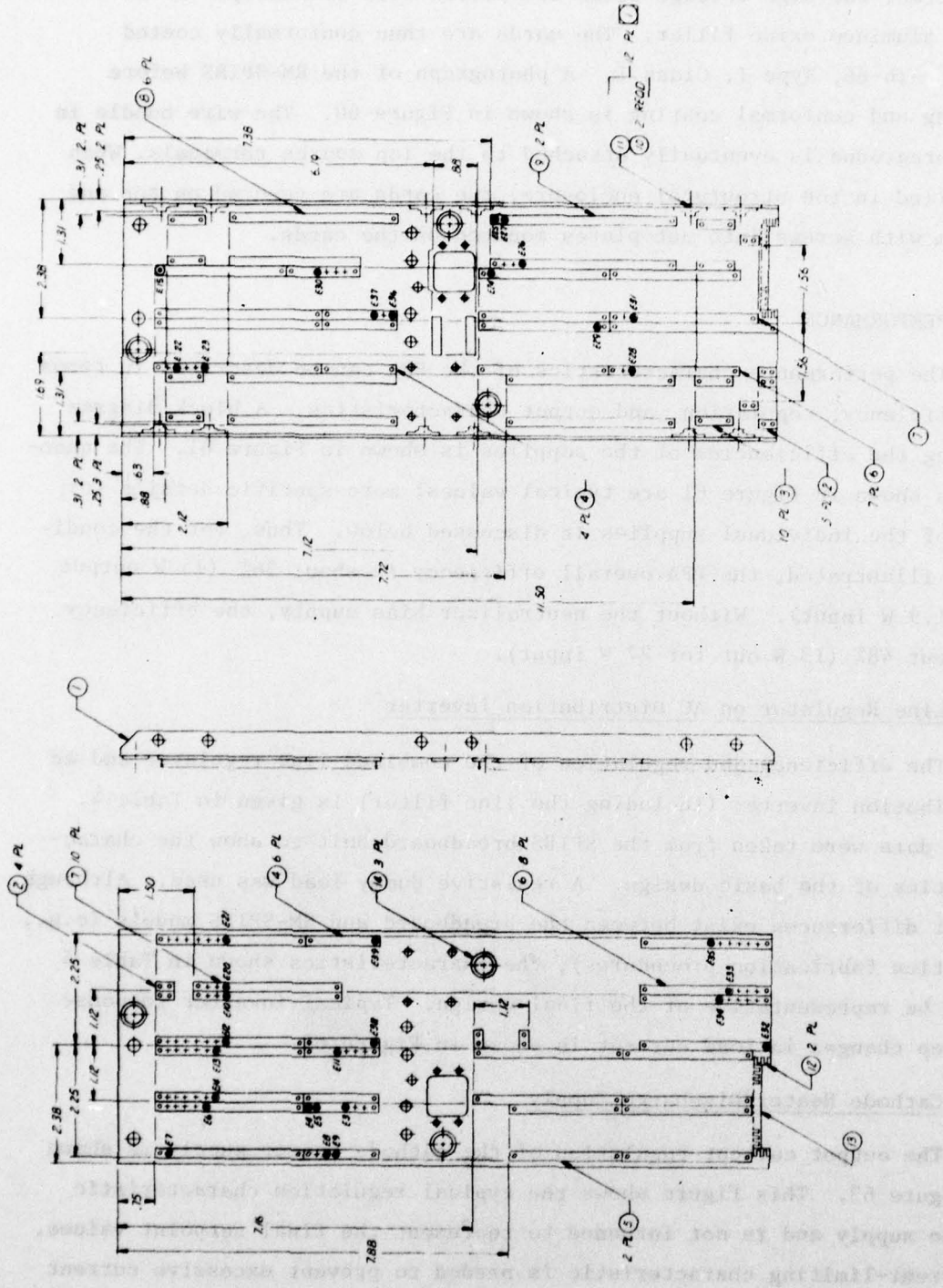

Figure 59. Continued.

together. After initial electrical testing of the circuit cards is completed, the high-voltage areas are potted with uralane per HP 16-8 using aluminum oxide filler. The cards are then conformally coated with HP-16-66, Type I, Class I. A photograph of the RM-SPIBS before potting and conformal coating is shown in Figure 60. The wire bundle in the foreground is eventually attached to the ion source terminals. When installed in the structural enclosure, the cards are secured on top and bottom with screws into nut plates mounted on the cards.

C. PERFORMANCE

The performance characteristics of the PPA can be described in terms of efficiency, regulation, and output characteristics. A block diagram showing the efficiencies of the supplies is shown in Figure 61. The quantities shown in Figure 61 are typical values; more specific details for each of the individual supplies is discussed below. Thus, for the conditions illustrated, the PPA overall efficiency is about 36% (15 W output for 41.9 W input). Without the neutralizer bias supply, the efficiency is about 48% (13 W out for 27 W input).

1. Line Regulator on AC Distribution Inverter

The efficiency and regulation of the combined line regulator and ac distribution inverter (including the line filter) is given in Table 4. These data were taken from the SPIBS breadboard unit to show the characteristics of the basic design. A resistive dummy load was used. Although slight differences exist between the breadboard and RM-SPIBS models (e.g., magnetics fabrication procedures), the characteristics shown in Table 4 would be representative of the final design. Typical inverter response to step changes in load current is shown in Figure 62.

2. Cathode Heater/Discharge Supply

The output current regulation of the cathode heater supply is shown in Figure 63. This figure shows the typical regulation characteristic of the supply and is not intended to represent the final setpoint values. A current-limiting characteristic is needed to prevent excessive current at turn-on when heater resistance is low (i.e., about 0.1 Ω hot).

7844-85

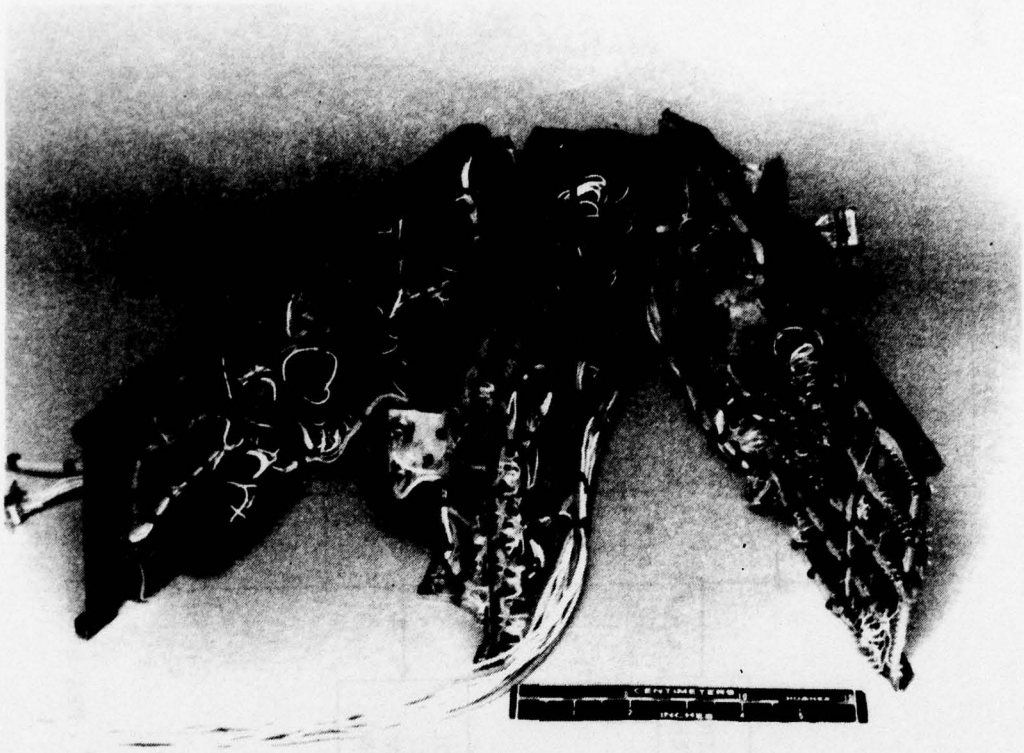

Figure 60. Flight PPA before potting and conformal coating.

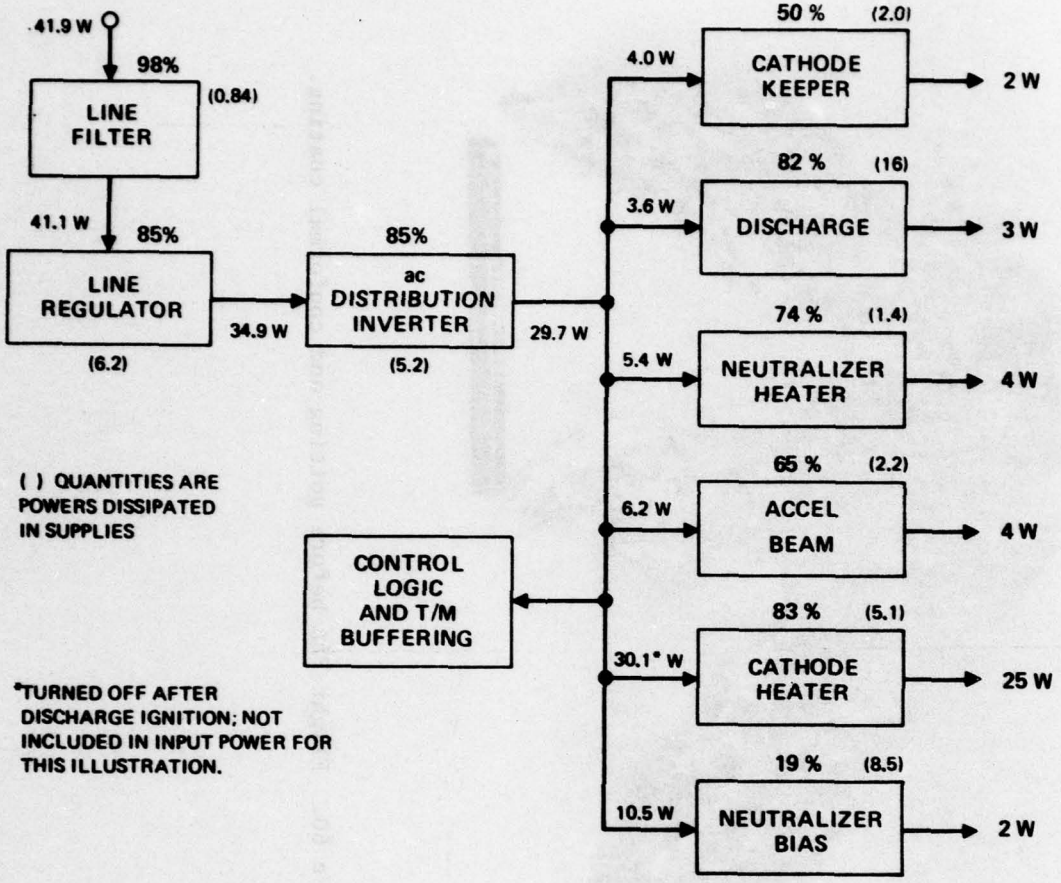

Figure 61. PPA efficiency block diagram.

Table 4. Line Regulator and AC Inverter Efficiency

Input Voltage, Vdc	Input Current, A	Input Power, W	Output Voltage, Vrms	Output Current, A	Output Power, W	Efficiency, %
21	1.3	27.3	41.5	0.5	20.75	76.01
	2.39	50.19	39.9	1.0	39.9	79.50
	3.15	66.15	37.0	1.5	55.5	83.90
25	1.28	32.0	42.3	0.5	21.5	66.09
	2.2	55.0	41.8	1.0	41.8	76.00
	3.25	81.25	40.5	1.6	64.8	79.75
30	1.0	30.0	42.3	0.5	21.15	70.5
	1.86	55.8	42.0	1.0	42.0	75.27
	2.76	82.8	40.5	1.6	64.8	78.26
35	0.87	30.45	42.3	0.5	21.15	69.46
	1.64	57.4	42.0	1.0	42.0	73.17
	2.3	80.5	40.5	1.5	60.75	75.46

T6327

The cathode heater supply efficiency as a function of output power is presented in Figure 64. This typical (breadboard) curve demonstrates the effect of load resistance on the efficiency of the supply. Since the output power is 15 to 20 W, efficiencies of 85 to 90% are achieved with this supply.

The discharge supply output current regulation for several setpoints is shown in Figure 65. Discharge voltage is determined by plasma characteristics, which in turn depend on xenon flow rate. Discharge current

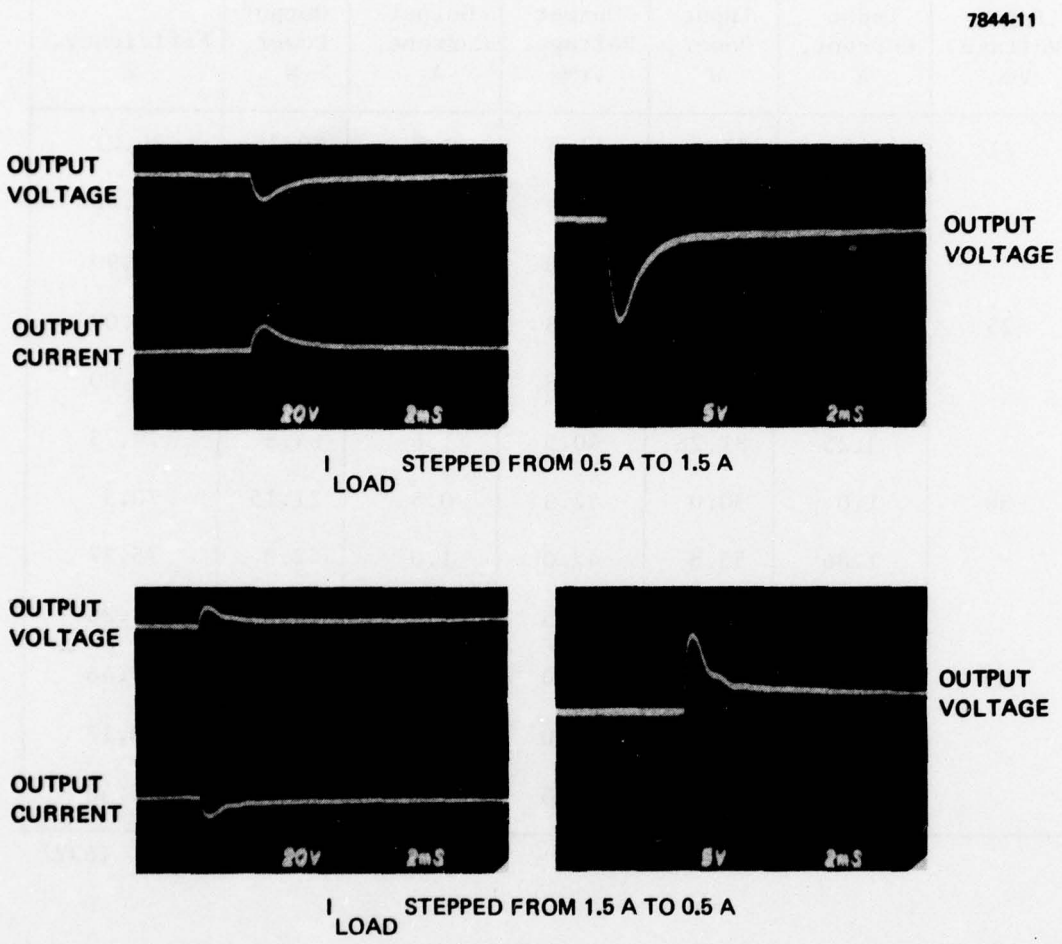

Figure 62. Inverter response to step changes in load current.

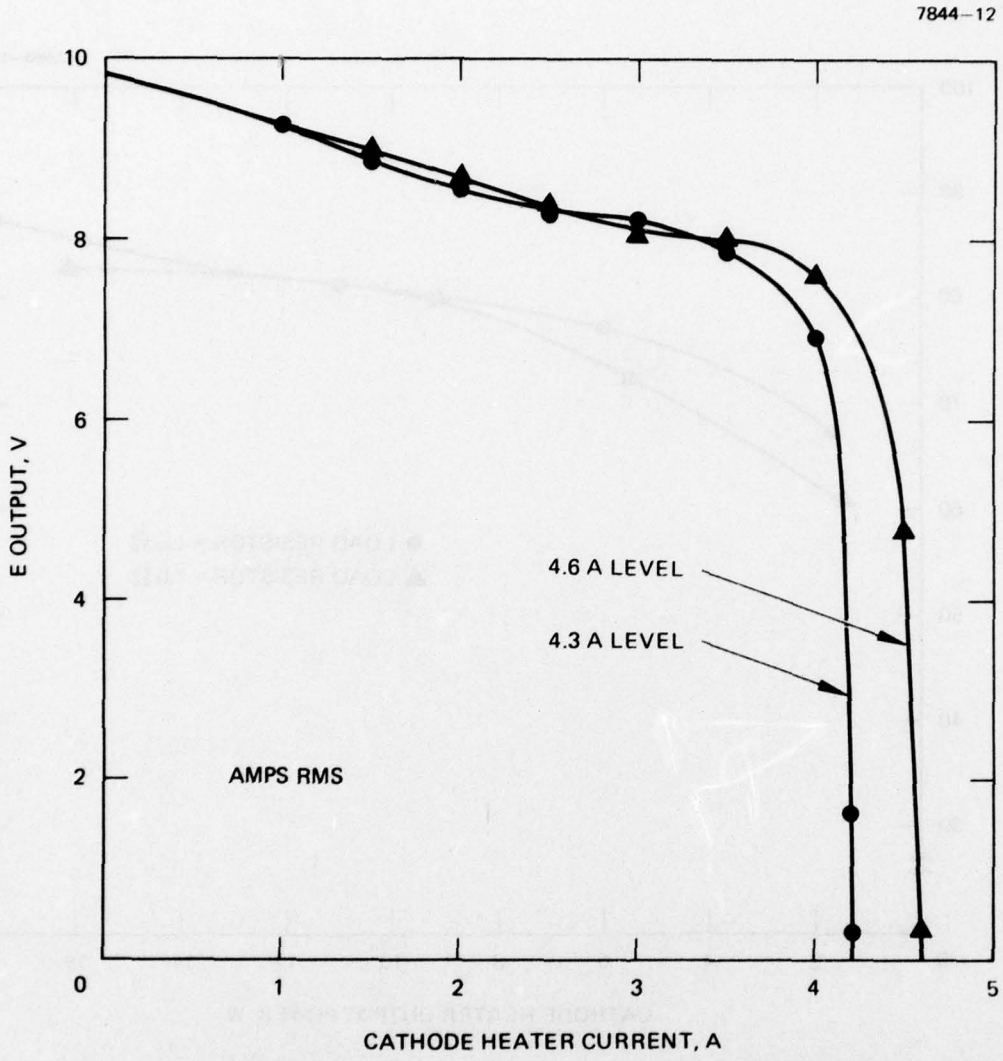

Figure 63. Cathode heater supply output characteristics.

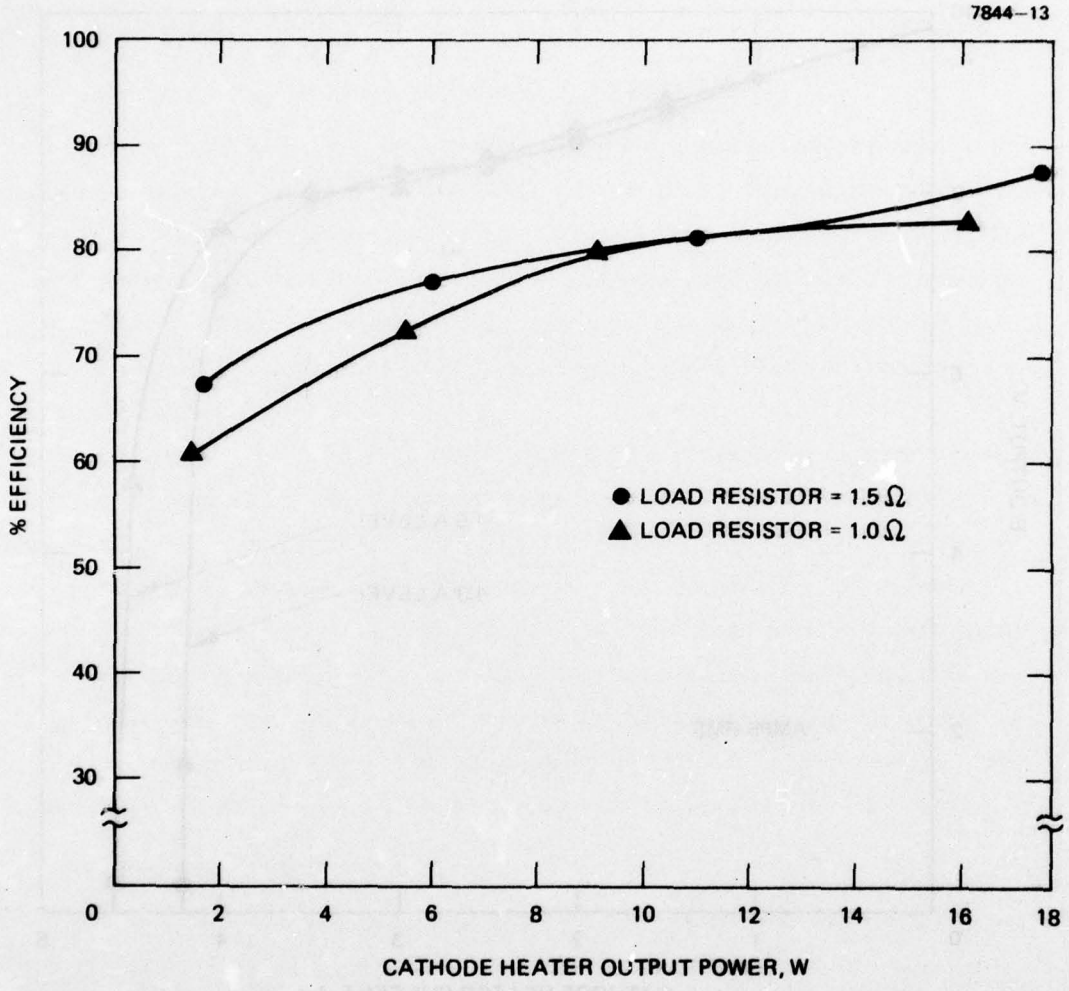

Figure 64. Cathode heater supply efficiency versus output power.

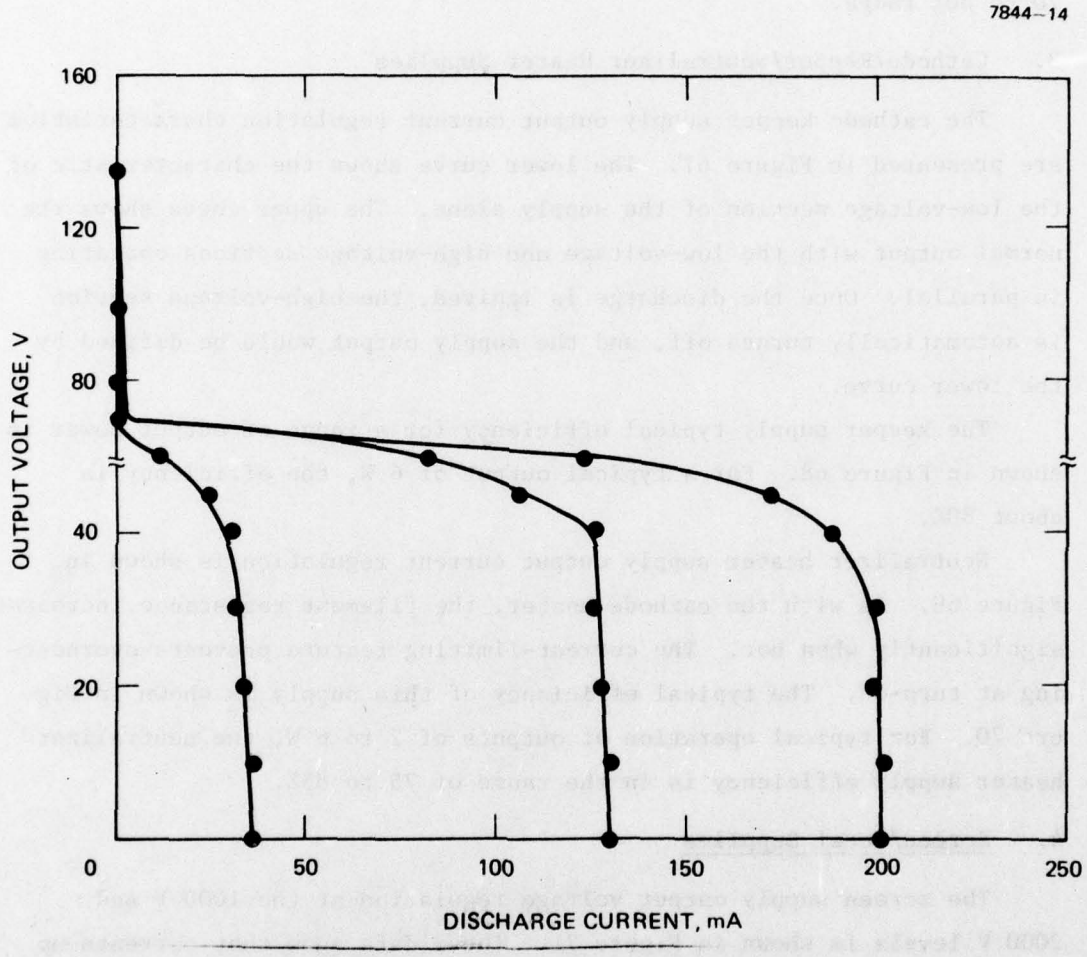

Figure 65. Discharge supply output characteristic.

levels are adjusted to produce the desired beam current. The typical efficiency of the supply when operating into a fixed load impedance and when operating at a fixed output voltage is shown in Figure 66. Thus, for most operating conditions, the discharge supply efficiency is in the 70 to 80% range.

3. Cathode/Keeper/Neutralizer Heater Supplies

The cathode keeper supply output current regulation characteristics are presented in Figure 67. The lower curve shows the characteristic of the low-voltage section of the supply alone. The upper curve shows the normal output with the low-voltage and high-voltage sections operating in parallel. Once the discharge is ignited, the high-voltage section is automatically turned off, and the supply output would be defined by the lower curve.

The keeper supply typical efficiency for a range of output power is shown in Figure 68. For a typical output of 6 W, the efficiency is about 80%.

Neutralizer heater supply output current regulation is shown in Figure 69. As with the cathode heater, the filament resistance increases significantly when hot. The current-limiting feature prevents overheating at turn-on. The typical efficiency of this supply is shown in Figure 70. For typical operation at outputs of 2 to 6 W, the neutralizer heater supply efficiency is in the range of 75 to 85%.

4. Screen/Accel Supplies

The screen supply output voltage regulation at the 1000 V and 2000 V levels is shown in Figure 71. These data show that currents up to 3 mA can be obtained at full voltage. The combined efficiency of the screen/accel supplies is presented in Figure 72. The typical efficiency curve is plotted against combined output power, with the two major operating levels noted. Since accel power represents less than 5% of the total power, the power scale is essentially beam power.

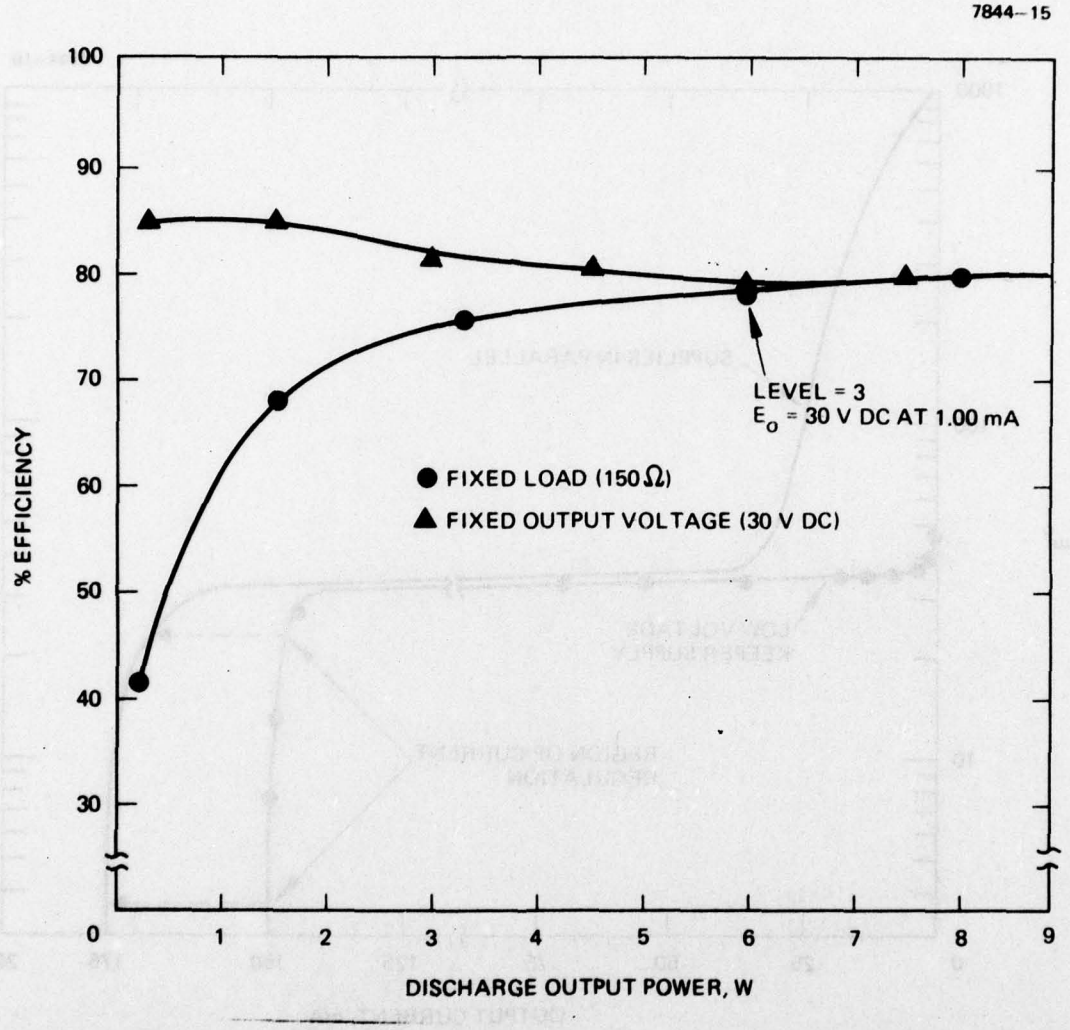

Figure 66. Discharge supply efficiency versus output power.

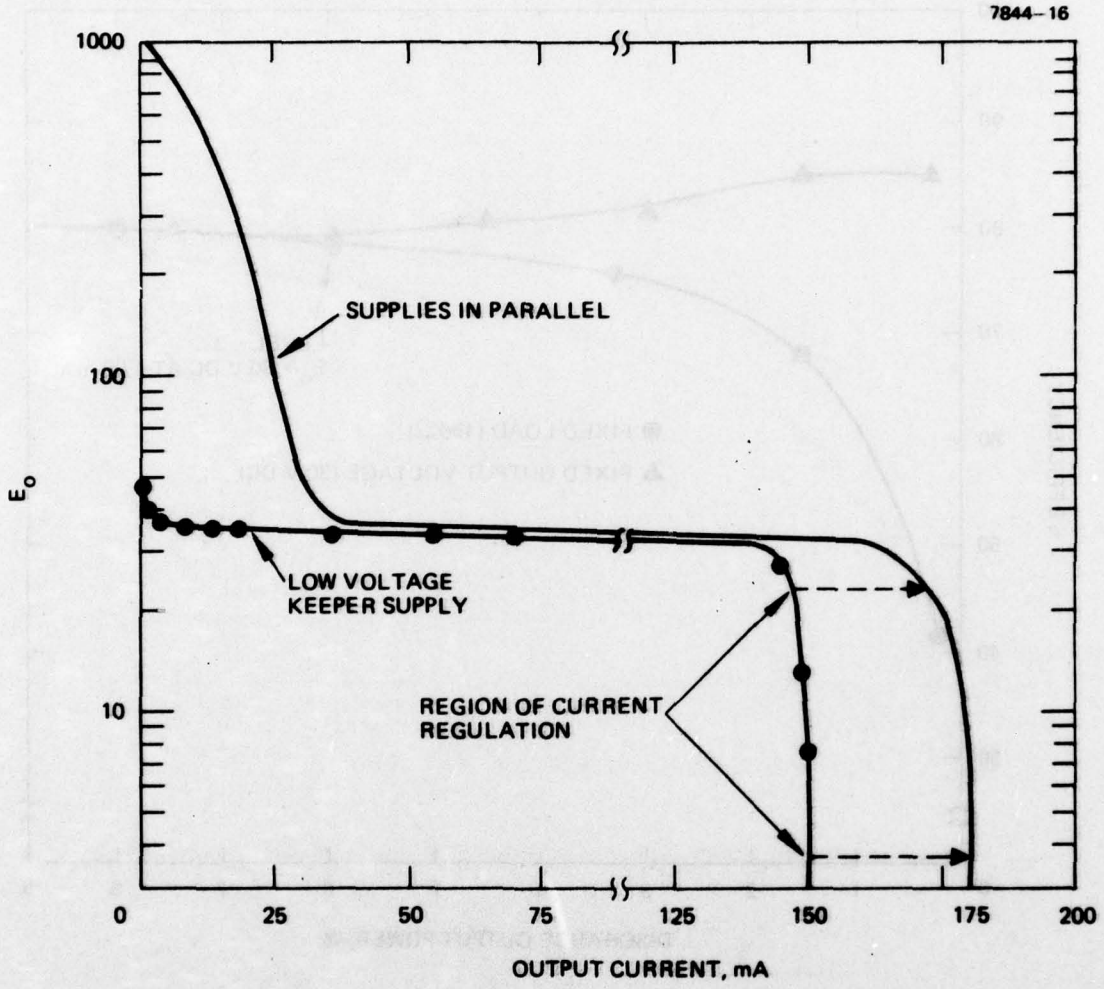

Figure 67. Keeper supply output current regulation.

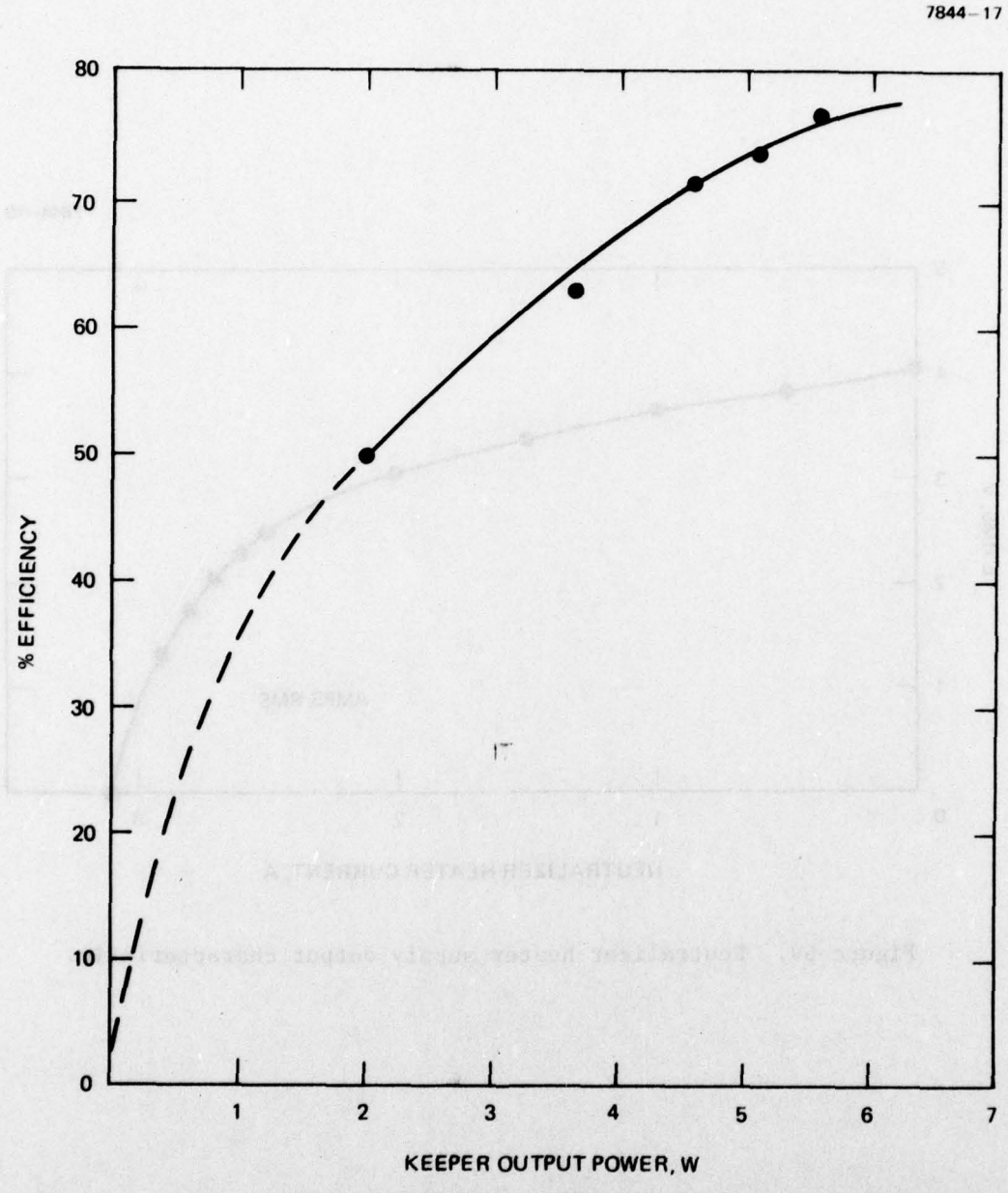

Figure 68. Keeper supply efficiency versus output power.

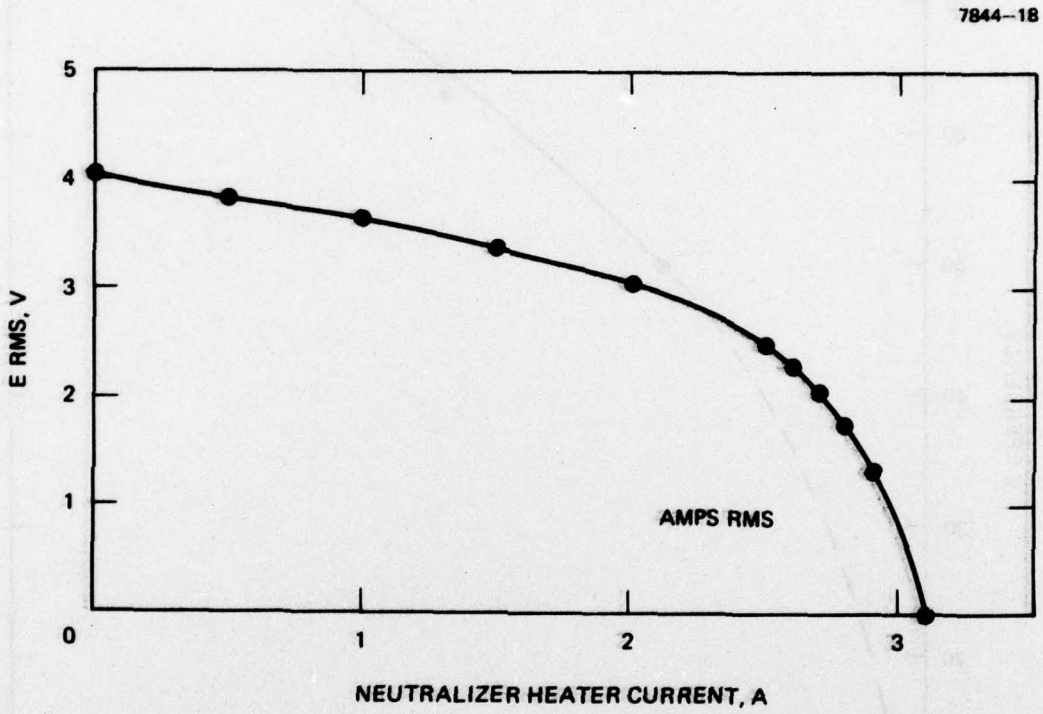

Figure 69. Neutralizer heater supply output characteristic.

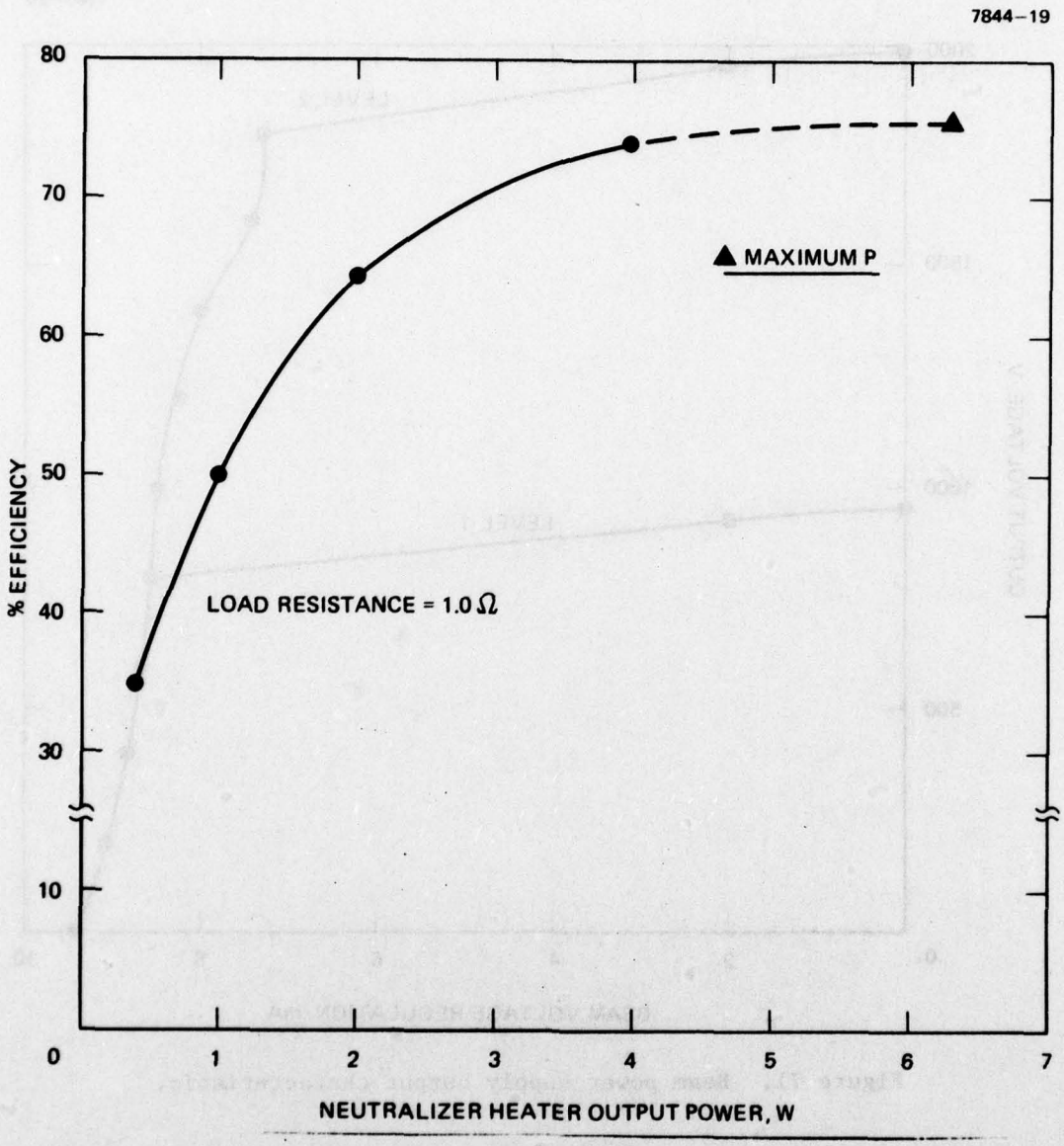

Figure 70. Neutralizer heater supply output characteristic.

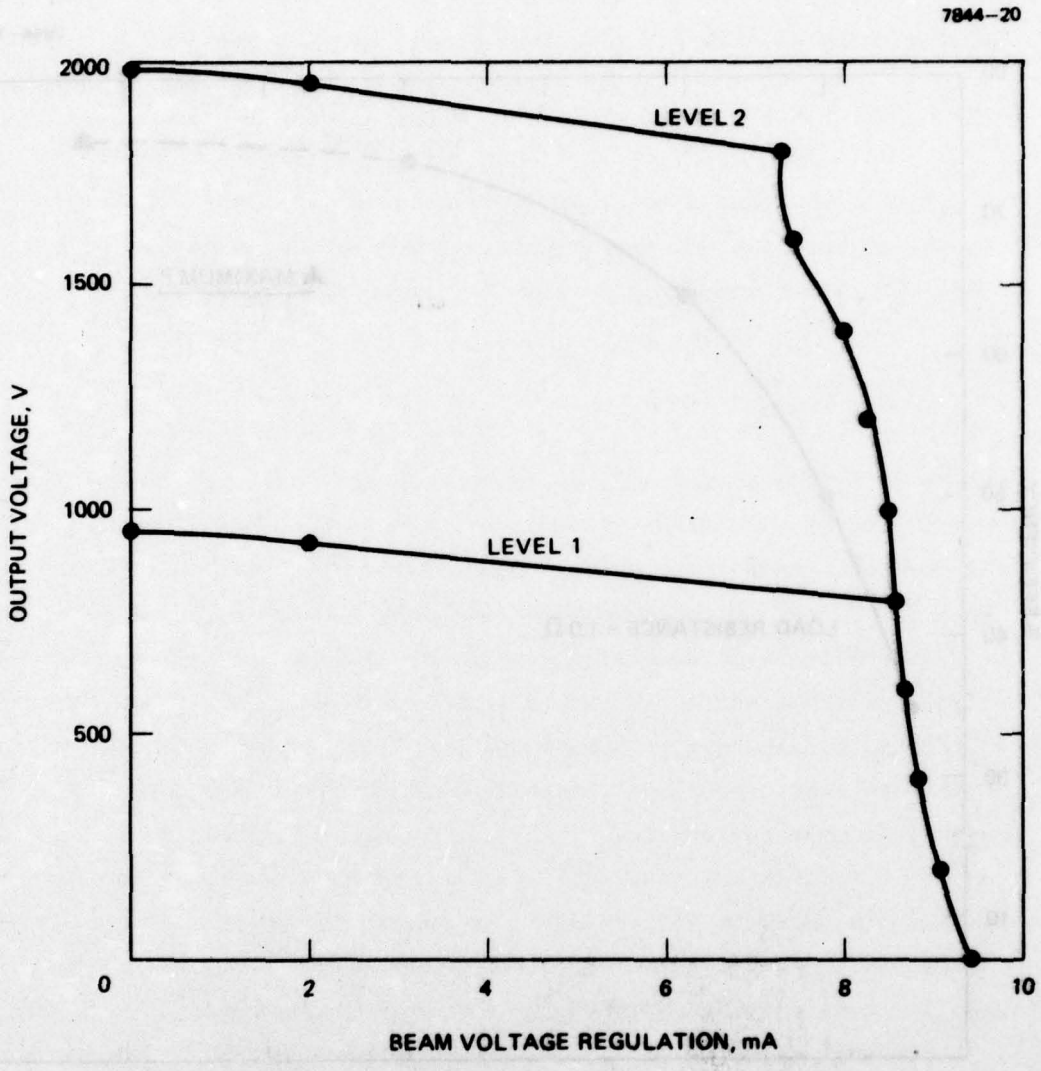

Figure 71. Beam power supply output characteristic.

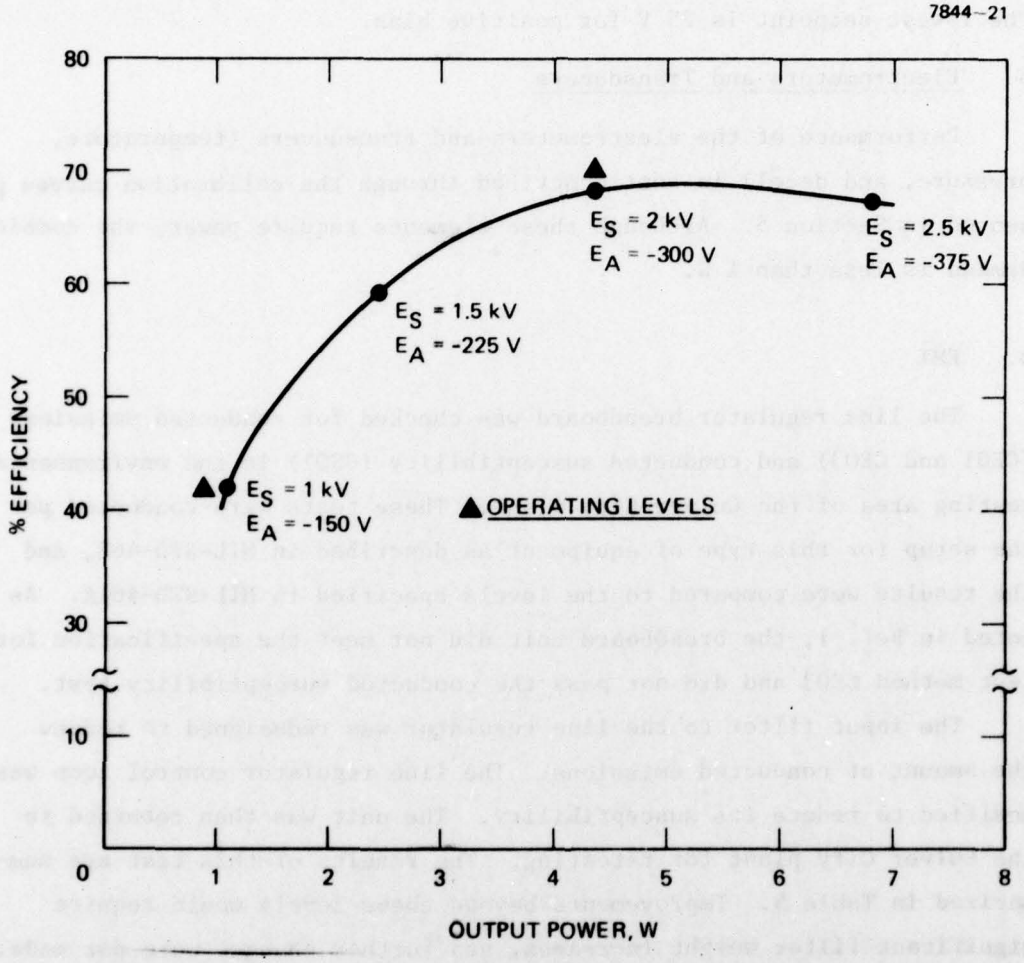

Figure 72. Beam power supply efficiency versus output power.

5. Neutralizer Bias Supply

Output voltage regulation curves for the neutralizer bias supply with negative and positive bias are shown in Figures 73 and 74, respectively. The curves in each figure represent the five setpoint levels. The lowest setpoint is 25 V for positive bias.

6. Electrometers and Transducers

Performance of the electrometers and transducers (temperature, pressure, and decel) is best described through the calibration curves presented in Section 5. Although these elements require power, the combined demand is less than 1 W.

D. EMI

The line regulator breadboard was checked for conducted emissions (CE01 and CE03) and conducted susceptibility (CS01) in the environmental testing area of the Culver City plant. These tests were conducted per the setup for this type of equipment as described in MIL-STD-462, and the results were compared to the levels specified in MIL-STD-461A. As noted in Ref. 1, the breadboard unit did not meet the specification for test method CE03 and did not pass the conducted susceptibility test.

The input filter to the line regulator was redesigned to reduce the amount of conducted emissions. The line regulator control loop was modified to reduce its susceptibility. The unit was then returned to the Culver City plant for retesting. The results of this test are summarized in Table 5. Improvements beyond these levels would require significant filter weight increases, and further changes were not made. Additional EMI tests conducted by AFGL with the EM system indicated satisfactory performance.

E. INPUT LINE TRANSIENTS

The major transient on the power bus occurs when power is applied to the PPA (*Instrument on* command). The current surge observed is the result of charging the line regulator input filter capacitor. Tests

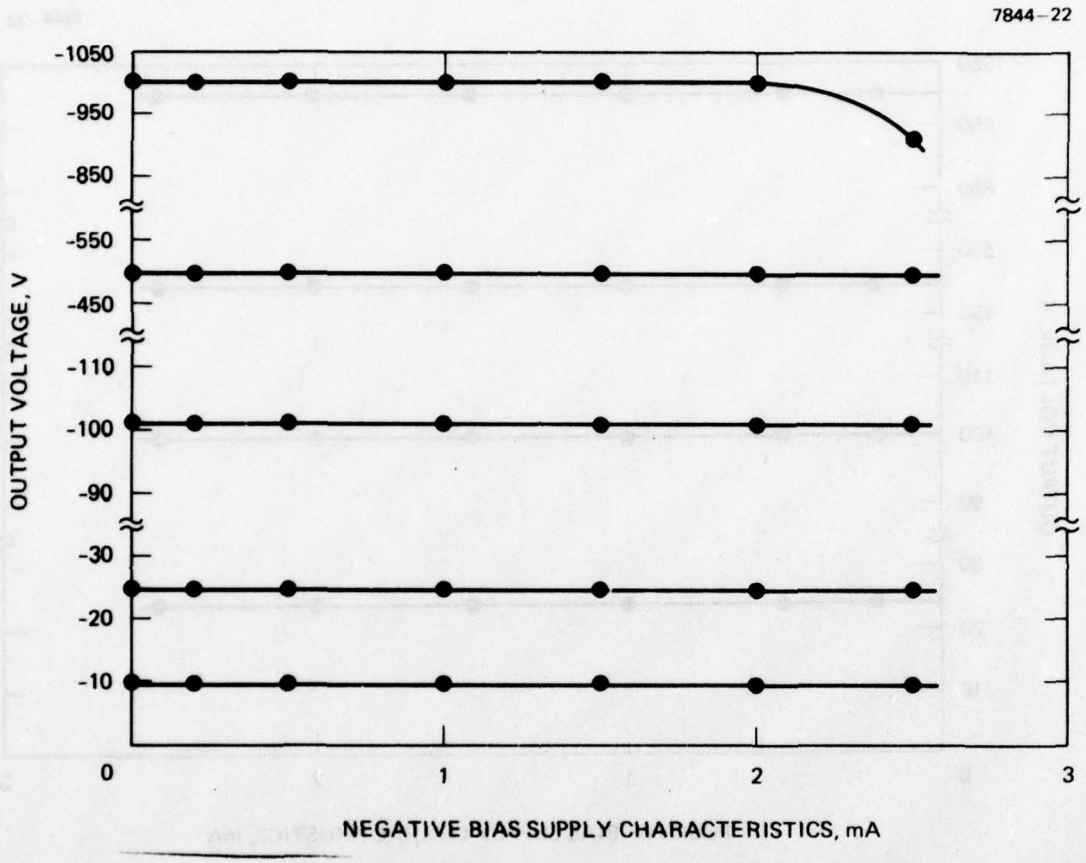

Figure 73. Bias supply negative output characteristic.

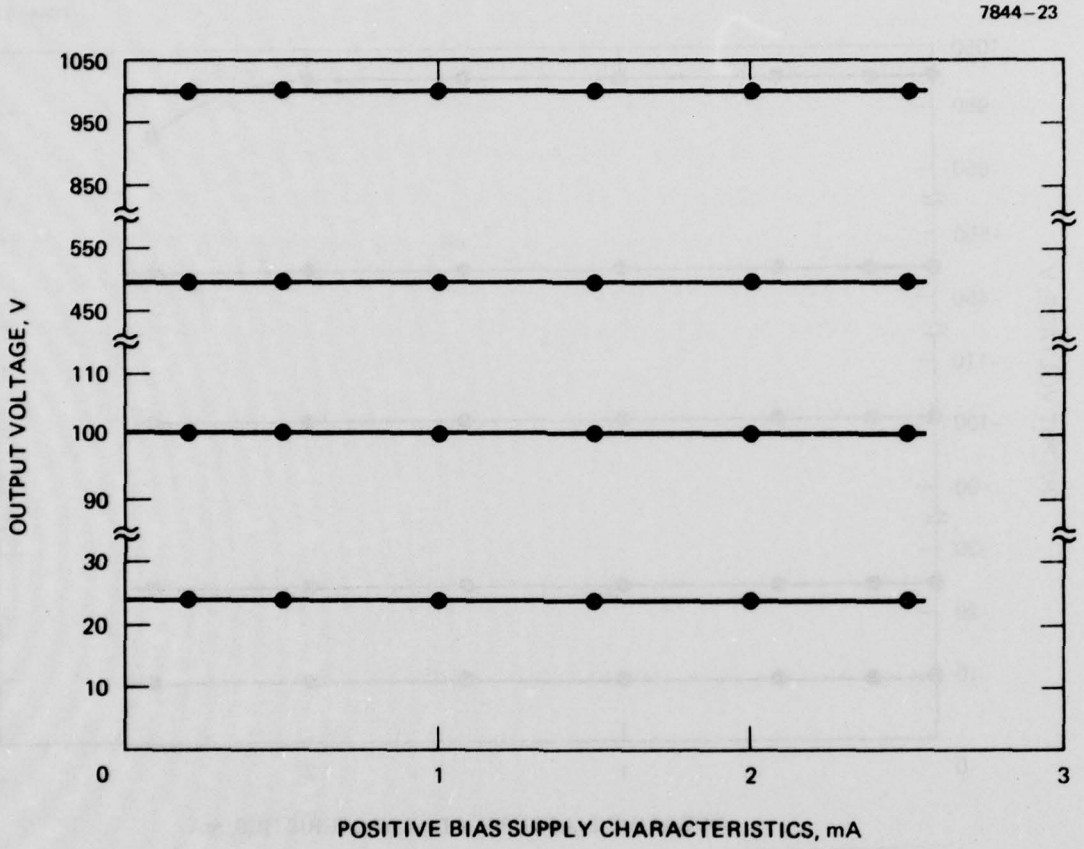

Figure 74. Bias supply positive output characteristic.

Table 5. Summary of EMI Test Data: SPIBS Line Regulator

(9 July 1976)

Operating Mode	Test Method	Test Point	Type of Int.	Max Over Spec.
32 V	CE01	+28 Vdc	Broadband	Within specified limits
	CE01	+28 Vdc	Narrowband	Within specified limits
	CE01	DC return	Broadband	Within specified limits
	CE01	DC return	Narrowband	Within specified limits
	CE03	+28 Vdc	Broadband	+2 dB at 2.29 MHz
	CE03	+28 Vdc	Narrowband	+11 dB at 1.85 MHz
	CE03	DC return	Broadband	+10 dB at 2.27 MHz
	CE03	DC return	Narrowband	+9 dB at 1.7 MHz
24 V	CE01	+28 Vdc	Broadband	Within specified limits
	CE01	+28 Vdc	Narrowband	Within specified limits
	CE01	DC return	Broadband	Within specified limits
	CE01	DC return	Narrowband	Within specified limits
	CE03	+28 Vdc	Broadband	Within specified limits
	CE03	+28 Vdc	Narrowband	+8 dB at 1.66 MHz
	CE03	DC return	Broadband	+2 dB at 2.28 MHz
	CE03	DC return	Narrowband	+10 dB at 1.73 MHz

were performed on the breadboard system to determine the peak value of the turn on current surge. The first test performed used the input filter configuration present during the 10 March 1976 EMI test. A photograph of the surge current is shown in Figure 75. The peak current observed in this figure is 30 A. The line regulator was retested using the EMI filter additions, with the results shown in Figure 76. The initial 43-A peak observed in this test, and not observed in the previous test, is due to the addition of capacitance between the input filter choke and the input power bus. Since the additional current peak is of short duration and would not adversely affect the spacecraft fusing requirements, it was decided to finalize the filter design in the configuration used in the 9 July 1976 EMI test. The RM-SPIBS instrument characteristic is expected to be similar to that shown in Figure 76.

7844-24

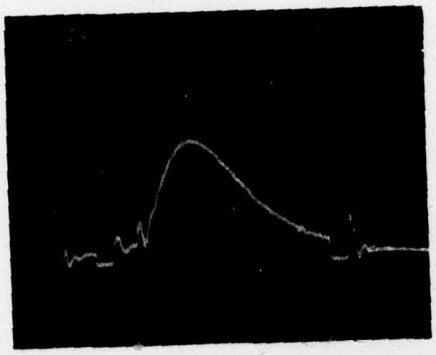

Figure 75. PPA input current turn-on characteristic using initial filter design.

7844-86

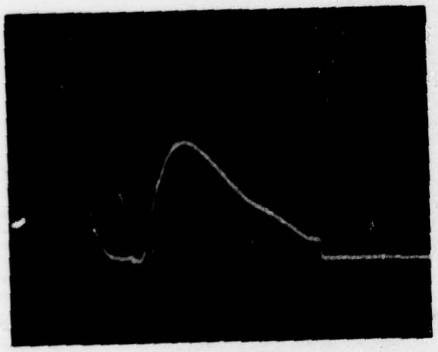

Figure 76. PPA input current turn-on characteristic using final filter design.

SECTION 5

ROCKET MODEL SYSTEM

The SPIBS system design evolution process is presented in depth in Ref. 1. The RM-SPIBS was phased into the main SPIBS program at about the time the EM went into fabrication. The two systems were largely built in parallel. However, to meet rocket test schedules, the RM-SPIBS model was completed first, with delivery in May 1977. A series of tests were subsequently performed at AFGL, some of which identified design weaknesses that were corrected in all SPIBS models (e.g., potting of the ion source vacuum feedthroughs to prevent breakdown in air).

A. SYSTEM DESIGN

The RM-SPIBS design is shown in Figures 77 through 79. Except for Figure 79, these figures apply equally to the engineering and the flight models. The reservoir clamp, shown correctly in Figure 77, was modified after the photographs were taken. The loop in the reservoir clamp extended beyond the base interface and was subsequently relocated. The photographs in Figures 78 and 79 show many details of the SPIBS system during and after final assembly. The wires protruding from the PPA enclosure in Figure 78 attach to terminals on the ion source.

Fabrication and assembly procedures for the RM system were similar to those used for the EM[1]. All mechanical or machined parts were fabricated through the HRL shops as "controlled hardware." The process does not involve inspection of vendor facilities, but does provide 100% inspection of all fabricated parts. Electronics parts, except for magnetics, were purchased and controlled by HRL personnel. Magnetics parts were designed electrically at HRL and were built by Hughes Components and Material Laboratory in Culver City.

During the fabrication of the EM and RM ion source, a written assembly procedure was developed. All process steps were clarified and documented for use on the flight source. The assembled ion source was inspected by the assembly supervisor. Although the quality

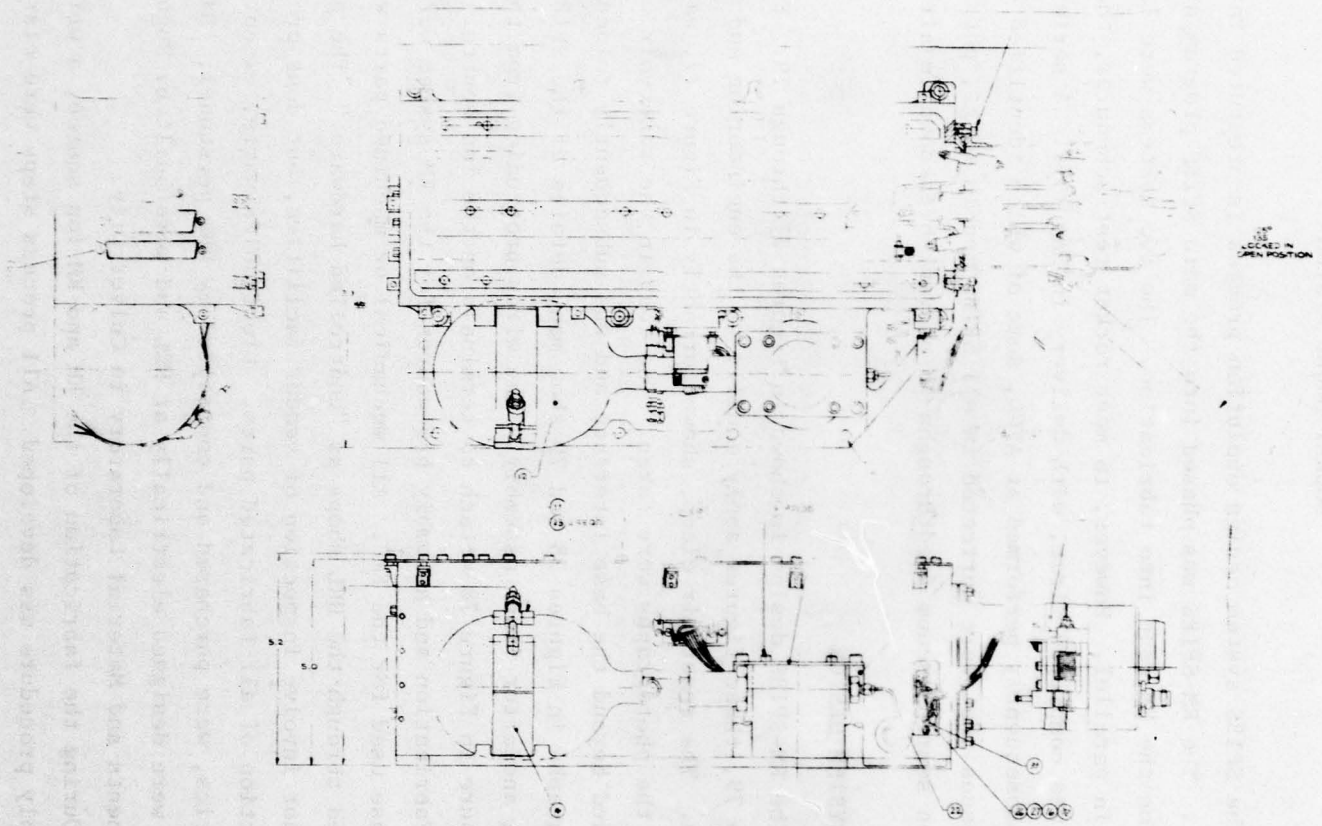

Figure 77. SPIBS layout drawing.

M12247

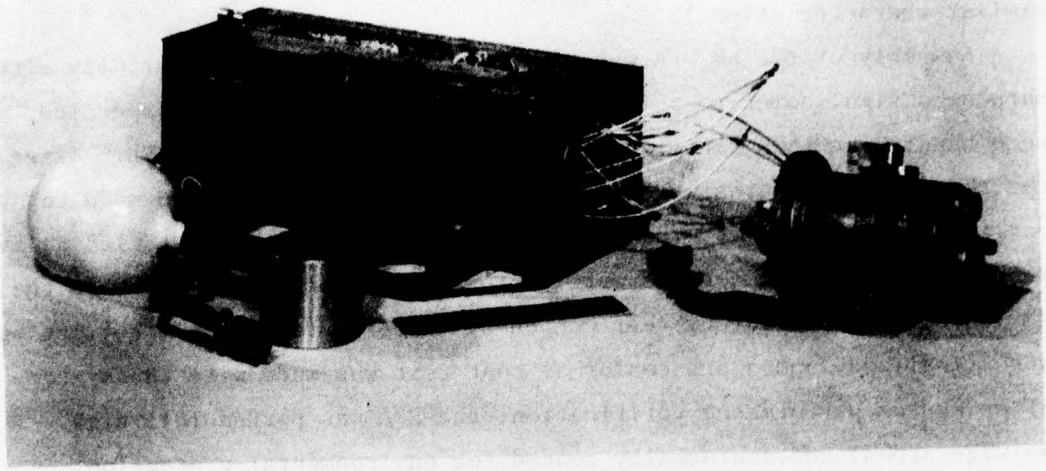

Figure 78. Typical assembly.

M12244

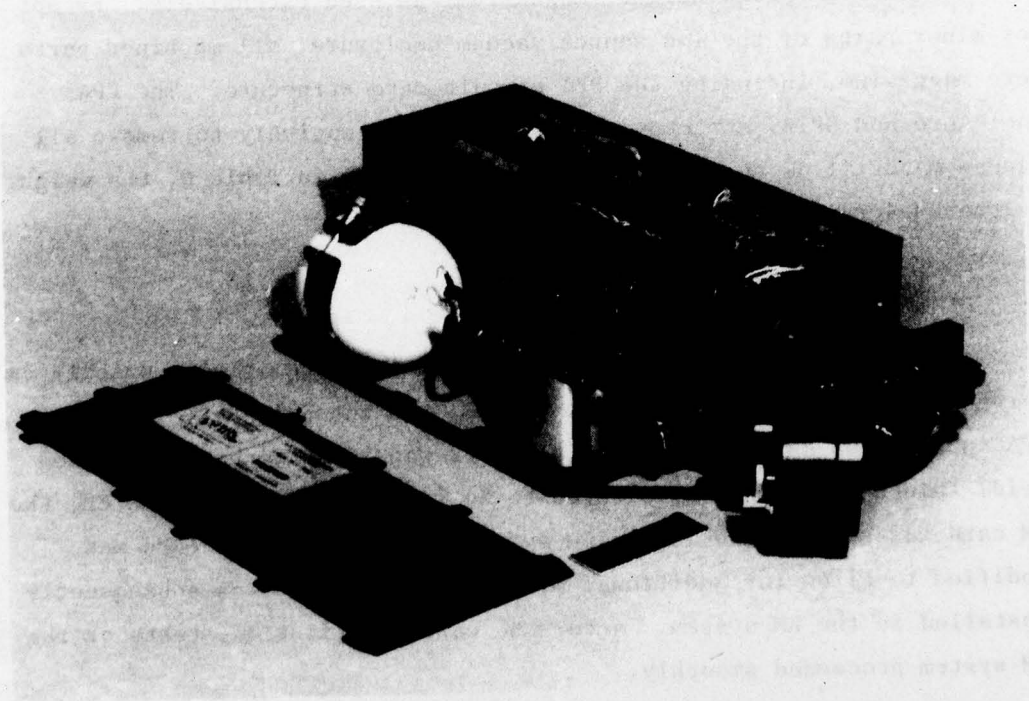

Figure 79. Completed RM-SPIBS.

assurance program for the ion source was simple, few errors resulted. (All sources operated properly from the first startup and had remarkably similar characteristics.)

Assembly of the RM PPA was performed at the Hughes Culver City site. Harness design, point-to-point wiring lists, assembly, and inspection were handled at this facility. Parts kits were supplied by HRL. After the three circuit cards were assembled, electrical tests were made to verify proper assembly. The inner-card harness was then installed as shown in Figure 80 and tests were performed on dummy loads and with the RM ion source. Select-by-test components were installed, all corrections were finalized, and a pre-conformal coat test was made with the system. After system performance verification, the PPA was potted (all high voltage areas) and conformally coated for environmental protection.

The ion source, PPA, and expellant assembly were then integrated. The various tests performed during the assembly phase are discussed in the following section.

To minimize SPIBS weight, magnesium was used extensively. Except for minor parts of the ion source vacuum enclosure, all machined parts were magnesium, including the PPA circuit card structure. The PPA enclosure and SPIBS structure were machined extensively to remove all excess material as shown in Figure 81. As shown in Table 6, the weight of the RM-SPIBS was 7.5 kg.

B. SYSTEM TESTING

Testing of the RM-SPIBS system was completed relatively quickly as a result of prior experience with the EM. As noted in Ref. 1, during PPA integration on the EM, circuit card 2 was found to have a cracked weld. Since the RM was considered to be less critical than the EM, the RM card was substituted in the EM system. The cracked EM card was modified to allow for additional mounting screws, and was subsequently installed in the RM system. After the card substitution, tests of the RM system proceeded smoothly.

M12056

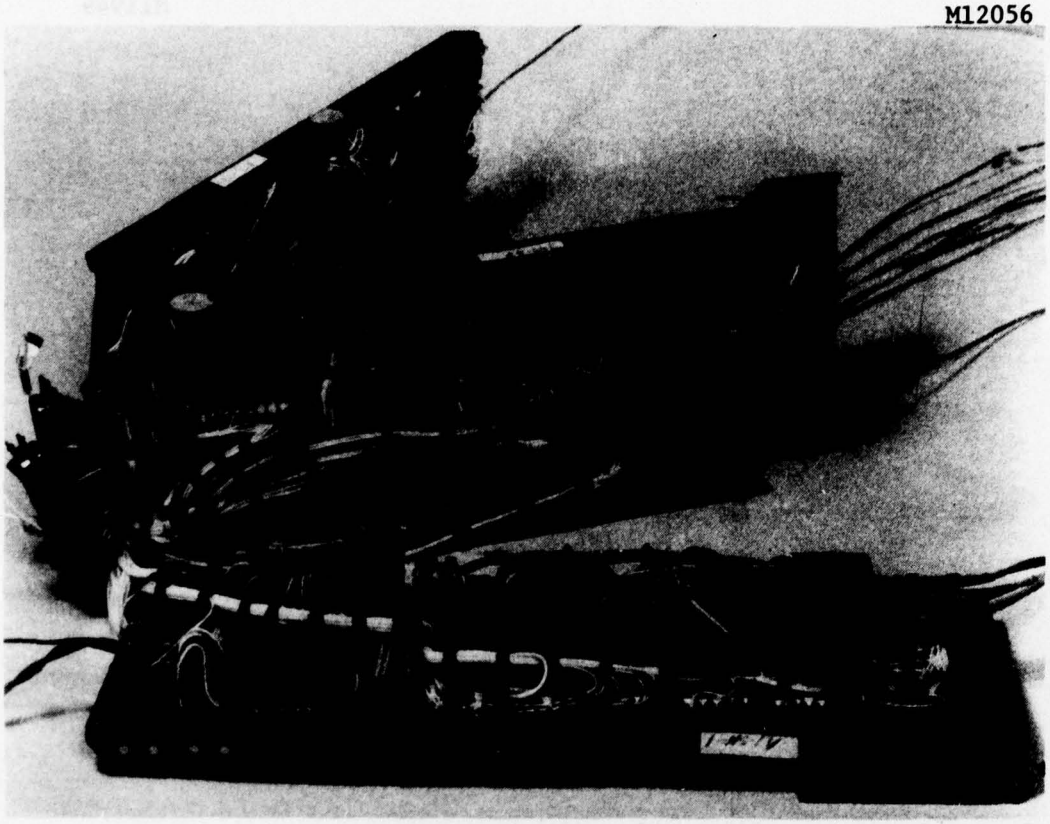

Figure 80. PPA cards and harness before potting.

M11949

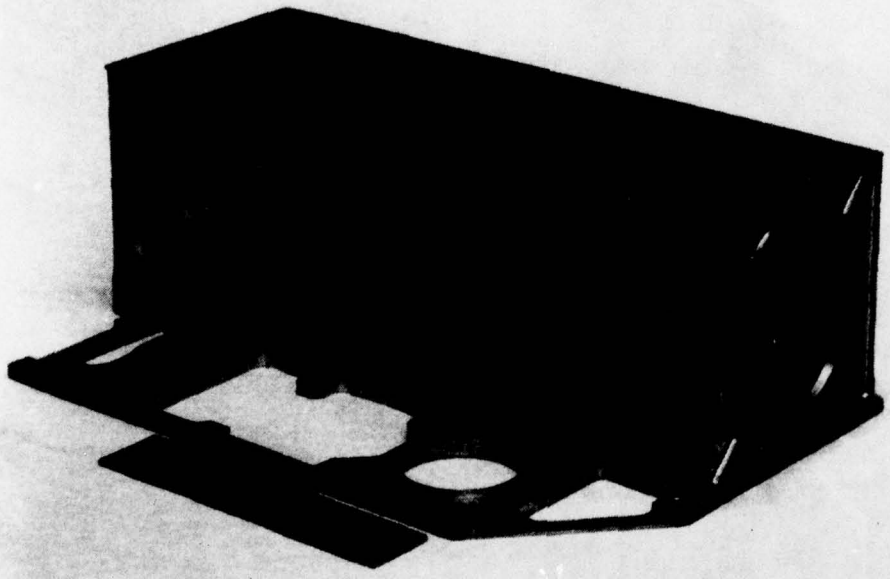

Figure 81. PPA structure.

Table 6. Engineering Model Weight Breakdown

Element	Weight, g Revised Estimate
Ion source assembly (ISA)	490[a]
Ion source	
Enclosure endplate	
Insulators, wiring, and fasteners	
Expellant assembly (EA)	
Tank (empty)	1253[a]
Valve, fill fitting, and transfer	
Regulator	
Xenon	270
Lines and fittings	20
Connectors and misc.	50
Power processor assembly (PPA)	
Circuit card 1	961[a]
Circuit card 2	1026[a]
Circuit card 3	810[a]
Conformal coating and potting	300
Connectors and wiring	550[a]
Structure and mechanisms	
Blowoff cover assembly	540
PPA enclosure	850[a]
Clamps and fasteners	230
Contingency	150
	7,500 g

[a]Measured EM weights

Six test runs were conducted during system integration, as shown in Table 7. The few problems encountered were limited to gas (or gas supply line) purity and PPA minor component failures. Run RM-1 was directed toward checkout of the RM ion source. The EM-PPA and EM-EA, mounted outside the vacuum chamber, were used to support this test. The RM-PPA was in the final steps of assembly when this test was conducted.

Test run RM-2 was primarily dedicated to checkout of the harnessed PPA and to determining select-by-test component values for the heater circuits and neutralizer emission levels. The EM-EA was also used for this run as a matter of convenience and availability.

The PPA was then returned to Hughes Culver City facility for potting and conformal coating. Prior to final system assembly, test run RM-3 was conducted to assure that no significant changes in PPA operation had occurred due to potting. For this test, the RM-EA was used, but test results indicated a possible gas contamination or gas line purity problem. Except for difficulty in operating at the low beam current level, the system performed satisfactorily.

A complete system test in vacuum was conducted in run RM-4, using the EM-EA because of previous success. Performance and full functional capabilities were satisfactorily demonstrated. This test was a major milestone in the RM-SPIBS program.

Run RM-5 was devoted to evaluating the RM-EA with the EM system. Satisfactory performance was achieved, and the RM-EA was made part of the EM. The apparent purity problem noted in run RM-3 was not clearly resolved since the RM reservoir gas apparently was clean.

A final ground test simulation run was conducted in run RM-6. In this test, the RM-SPIBS pumpout port (with the cover closed) was "plugged in" to a fitting on the vacuum chamber. In this configuration, sputtering limits operating time to a few minutes. Beam current was detected on the collector mounted in the cover. However, in the confined volume of the cover, neutralizer performance cannot be evaluated. Following this run, the RM-SPIBS instrument was packaged and shipped to AFGL.

Table 7. Summary of Integration Test Objectives and Results

Run	Objective	Result
RM-1	RM ion source checkout using EM PPA and EA.	Ion source starts and operates within normal tolerances.
RM-2	Checkout of RM-PPA cards, harnessed, but in air; install select-by-test components; EM EA	Adjustment, minor corrections, and SBT component installation completed; operation normal.
RM-3	Checkout following PPA conformal coating and potting; PPA and EA in air; RM EA.	PPA checks OK; RM EA gas system purity in question; operation at beam level 1 difficult.
RM-4	Checkout of PPA in vacuum; return to EM EA; total system in vacuum.	PPA operates satisfactorily; operation at beam level 1 more stable.
RM-5	Checkout of RM EA with EM ion source and EM PPA.	Operation seems to be satisfactory. RM EA to be used with EM system.
RM-6	Final checkout of RM system in "ground test" mode, pumping through pumpout port.	Startup and operation satisfactory; collector current satisfactory.

An operating mode not originally anticipated was experienced during the SPIBS and RM-SPIBS testing. This mode is one in which the keeper is ignited at a low value (less than 30 mA), the discharge current is essentially zero, and the cathode heater is limited to about 1 A. Such a condition arises if the discharge goes out but the keeper discharge remains at a level sufficient to be self-sustaining. The cathode heater supply and the keeper supply share a high voltage transformer to minimize parasitic power during normal operation; however, when the keeper drains even small currents, the cathode heater current is limited to about 1 A. Since it was expected that the keeper and cathode heater would never be on together, algorithms to accommodate this mode were not planned.

However, as a result of the rocket test of the RM-SPIBS, it was determined that beam current levels below 0.3 mA might be desirable and necessary for full evaluation of SPIBS on SCATHA. The "low keeper current only" mode can probably be achieved repeatably by turning the ion source on in the low discharge current mode (25 mA) without initially starting at higher discharge current. Such a startup process probably does not allow the cathode emission process to stabilize sufficiently to operate as an "auto cathode." The beam current obtained in this low keeper current mode is about 0.1 mA, giving the SPIBS a beam current dynamic range of about 20 to 1.

C. ANALOG OUTPUTS

Operation of the RM-SPIBS instrument is monitored with the 18 analog outputs listed in Table 2. Calibrations for these channels are presented in Figures 82 through 99. These data were obtained using resistive loads on the supplies individually. However, during system integration, the PPA was connected through a meter panel to verify calibrations and to set select-by-test components. Most of the calibration curves are believed to be accurate to within ±5% of the true value. The electrometers are believed to be accurate to about ±10%.

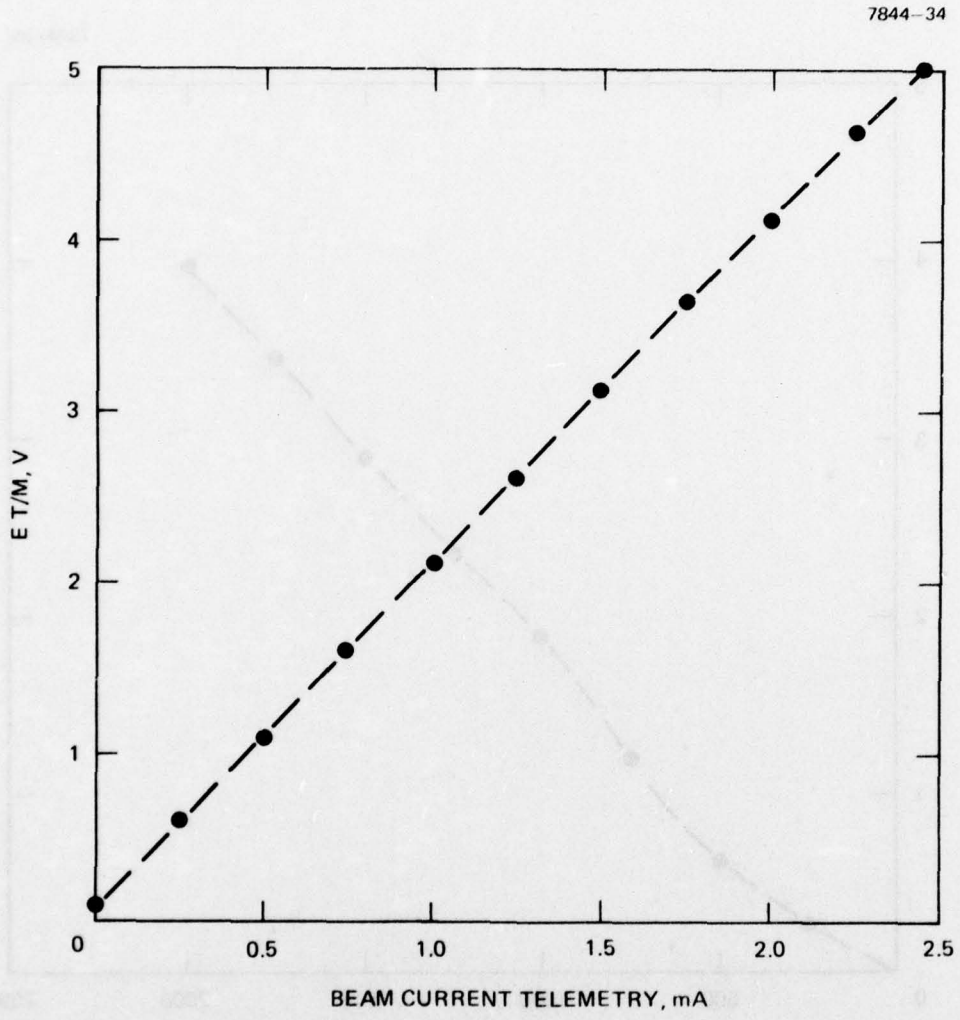

Figure 82. EM beam current telemetry calibration.

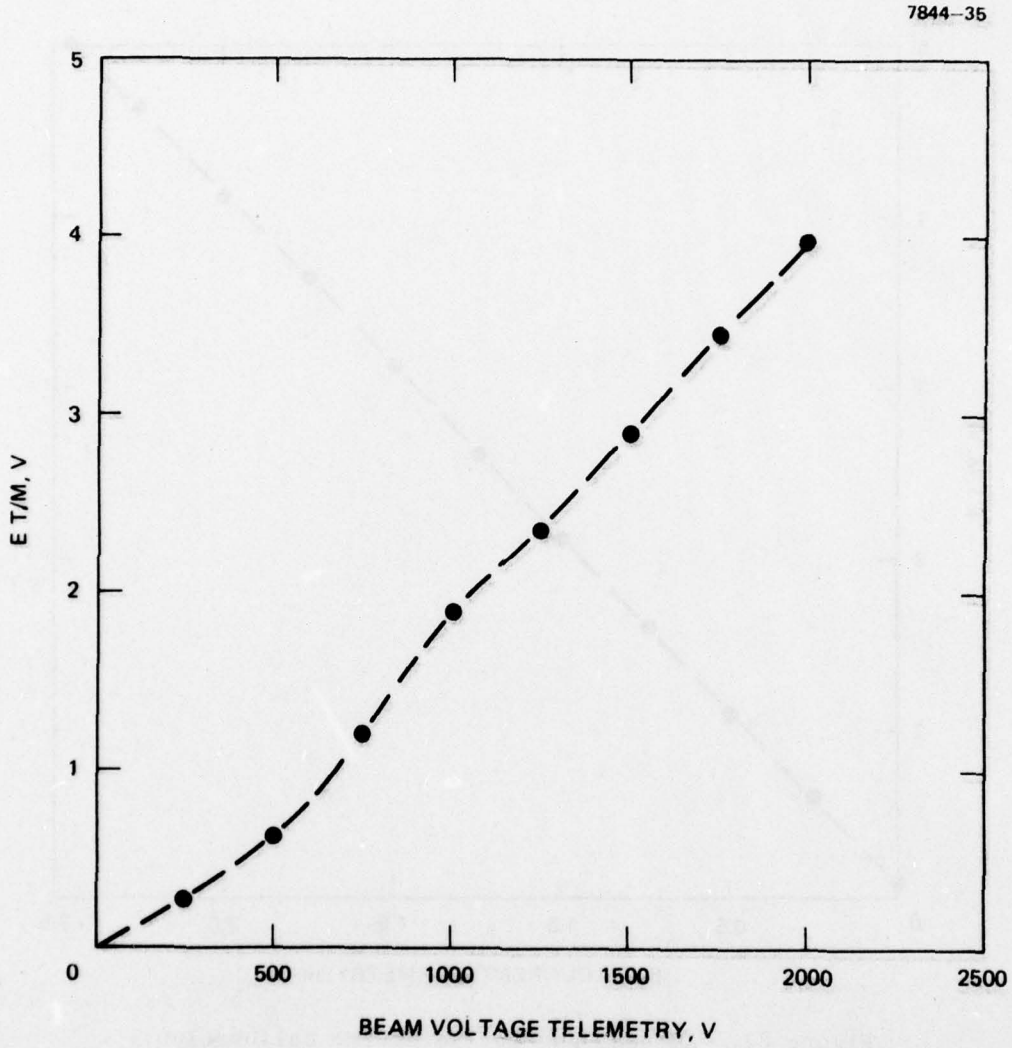

Figure 83. EM beam voltage telemetry calibration.

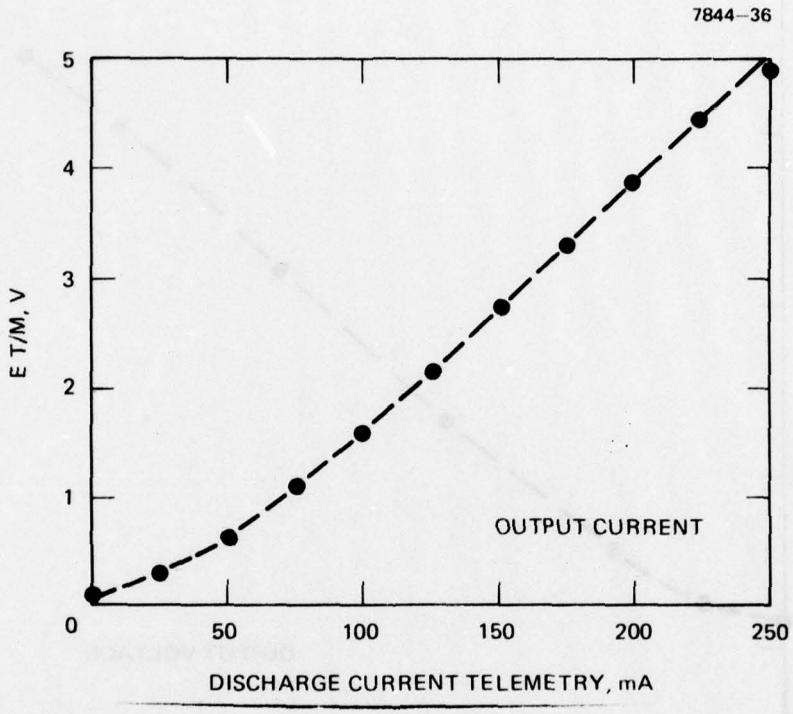

Figure 84. EM discharge current telemetry calibration.

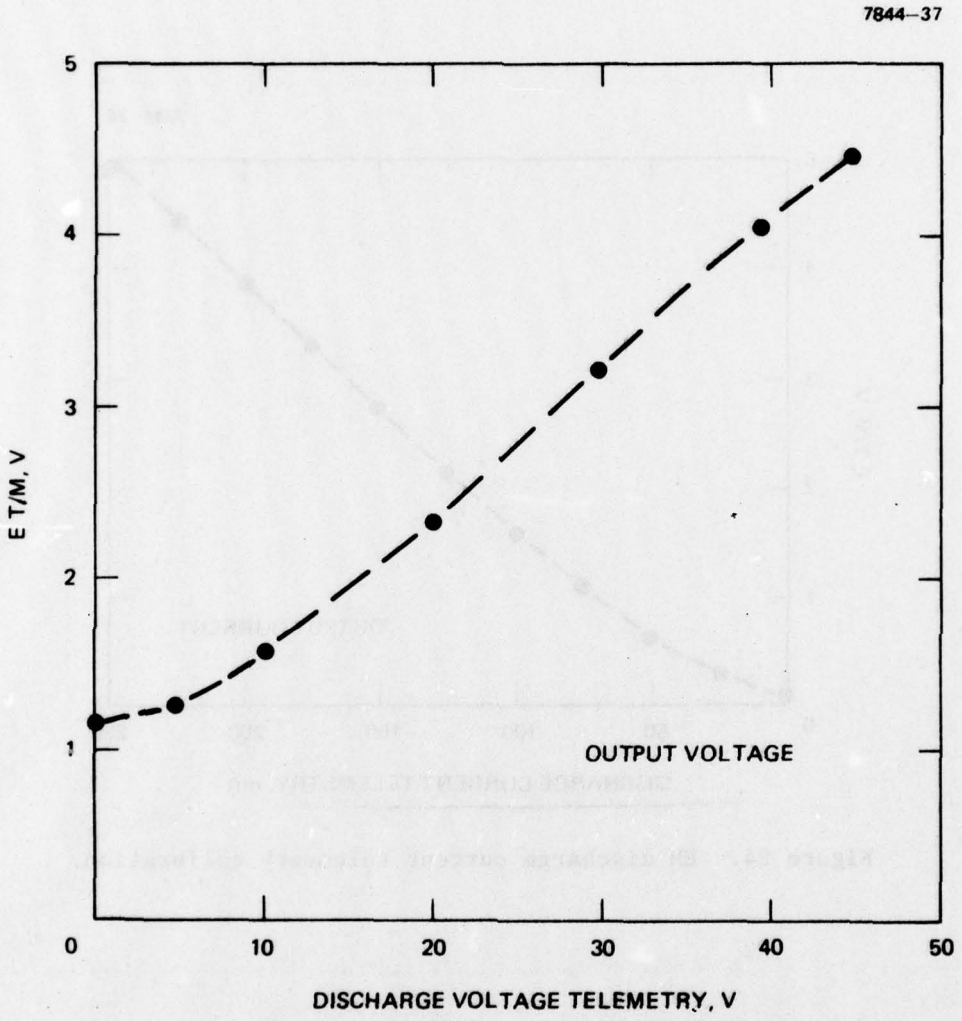

Figure 85. EM discharge voltage telemetry calibration.

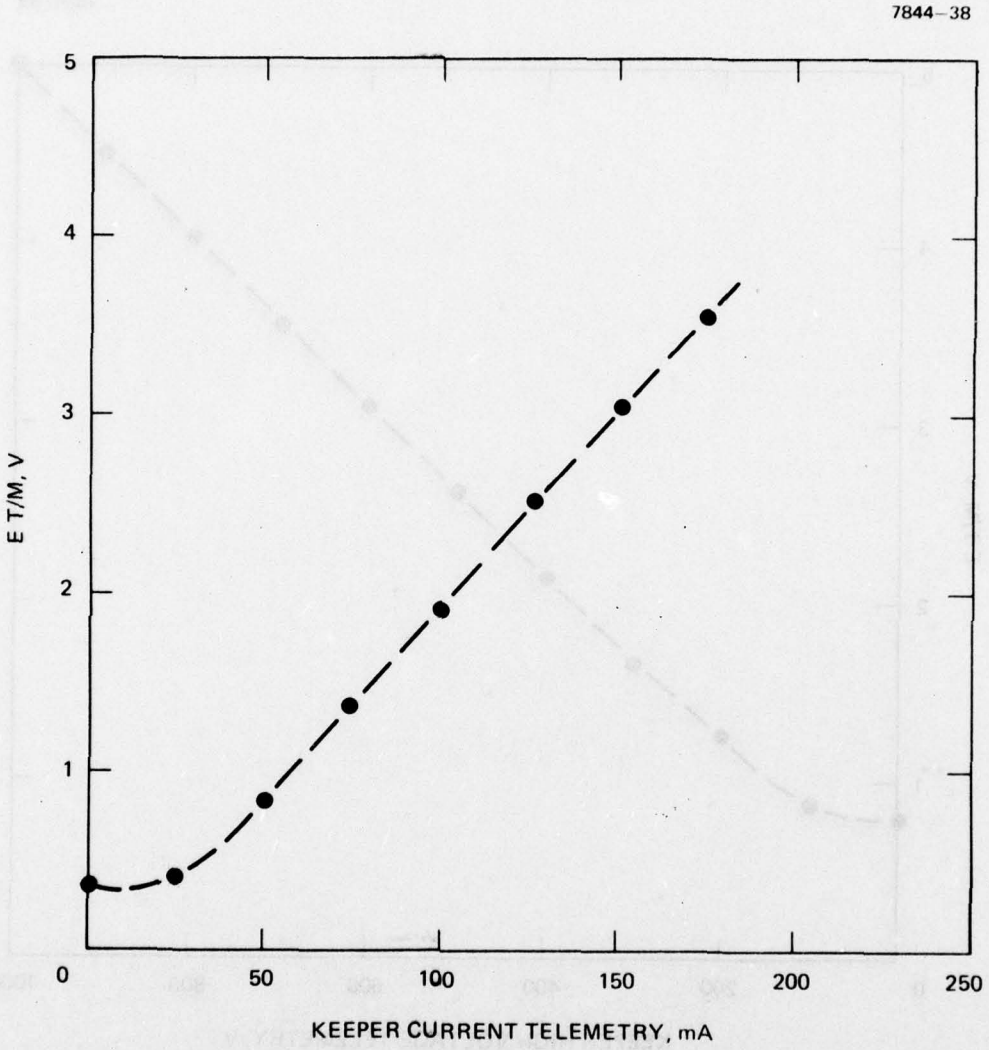

Figure 86. EM keeper current telemetry calibration.

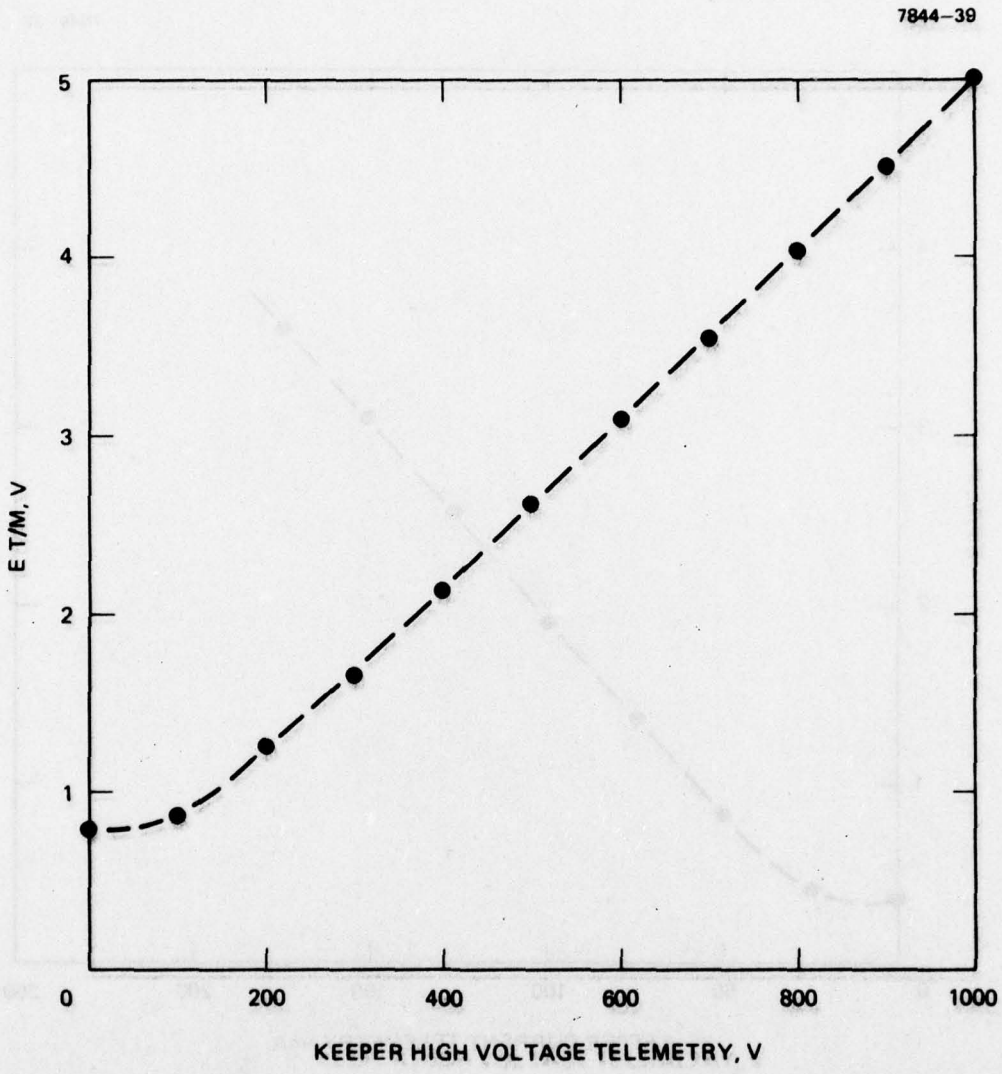

Figure 87. EM keeper high voltage telemetry calibration.

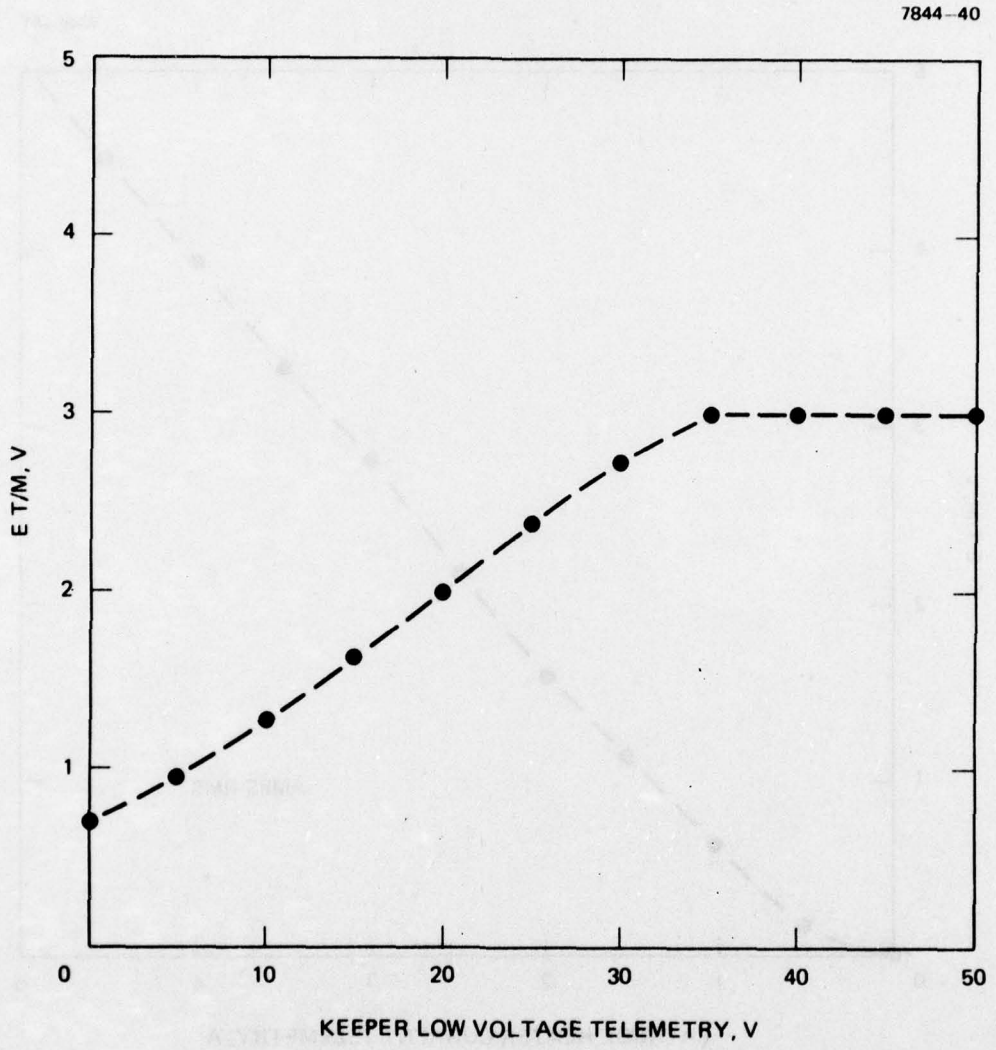

Figure 88. EM keeper low voltage telemetry calibration.

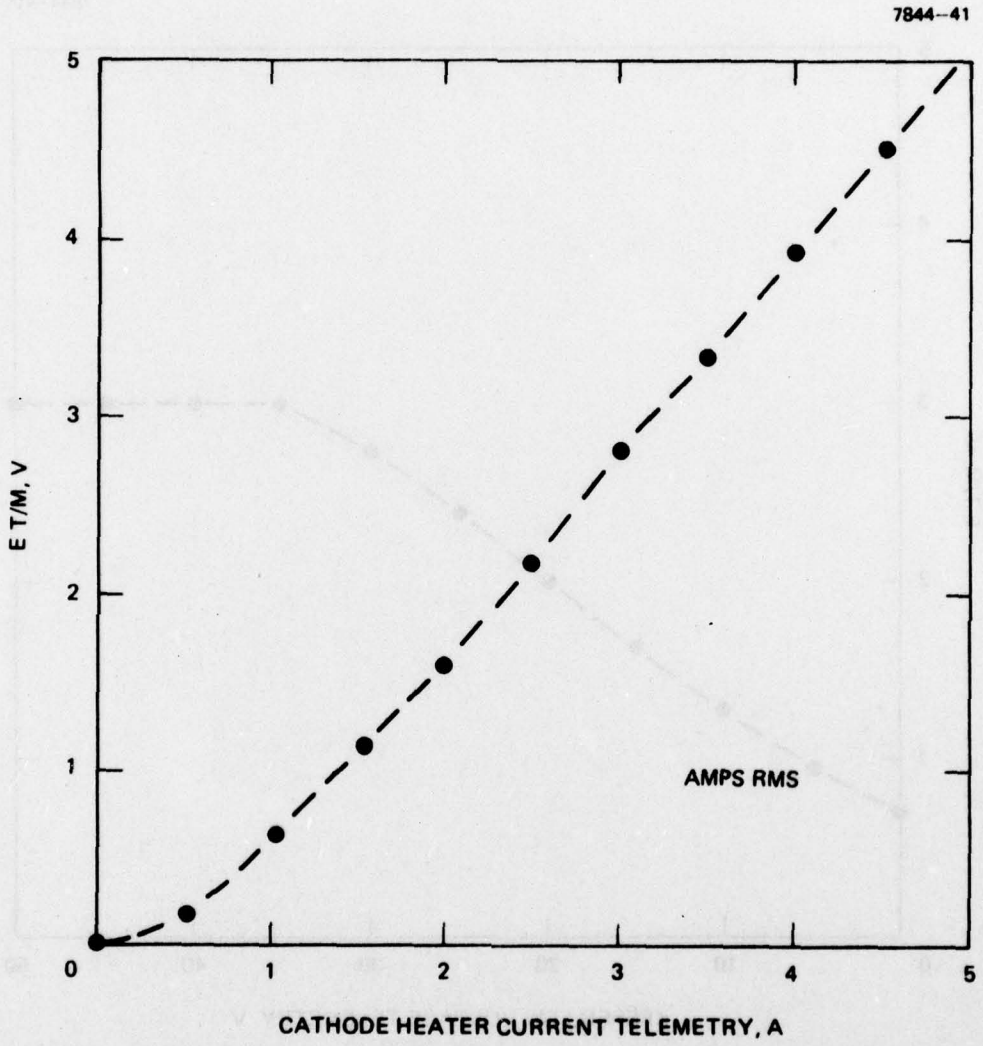

Figure 89. EM cathode heater current telemetry calibration.

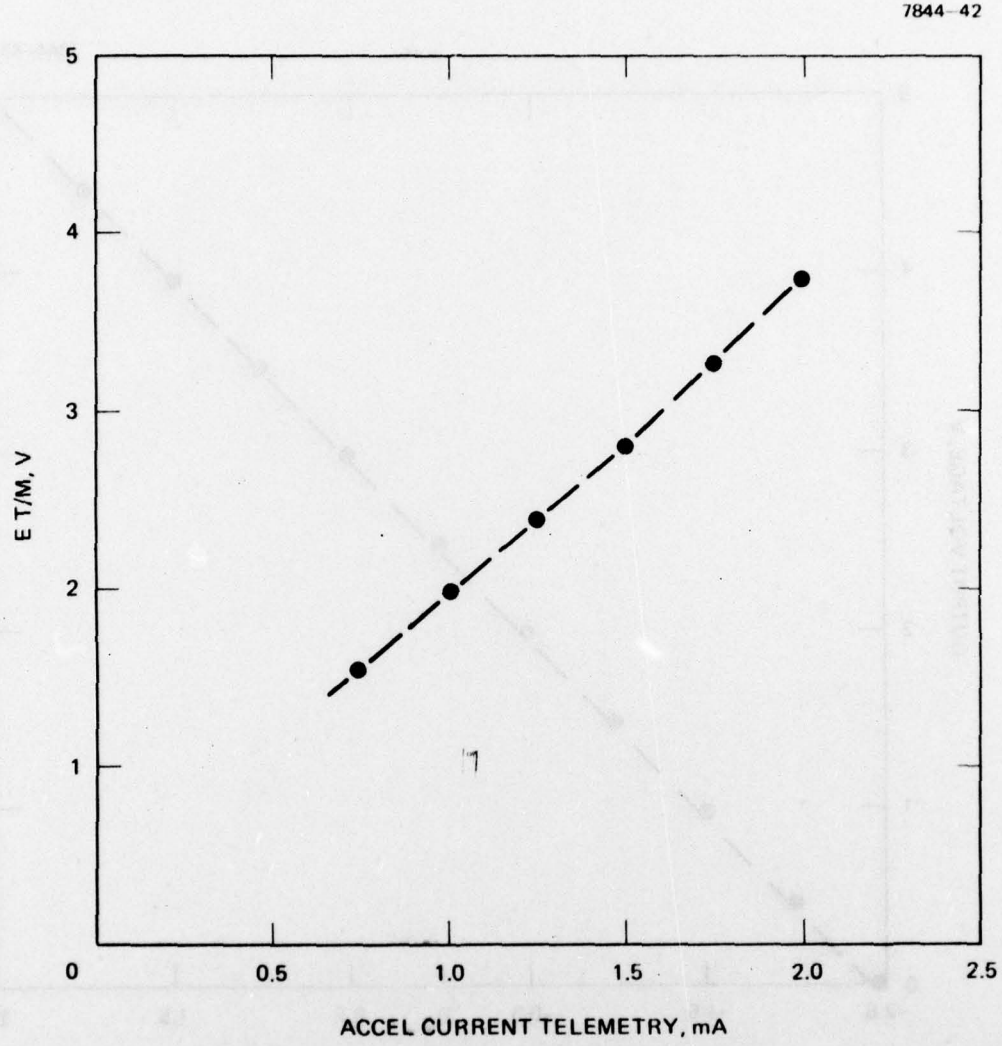

Figure 90. EM accel current telemetry calibration.

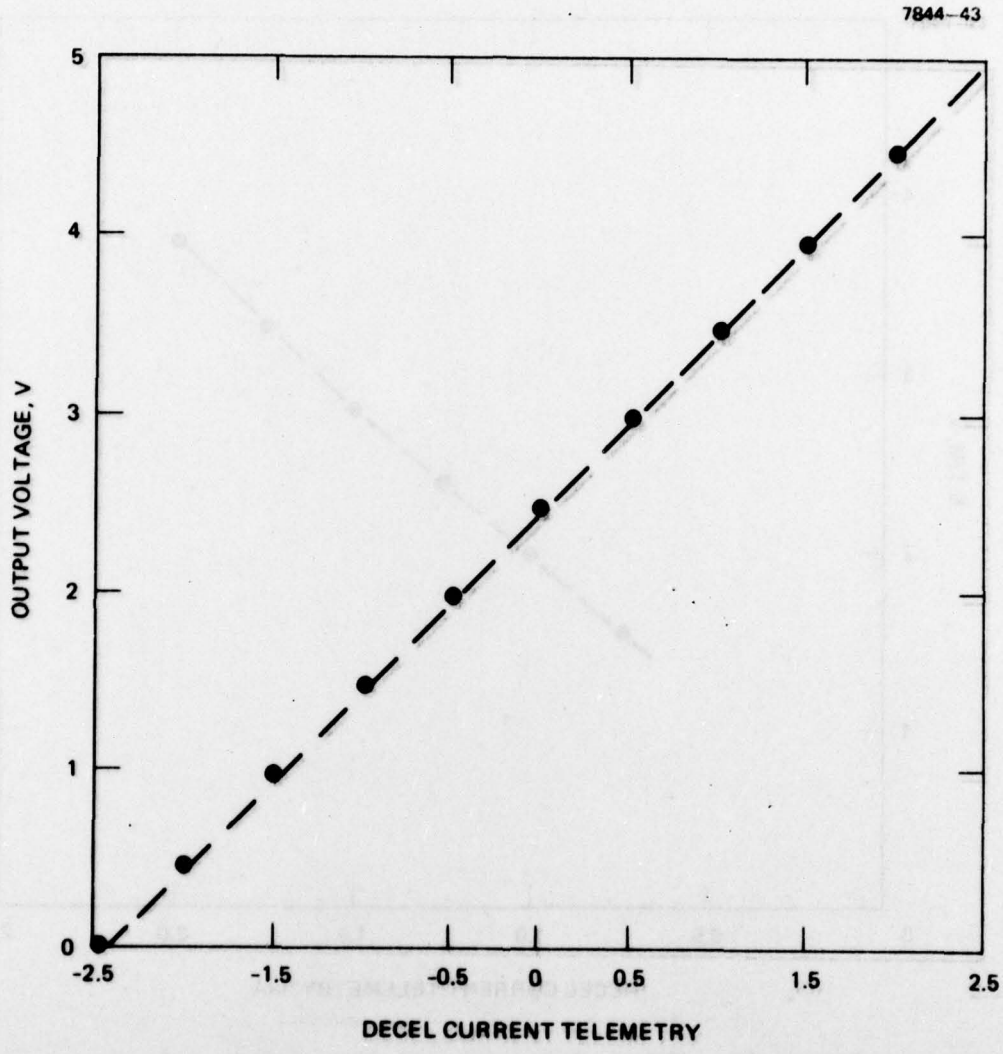

Figure 91. EM decel current telemetry calibration.

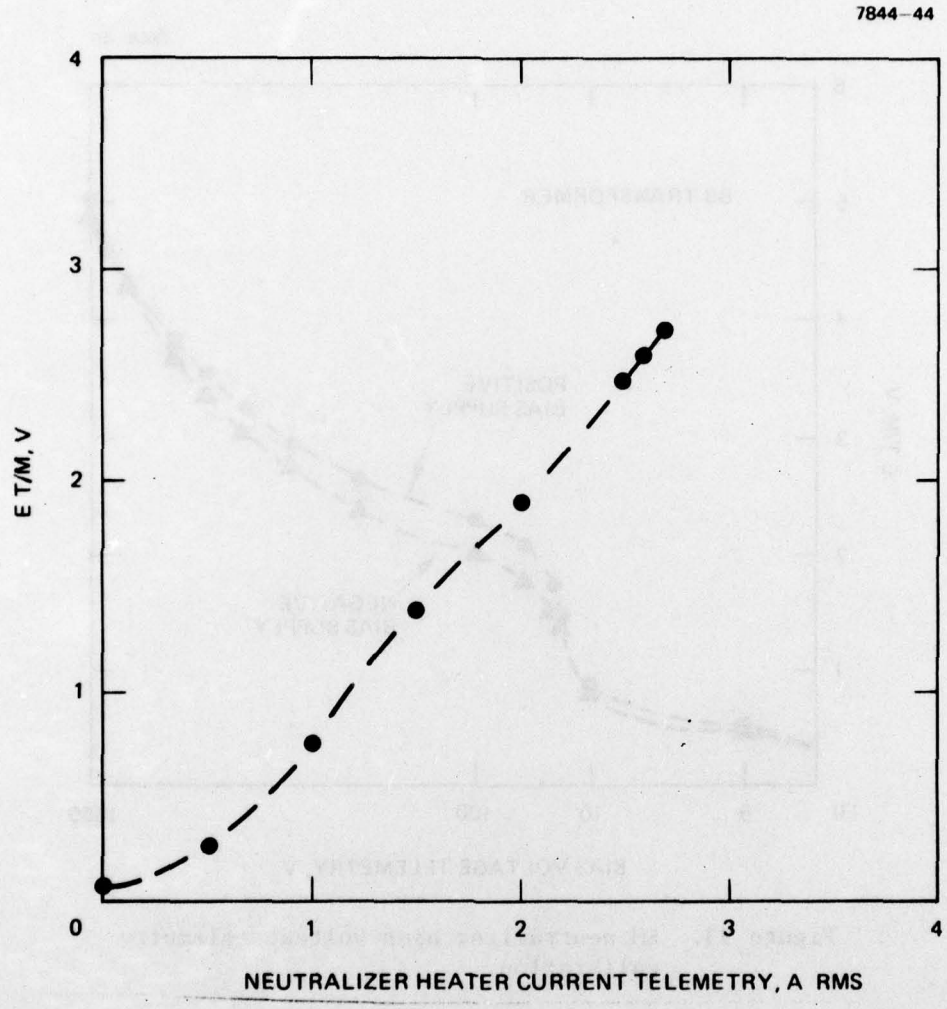

Figure 92. EM neutralizer heater current telemetry calibration.

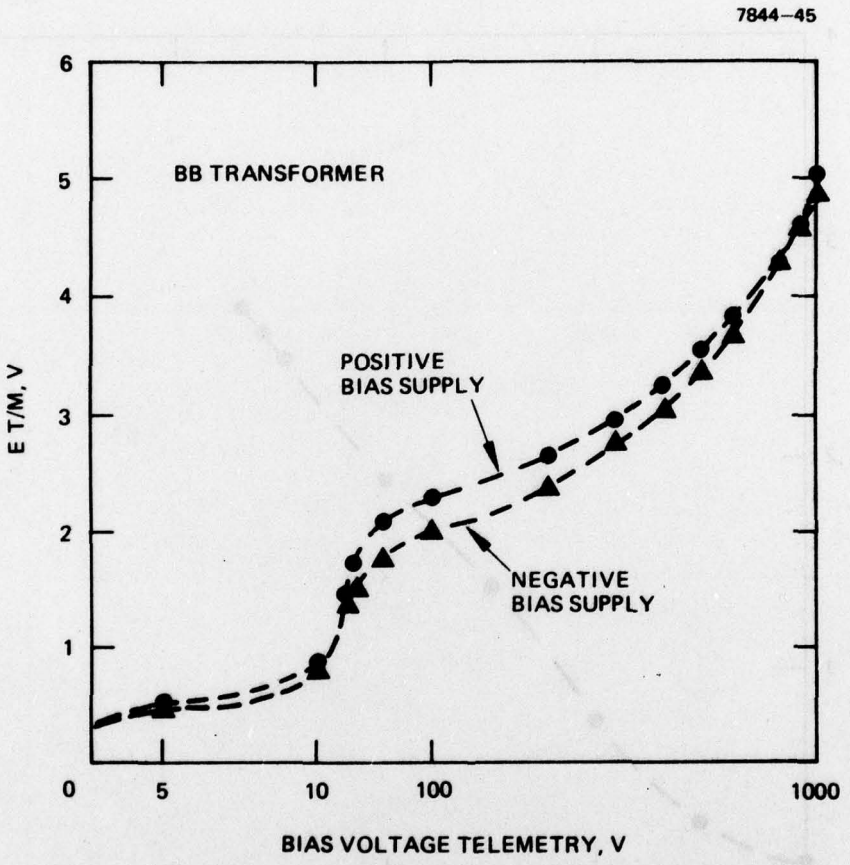

Figure 93. EM neutralizer bias voltage telemetry calibration.

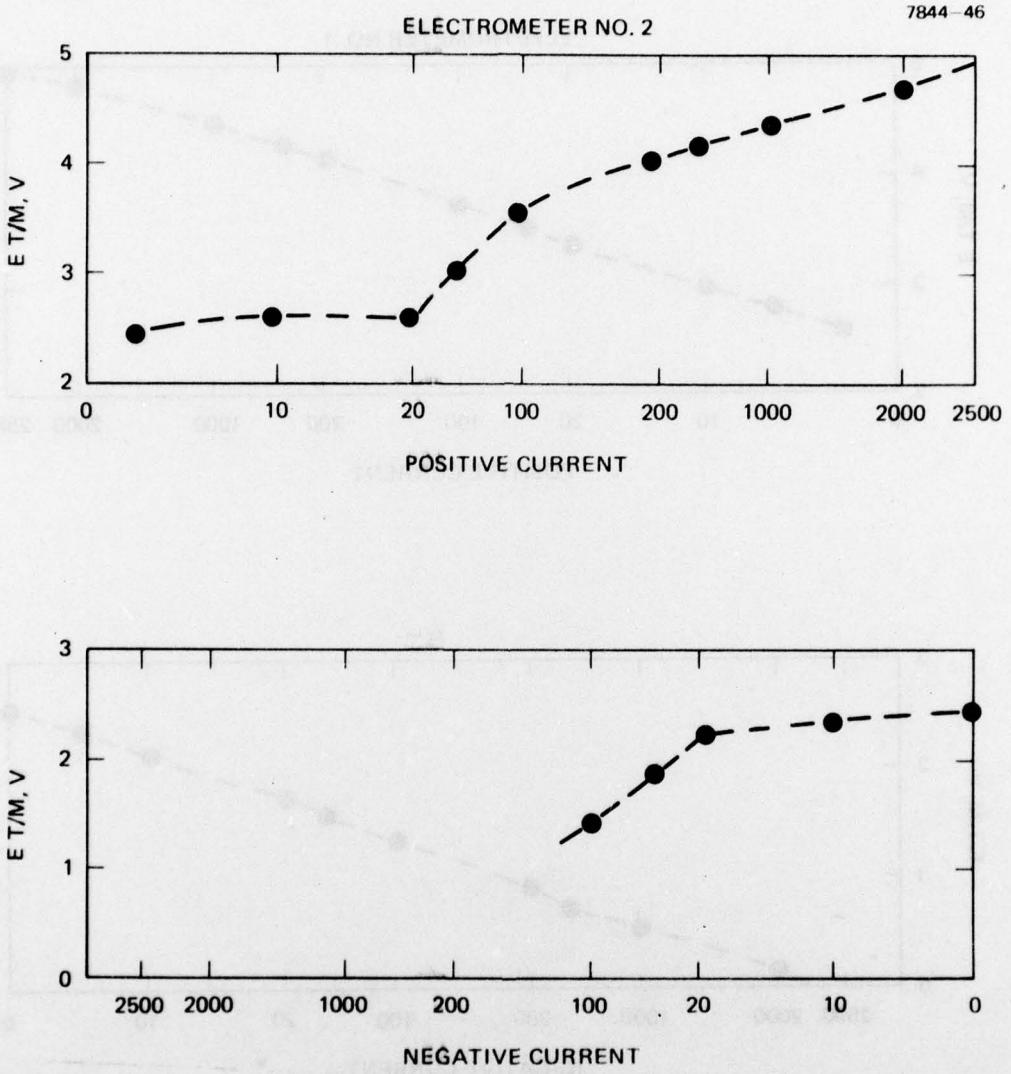

Figure 94. EM neutralizer emission telemetry calibration.

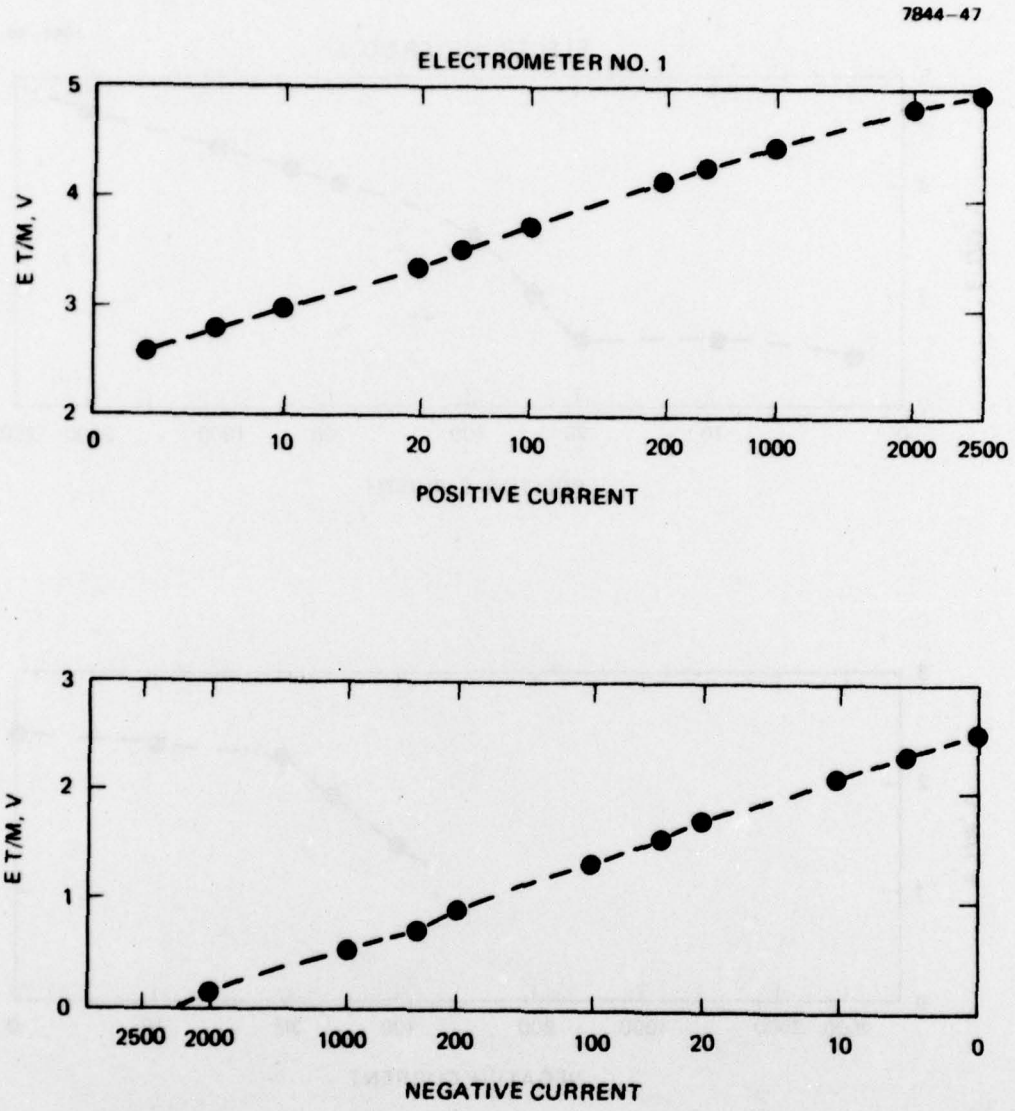

Figure 95. EM SPIBS net current telemetry calibration.

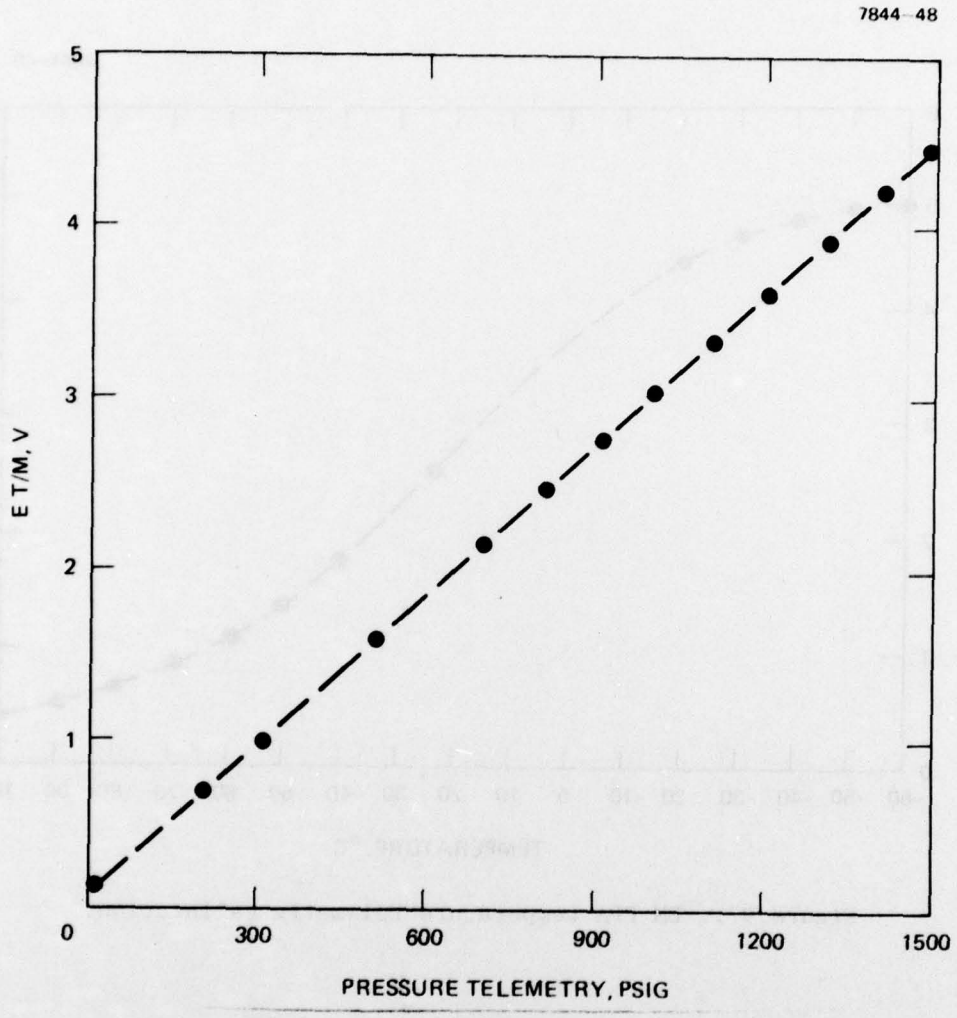

Figure 96. EM reservoir pressure telemetry calibration.

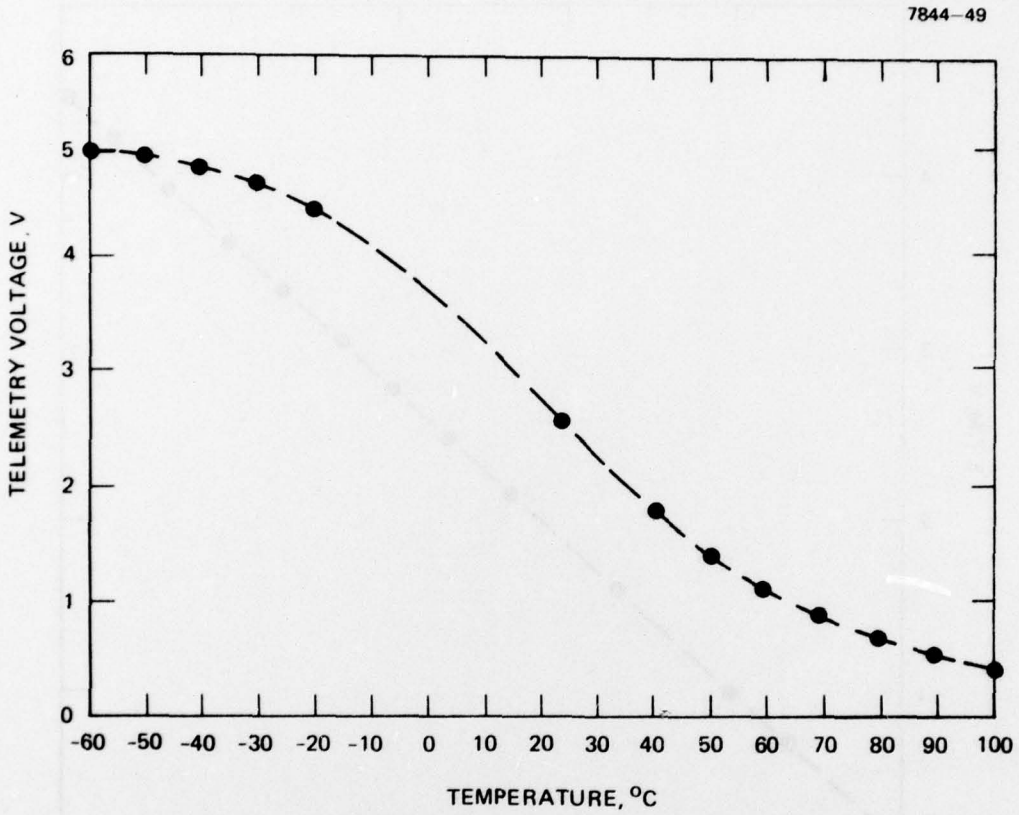

Figure 97. EM PPA temperature telemetry calibration.

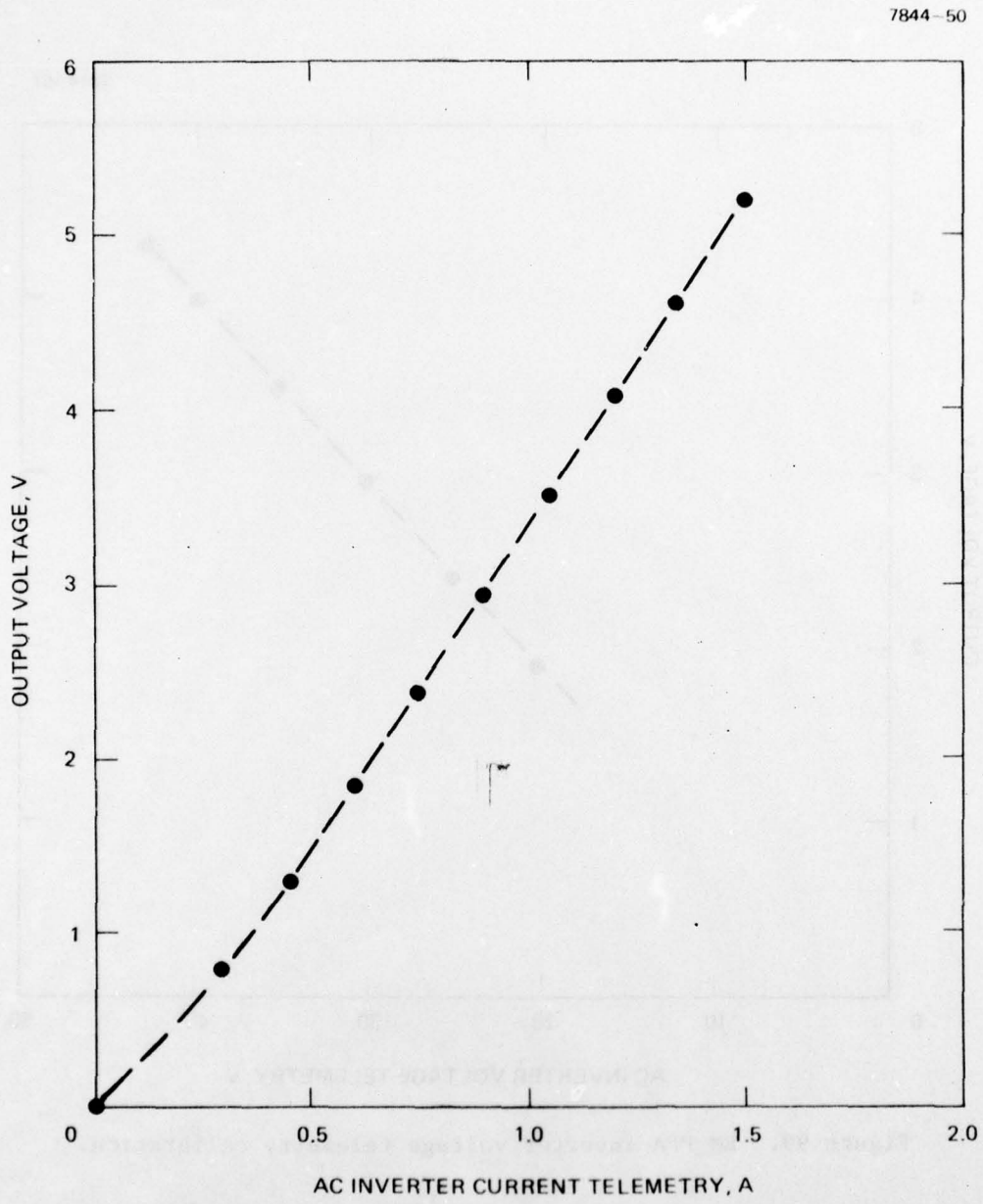

Figure 98. EM PPA inverter current telemetry calibration.

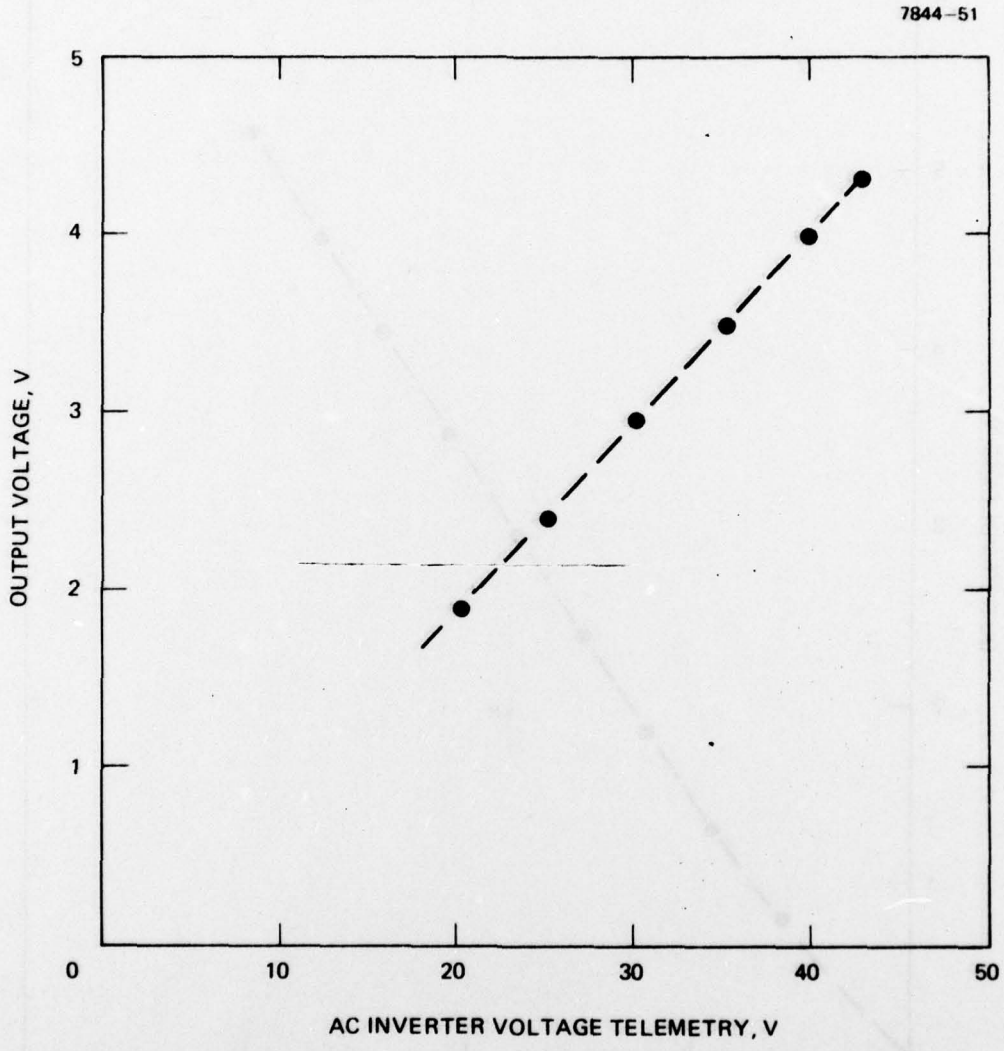

Figure 99. EM PPA inverter voltage telemetry calibration.

SECTION 6

CONCLUSIONS

The RM SPIBS program was successfully carried out with a minimum of serious setbacks. Essentially, all objectives were met and an operational instrument was delivered to AFGL. This instrument was subsequently used successfully in a rocket flight test program. Although the RM-SPIBS as delivered had a few shortcomings that were discovered later in the program, modifications were made relatively easily by AFGL personnel. These modifications included: (1) ion source insulator potting and (2) the addition of a noise filter on the analog outputs. A PPA component failure was also corrected at AFGL with Hughes support.

Significant points to be noted regarding the instrument include:

- The RM-SPIBS performed as specified with reproducible characteristics and satisfied requirements on input power, envelope dimensions, and weight.

- Rocket qualification tests were completed by AFGL personnel and demonstrated that RM-SPIBS met rigid requirements on vibration, thermal-vacuum, and EMI.

- The flexibility of the SPIBS design was demonstrated during the rocket flight test. As a result of this flight, an additional operating mode will be included on SCATHA to obtain beam currents as low as 0.1 mA. With this "keeper only" mode, the beam current dynamic range is about 20 to 1.

- Over 300 operating modes are available, including operation with an un-neutralized ion beam, partial neutralization, full neutralization, or neutralizer only. Neutralizer biasing of ±1000 V is possible in all modes.

- The SPIBS ion source has many novel features and characteristics, including: (1) xenon expellant, (2) decel grid, (3) graphite screen and accel grids, (4) compact and rugged hollow cathode using a porous tungsten oxide impregnated insert, (5) startup in less than 3 min, (6) stable operation over a wide beam current range, (7) operating life in excess of 1000 hr, (8) low input power considering overall capabilities, and (9) an extremely high tolerance to abnormal gas conditions (e.g., exposure to air during operation).

Several important related subjects were not addressed as part of this program. Neutral efflux, ion beam divergence, and charge exchange are of concern to other experimenters on SCATHA. AFGL personnel are conducting experiments and analyses to accurately define and assess these areas. Notwithstanding these questions, SPIBS should prove to be a valuable tool in the study of vehicle charging.

SECTION 7

REFERENCES

1. "Satellite Positive Ion Beam System," Final Report on Contract F19628-76-C-0066, Hughes Research Laboratories, August 1978.

2. DeForest, S.E., "Spacecraft Charging at Synchronous Orbit," *Journal of Geophysical Research* 77: 4, p. 651-659 (1972).

3. Fredricks, R.W. and Scarf, F.L., "Observations of Spacecraft Charging Effects in Energetic Plasma Regions," *Photon and Particle Interactions with Surface in Space*, D. Reidel Publishing Co., Dororecht-Holland, 1973, pp. 277-308.

4. Rosen, A, "Large Discharges and Arcs on Spacecraft," AIAA Astronautics and Aeronautics, p. 36-44, June 1975.

5. McPherson, D.A., Cauffman, D.P., and Schober, W., "Spacecraft Charging at High Altitudes: The SCATHA Satellite Program," AIAA Paper 75-92, AIAA 13th Aerospace Sciences Meeting, Pasadena, California, January 1975.

6. Bartlett, R.O., DeForest, S.E., and Goldstein, R., "Spacecraft Charging Control Demonstration at Geosynchronous Altitude," AIAA Paper 75-357, 11th Electric Propulsion Conference, March 1975.

7. DeForest, S.E., and Goldstein, R., "A Study of Electrostatic Charging of ATS-5 Satellite During Ion Thruster Operation," Final Technical Report, Contract NAS JPL 953675, Jet Propulsion Laboratory, Pasadena, California, December 1973.

8. Masek, T.D. and Cohen, H.A., "Satellite Positive Ion Beam System," *Jour. of Space and Rockets*, 15: 1, pp. 27-33, Jan. 1978.

9. Gallagher, H.E. and Knauer, W., "Advanced Thermionic Cathodes for Kaufman Thrusters," AIAA Paper 67-678, Colorado Springs, Sept. 1967.

10. Kramer, N.B. and King, H.J., "Extraction of Dense Ion Beams from Plasma," *J.A.P.* 38: 10, p. 4021, Sept. 1967.

11. Worlock, R., Davis, J.J., James, E., Ramirez, P., and Wood, O., "An Advanced Contact Ion Microthruster System," AIAA Paper 68-552, AIAA 4th Propulsion Joint Specialist Conference, Cleveland, Ohio, June 1968.

12. Hyman, J., Dulgeroff, C.R., Kami, S., and Williamson, W.S., "One-Millipound Mercury Ion Thruster," *Journal of Spacecraft and Rockets* 13: 366-372, June 1976.

13. Hyman, J., "Development of a 5-CM Flight-Qualified Mercury Ion Thruster," *Journal of Spacecraft and Rockets* 10: 503-509, August 1973.